NOTE TO USERS

uOttawa

L'Université canadienne
Canada's university

FACULTÉ DES ÉTUDES SUPÉRIEURES ET POSTOCTORALES

uOttawa

L'Université canadienne
Canada's university

FACULTY OF GRADUATE AND POSDOCTORAL STUDIES

Manzoor Qadir
AUTEUR DE LA THÈSE / AUTHOR OF THESIS

M.A.Sc. (Mechanical Engineering)
GRADE / DEGREE

Department of Mechanical Engineering
FACULTÉ, ÉCOLE, DÉPARTEMENT / FACULTY, SCHOOL, DEPARTMENT

Stress and Fatigue Analysis of Pressurised Vessel-Nozzle Intersections with and without Local Wall Thinning

TITRE DE LA THÈSE / TITLE OF THESIS

David Redekop
DIRECTEUR (DIRECTRICE) DE LA THÈSE / THESIS SUPERVISOR

CO-DIRECTEUR (CO-DIRECTRICE) DE LA THÈSE / THESIS CO-SUPERVISOR

EXAMINATEURS (EXAMINATRICES) DE LA THÈSE / THESIS EXAMINERS

R. Langlois

M. Nganbe

Gary W. Slater
Le Doyen de la Faculté des études supérieures et postdoctorales / Dean of the Faculty of Graduate and Postdoctoral Studies

STRESS AND FATIGUE ANALYSIS OF PRESSURISED VESSEL-NOZZLE INTERSECTIONS WITH AND WITHOUT LOCAL WALL THINNING

MANZOOR QADIR

Thesis submitted to the Faculty of Graduate and Post Doctoral Studies as partial fulfillment for the degree of

M.A.Sc. in Mechanical Engineering.

uOttawa

L'Université canadienne
Canada's university

OTTAWA-CARLETON INSTITUTE

OF

MECHANICAL AND AEROSPACE ENGINEERING (OCIMAE)

UNIVERSITY OF OTTAWA CANADA

Your file Votre référence
ISBN: 978-0-494-46495-3
Our file Notre référence
ISBN: 978-0-494-46495-3

ABSTRACT

Pressure vessel and piping systems are essential components of all power plants. After long-term service, metallic components in plants will experience wear, leading to wall thinning. Severe thinning will affect the structural integrity, and thus a capability is required to assess the thinned components. The greatest weakening is normally near the intersection of two components. In this work, the finite element method is used to determine the remaining structural capacity of components which have been subjected to local wall thinning. The work is divided into two main parts; a stress analysis at the intersection of pressurized vessels and piping having wall thinning, and a fatigue analysis of damaged intersections subject to cyclical loading.

In the first part of the study, a finite element analysis (FEA) is carried out for the common sphere-nozzle and cylinder-nozzle intersections, to determine the stress concentration factor (SCF). Axi-symmetric (2D) and 3D elements, respectively, are used for the two geometries. In convergence-validation studies, the SCF values obtained for vessels with uniform wall thickness are compared with previously published experimental and analytical results. Comparisons are also made with results from standard formulae given in the literature, and good agreement is observed. An evaluation is made of the effect on the SCF of the growth of the thinning away from the intersection. Finally, a parametric study is conducted in which the SCF is computed for a number of intersections, initially considered undamaged, and then with wall thinning damage. Charts based on the results are provided for the convenience of engineers.

In the second part of the study, a preliminary fatigue analysis is carried out to compare the performance under cyclic loading of sphere-nozzle and cylinder-nozzle intersections, without and with wall thinning damage. The study consists of an elastic-plastic large displacement FEA analysis for simulated seismic action. Results are presented for the major parameters that affect fatigue life. The study ends with some conclusions about the suitability of the FEA for assessing damaged intersections.

ACKNOWLEDGEMENTS

I am thankful to my God who bestowed me good health and power of thinking to do this work. The author wishes to express his sincere gratitude to Professor Dr. David Redekop, the supervisor of this research, for his encouragement, valuable support, and continuous help to complete this study. I am thankful to faculty of graduate and post doctoral studies (FGPS), the faculty and staff members of Mechanical Engineering Department, University of Ottawa, Canada who provided me all kinds of possible support and a better working environment. I would like to appreciate the devotion of my parents, wife and kids who gave me enough time from their share to complete this work.

CONTENTS

LIST OF TABLES

LIST OF FIGURES

Nomenclature:

d_i,d,d_o	internal, mean, external diameter of nozzle
D_i,D,D_o	internal, mean, external diameter of sphere or cylinder
h, h_d	total length, thinned length of nozzle (sphere-nozzle)
p	internal pressure
r_i,r,r_o	internal, mean, external radius of nozzle
R_i,R,R_o	internal, mean, external radius of sphere or cylinder
t,T	wall thickness of nozzle, sphere or cylinder
T_d,T_u	damaged, undamaged diagonal thickness at junction
ε, $\Delta\varepsilon$	effective plastic strain, strain amplitude
ρ	non-dimensional parameter = $(d/D)\,(D/2T)^{1/2} = r/(RT)^{1/2}$
σ_1,σ_2,σ_3	principal stresses
σ_{max}	von Mises stress = effective stress
σ_{nom}	nominal stress = sphere hoop stress
σ_t	tensile stress in nozzle due to p
l,L	length of nozzle, vessel
L_n,L_v	length of thinned section of nozzle, vessel (tee-joint)
ε, $\Delta\varepsilon$	effective plastic strain, strain amplitude
σ_y,σ_u	yield, ultimate tensile stress

CHAPTER 1: INTRODUCTION

1.1 The problem - intersection of pressure vessel and nozzle

Carbon steel vessels and piping are widely used in gas processing plants, oil refineries, chemical plants, and nuclear power plants. Pressure vessels commonly have the form of spheres, cylinders, ellipsoids, or some combination of these. Their main function is to contain media under pressure and temperature. They are also subjected to the action of steady and dynamic loading, piping and supports reactions, and thermal shocks which require an overall knowledge of the stresses imposed by these conditions on various vessel shapes. The spherical vessels with attached radial nozzles and cylinder-cylinder intersections or tee-junctions, are two principal components of many industries like gas processing plants, oil refineries, chemical plants, and nuclear power plants etc. Some of the examples of vessels with attached nozzles are heat exchangers, process columns, pressure vessels, fluid storage tanks, and two intersecting pipes in any piping system.

The aging of vessels and piping of nuclear power plants, refineries, and chemical industries have led to the need to assess the integrity and functionality of existing vessels, piping and its components. Such aging vessels and piping experience metal loss due to erosion and corrosion. This metal loss or damage referred to as local area wall thinning (LTA) in this study is most likely and more severe near the junction or intersection of two components. Thus, an understanding of the behaviour of these types of structures is essential in developing design rules and safety criteria. The function of design is to ensure safe and long life of these components.

It has been recognized that when material is removed from a vessel in order to accommodate a nozzle, the opening in the vessel promotes increased stresses around the edge of the hole. The stress analysis of such a structure is complex due to the many geometric variables and various possible loading conditions. The stress analysts and designers of intersections have made considerable progress over the years to develop rules and establish relationships for stress concentration and distribution, limit and burst pressures. Progress has also been made in the study of fatigue and mechanical damage which leads to geometric imperfection such as cracks.

Various pressure vessel and piping codes are available for the design specifications of vessel-nozzle intersection. These are constantly being updated and revised. Some of the more common codes used for design and construction of equipment are as follows:

- ASME Boiler & Pressure Vessel Code, Section VIII, Division – 1: Rules for Construction of Pressure Vessels.
- ASME Boiler & Pressure Vessel Code, Section VIII, Division - 2: Alternative Rules for Construction of Pressure Vessels.
- ASME Boiler & Pressure Vessel Code, Section VIII, Division - 3: Alternative Rules for Construction of High Pressure Vessels.
- ASME Boiler & Pressure Vessel Code, Section I: Rules for Construction of Power Boilers.
- ASME B31.3: ASME Code for Process Piping.
- ASME B31.1: ASME Code for Power Piping.
- EJMA: Standards of the Expansion Joint Manufacturers Association, Inc.
- API 650: Welded Steel Tanks for Oil Storage.
- API 620: Design & Construction of large, welded, low pressure storage tanks.
- AWWA D100-96: Welded Steel Tanks for Water Storage TEMA: Standards of Tubular Exchanger Manufacturers Association.
- BS 5500: British Specification for Unfired Fusion welded pressure vessels.
- CODAP: French Code for Pressure Vessel Design.
- AD Merkblätter: German Pressure Vessel Code.

Each code has its own approach and provides guidelines for dealing with the problems involved in vessel-nozzle intersection. One of the most common approaches is to determine the stress concentration factor (SCF) of pressure vessel and piping connections based on theoretical, experimental, and finite element analysis (FEA). There is extensive literature available for both geometries in which experimental, analytical,

and numerical solutions and empirical formulae are available to find the SCF for an undamaged component.

In recent years, efforts have been made to perform Fitness-For-Service (FFS) analysis on components which have been in service for a number of years, and which have developed structural defects over time. FFS assessments are quantitative engineering evaluations that are performed to demonstrate the structural integrity of an in-service component containing a flaw or damage. One of these known flaws is LTA due to corrosion/erosion. Fitness-for-service is based on API-579 and other applicable codes, standards and specifications.

Recently great improvements in computer technology have made FEA a dominant means of analysis. A number of FEA softwares are available in the market which can address a variety of engineering problems without going into expensive experimental analysis.

In the FEA, a mathematical model is generated by subdividing the actual domain into a finite number of small sub-domains, called elements. The displacements and stresses are approximated using polynomial shape functions for each element. Adjacent elements are connected with each other through nodes, and interaction between them is given by the forces they exert through the nodes. Element material properties and geometry are used to generate the stiffness matrix of the whole structure. The solution requires the known loads, boundary conditions, and stiffness matrix to solve for the unknown displacements. The displacements are then used to find elements results such as stress, strain and reactions etc.

In the present work FEA is applied to find the SCF for the intersection of sphere-nozzle and cylinder-nozzle (tee-joints) intersections for both undamaged and damaged components due to corrosion/erosion. A preliminary seismic fatigue study using FEA was also carried out for both geometries to see the effect of LTA in case of seismic events.

1.2 Outline

The purpose of this research is to analyse sphere-nozzle and cylinder-nozzle junctions with and without LTA under internal pressure and seismic loading. In this study, linear and non-linear FEA based on axisymmetric 2D ring and 3D solid elements is performed to predict the SCF and fatigue characteristics of undamaged and thinned intersections. The effect of the extent of thinning on the SCF is assessed through the analysis of specific intersections with varying degrees of thinning. A parametric study is conducted of intersections both in the undamaged and thinned states and results are presented in chart form. Finally a preliminary fatigue analysis is performed comparing the effects of cyclical load on undamaged and thinned intersections. The commercial software *ADINA AUI 8.3.3* is used to carry out linear (elastic) and non-linear (elastic-plastic) finite element analysis. The approach is first validated through comparing the results with published data. Similar material properties, boundary conditions, and loading are used for this purpose.

The study has the following objectives:

- To determine the relationship between SCF and main geometric parameters of vessel and nozzle: diameter ratio (d/D), thickness ratio (t/T) and vessel diameter to its thickness ratio (D/T).
- To demonstrate the validity of the FEA by comparing results with experimental, analytical, numerical, and empirical formulae results available in the literature.
- To determine the change in SCF with LTA of different depth and extent.
- To study the fatigue characteristics near the high stress zone (intersection) of both geometries.

The present work is divided into seven chapters; after the introduction of the research topics as presented in chapter 1, a brief literature review is presented on vessel-nozzle and cylinder-nozzle intersections in chapter 2. Then, in chapter 3, a theoretical background is presented on the finite element approach and the use of commercial FEA software *ADINA AUI 8.3.3* is explained. In chapters 4 and 5 the stress analysis of the sphere-nozzle and cylinder-nozzle intersections is discussed and results with and without

LTA are presented. In chapter 6, the fatigue analysis for selected models with and without damage for both geometries is presented. In chapter 7, conclusions and suggestions for further research are given. Finally in the appendix software instructions are given for the SCF and fatigue analysis of sphere-nozzle and cylinder-nozzle intersections.

CHAPTER 2: LITERATURE REVIEW

2.1 Introduction

For safe operation and long life of structures at high pressure and temperature in nuclear plants, oil refineries and chemical plants etc. an application of stress analysis and failure theory is required. Beyond consideration of safety and design life of these structures, fabrication costs, and severity of functional performance requirements pose demanding design problems. A good engineering design is one which can provide approximate functionality, high level of safety, long life of the structure, and cost effectiveness.

Pressure vessels should have the ability to cope with extremes in pressure, temperature, and hostile environments. Through the use of an efficient design of pressure vessels nuclear power can be harnessed, energy systems can be controlled and the chemical and oil industry processes can be operated at high efficiency. Special attention must be paid to intersection problems involving sphere-nozzle and cylinder-nozzle combinations. The analysis of pressure vessels and piping problems can be divided into the following categories:

1 Linear and non-linear, static and dynamic, stress and deflection analysis

2 Stability problems

3 Thermal problems

4 Fracture mechanics problems

5 Contact problems

6 Fluid – structure interaction problems

7 Welded pipes and pressure vessel components

8 Fatigue Problems

The present work falls in categories (1), (7) and (8) i.e. stress concentration studies, damage due to corrosion and fatigue problems.

2.2 Sphere-nozzle intersection

Since the 1960s extensive research has been carried out to determine the linear and non-linear behaviour of undamaged intersections under pressure loading. Several studies [1-6] have addressed the problems of vessel nozzle intersection using different techniques. Rose [2] in 1962 suggested that the stress concentration factor (SCF) obtained from an elastic analysis should be used as a design criterion. Many analytical studies have dealt with the SCF in sphere-nozzle intersections including the works of Leckie and Penny [3]. They analyzed the sphere-nozzle intersection with or without pad reinforcement for external loadings and for internal pressure. The graphical data depicted in BS 5500 Appendix G is based on their work. The analytical work has application though only to thin shells. Lind and Taylor [4-6] from 1965-1967 determined the elastic SCF by performing a semi-empirical analysis, to find an average deviation of only 7% in magnitude when compared with photo elastic test values.

With the increased power of the digital computer in the last three decades, numerical solutions for complete geometries have become more practical. In particular, the finite element analysis (FEA) has played an increasingly important role in the area of pressure vessel design. In fact, today most designers use the FEA, and much work has been carried out on discontinuity analysis of shell structures.

In 1984, Wood [7] demonstrated that by using thin shell elements with six degrees of freedom per node, where the geometry is defined by wall centre lines and wall thicknesses, the shape of the stress distributions agree with three-dimensional analysis, but their location was offset. He showed that the element selections for intersection problems are important, as well as that the maximum stresses were significantly overestimated. Then in 1989, work by Primm [8] showed that major obstacles can exist when analysing finite element models of shell intersections, due to the rapidly varying nonlinear through the thickness stress states and the presence of geometric discontinuities. Highlighting the effects of element density at the intersection region, they indicated that it is difficult to predict whether high density of lower-order elements gives a better performance than a lower density system of higher-order elements.

Attwater [9] in 1994 conducted a three-dimensional FEA study of practical spherical pressure vessels with radially disposed cylindrical nozzles subjected to internal pressure loading. Weiz and Rudolph [10] in 1995 used the FEA to examine the fatigue strength of nozzle to spherical shell intersections subjected to internal pressure, axial force, bending, and torsional moments. They used the axisymmetric element plane 82 (eight nodes, two degrees of freedom per node) of the ANSYS elements library in the case of axi-symmetric loads (internal pressure, axial force) and the corresponding harmonic element plane 83 for parameters of d/D = 0.02. . . 07, t/T = 0.2. . 1.2, T/D = 0.002 . . . 0.007. The results of the linear analyses were depicted in terms of SCF for the different loads (internal pressure, axial force, bending, and torsional moments). They showed that in the case of approximately equal wall thickness of both the nozzle and vessel, the influence of the vessel thickness-diameter ratio T/D on the maximum equivalent stress is minimal.

Dekker and Brink [11] in 2000 studied the stresses at nozzle-vessel junctions, by various analysis methods based on thin shell theory. Results were obtained for various ratios of the d/D parameter. They concluded that simple discontinuity analysis based on thin shell theory and the FEA analysis with plate/shell elements resulted in very much the same stresses. The spherical shell equations with their approximations even at the lower limit of their range behave in a stable manner. To model the junction of the nozzle with the spherical shell more accurately, and indeed to be able to introduce the possible beneficial influence of the weld, they devised a double discontinuity analysis of the nozzle/vessel junction under internal pressure. The double discontinuity analysis models the junction of the nozzle with the spherical shell far more accurately and gives results that do not much deviate from those given by the simple analysis methods. They showed that the double discontinuity analysis proved to be quite accurate when benchmarked against full 3D finite element analysis. In the case of thin nozzles, i.e. the nozzle wall thickness is less than the vessel wall thickness, the longitudinal bending stress in the nozzle will be over estimated by the above analysis, but they stated that the conservative deviation does not affect the maximum allowable internal pressure as the bending stresses do not control the maximum pressure.

Schindler [12] in 2003, conducted FEA analysis of a sphere-nozzle connection for fatigue behaviour. Results were plotted for circumferential stress, and stress components were found at critical points. Comparison was made with the SCF values of the British standard specification for unfired fusion welded pressure vessels. They observed a large variation in the results and suggested improvements related to cyclic fatigue calculations.

A number of finite element studies have been conducted on sphere-nozzle intersections [9, 12, and 13]. While finite element studies can give good results they require a lot of computational effort, and therefore simple formulae have been developed to predict the main elastic stress characteristics [6, and 19-23].

2.3 Cylinder-nozzle intersection (tee-joint)

There is a vast literature on analytical solutions for the state of stress in pressurized tee joints without wall thinning [13-14]. These analytical solutions though apply only to thin shells. A number of finite element studies have dealt with this geometry, including the works of Moini and Mitchell [15], Dekker and Stikvoort [16], Finlayson [17] and Diamantoudis and Kermanidis [18]. It has been established that three-dimensional elements are required to obtain accurate results for practical tee joints with a weld. Prior to the use of the FEA many researchers [19-24] sought to develop simple equations to predict the SCF in tee joints. In the various investigations it was concluded that the diameter and thickness ratios, as well as local characteristics at the junction, were primary factors affecting the SCF in tee joints.

Finlay [24] presented finite element data for 92 reinforced butt-welded branch outlet piping junctions designed according to the ASME B31.3 process piping code, for investigating their effectiveness in the light of data for an un-reinforced fabricated tee junction (UFT). All the analysis in this study was linear elastic. The concluded data suggested that the reinforcement provided under ASME B31.3 design was effective for the internal pressure loading and all external bending moment loads with the exception of branch out-of-plane bending for thin-walled assemblies.

2.3.1 Theoretical values for SCF for tees without wall thinning

Prior to the availability of powerful numerical capabilities a number of simple formulas were developed for the SCF in pressurized tees based on theoretical or experimental considerations. Subsequently, some simple formulas were developed based on statistical analysis of numerical results for tees determined using the FEA.

Lind [6], using the 'area method', developed the set of formulas

$$K_1 = \frac{[1+1.77(d/D)\sqrt{D/T}+(d/D)^2\sqrt{s/S}][1+(T/D)/\sqrt{s/S}]}{1+(d/D)^2/(s/S)\sqrt{s/S}}$$
$$K_2 = \frac{[1.67\sqrt{s/S}\sqrt{D/T}+0.565(d/D)][1+(T/D)/\sqrt{s/S}]}{0.67\sqrt{s/S}\sqrt{D/T}+0.565(d/D)/(s/S)} \qquad (2.1)$$
$$SCF = \max\{K_1, K_2\}$$

where s=d/(2t), S=D/(2T), and *t, d* are the thickness and the mean diameter of the nozzle.

Expressions for the SCF were given by Money [19], on the basis of experimental results for many tee joints. According to his work, SCF formulas valid for $r/R < 0.7$ and $r/R > 0.7$, respectively, are given by

$$SCF = 2.5\left[\left(\frac{r}{t}\right)^2\frac{T}{R}\right]^{0.2042} \quad \text{and} \quad SCF = 2.5\left[\left(\frac{r}{t}\right)^2\frac{T}{R}\right]^{0.24145} \qquad (2.2)$$

In these two relations *R* and *r* are the mean radii of the vessel and nozzle.

Decock [20], based on results from experimental data, and presented a formula for the SCF in terms of non-dimensional parameters as:

$$SCF = \frac{\left[2+2\frac{d}{D}\sqrt{\left(\frac{d}{D}\times\frac{t}{T}\right)}+1.25\frac{d}{D}\sqrt{\frac{D}{T}}\right]}{\left[1+\frac{t}{T}\sqrt{\left(\frac{d}{D}\times\frac{t}{T}\right)}\right]} \qquad (2.3)$$

This correlation equation was considered applicable in the determination of the SCF at the crotch corner in tee joints.

Moffat et al [21-22] have derived a formula for the effective stress factor (ESF) based on a parametric analysis of tees using three-dimensional FEA. The ESF is essentially equivalent to the SCF. The formula for the ESF is given by

$$EFS = [a_1 + a_2 (d/D) + a_3 (d/D)^2 + a_4 (d/D)^3] + [a_5 + a_6 (d/D) + a_7 (d/D)^2 + a_8 (d/D)^3] (t/T) + [a_9 + a_{10} (d/D) + a_{11} (d/D)^2 + a_{12} (d/D)^3] (D/T)^p + [a_{13} + a_{14} (d/D) + a_{15} (d/D)^2 + a_{16} (d/D)^3] (t/T) (d/T)^p \quad (2.4)$$

where p = 1.2, and the constants a_1 - a_{16} are given by; 2.5, 2.715, 8.125, -6.877, -0.5, -1.193, -5.416, 5.2, 0.0, 0.078, -0.195, 0.11, 0.0, -0.043, 0.152, -0.097.

Recently Gurumurthy [23], based on a shell theory FEA parametric study, developed a formula for the SCF. These authors observed that traditional design methodology for pressure reinforcement of openings in the pressure vessels is usually accomplished by utilizing the equivalent area replacement as specified in ASME Boiler & Pressure Vessel code. It was found that, in some cases, the stresses at the nozzle shell junction exceeded the allowable limits for stress, even though the code requirements of area replacement rules were met. A parametric study was carried out using the axisymmetric 2D FEA using (*FSTRIP* program) to arrive at a simplified formula for SCF under internal pressure loading. The formula was derived based on the data generated for maximum membrane stress intensity at the junction in terms of non-dimensional parameters as:

$$SCF = 1.75(T/t)^{0.4}(d/D)^{-0.08}(\lambda)^{0.6} \quad (2.5)$$

where $\lambda = d/(DT)^{1/2}$ is the pipe factor.

2.4 Local area thinning (LTA)

There is a need to perform Fitness-For-Service (FFS) analysis on components that have been in service for a number of years, and have developed structural defects over time. FFS are quantitative engineering evaluations that are performed to demonstrate the structural integrity of an in-service component containing a flaw or damage. One of these known flaws is LTA due to corrosion/erosion or excessive grinding of the weld. The ability to analyze the impact of structural defects on the overall behavior of pressure vessels is greatly enhanced due to rapid technological advancements. The availability of

FEA software has made it possible to analyze vessel shells and heads with LTA to determine its effect on structural integrity of the vessel and its suitability for continued service. The current study attempts to utilize the FEA to determine the SCF (K) of sphere-nozzle and cylinder-nozzle intersection subjected to inner wall thinning.

A series of papers have dealt with the wall thinning problem in the pressure vessels and piping field. Recently, interest has turned to the determination of the characteristics of such structures damaged by wall thinning. The aim is to determine the structural integrity of the damaged vessels and their suitability for the continued service. Recent studies on thinning and its structural effect on vessels include those of Netto et al [25] and Dooley and Chexal [26]. Shiratori et al [27] carried out a series of static elastic-plastic finite element analysis to investigate the failure behaviour of degraded pipe bends with local thinning subject to seismic loading.

Balan and Redekop [28] performed elastic-plastic finite element study to determine bi-directional loading on the fatigue characteristics of pressurized 90^0 piping elbow with LTA using *ADINA* finite element software. The comparisons were made for deformation patterns, hoop strain histories, and reaction forces. The same seismic wave as used in [28] was applied to both the sphere-nozzle and cylinder-nozzle intersection for the current cyclic fatigue analysis. There have been a number of numerical studies [25-28] on pipes and vessels with local thinned areas (LTA). Several studies have dealt with thinning in piping elbows [27-28].

Namita [29] presented a paper on a series of experiments performed by NUPEC on eroded piping components and piping systems. The objective of the study was to ascertain the seismic safety margins for eroded piping designed under current seismic design code in Japan and to clarify the elastic-plastic response and ultimate strength of eroded nuclear piping. It was determined that fatigue lives of piping components, such as elbow and tee, are about 1/5 of those of parent material, but enough longer than those of the design fatigue curve in the ASME Code. Ahmad et al [30] studied the tee-joint for SCF and burst pressure using 3D FEA. They found that LTA increase the SCF and decrease the burst pressure.

Hwang et al [31] have performed an experimental and numerical study seeking to identify the causes of shell wall thinning in a tee joint. There have been a number of studies on straight and curved pipes with wall thinning, including the works of Park et al [32] and Kim, Na, and Park et al [33]. Several studies have dealt with the effect of wall thinning on tee joints, including the works of Namita, Susuki, and Abe [34], Akahashi et al [35], and Ahmad [36]. The issue of fatigue of tees with thinning is significant, but so far studies have only been for undamaged intersections [38-40]. There is an extensive literature dealing with stress concentration of shell structures. Mackerle [41] in 2005 has published a survey of the research work on structural mechanics of pressure vessels and piping.

CHAPTER 3: FINITE ELEMENT ANALYSIS

3.1 Introduction

There are various techniques available for obtaining numerical solutions but the most popular and effective one is the finite element analysis (FEA). With the advancement of the digital computer in the last three decades, numerical solutions for complete geometries have become more practical. In particular, the FEA has an increasing role in the area of pressure vessel design. In fact, most designers are using this method, and much work has now been carried out on discontinuous shell structures.

In any analysis a mathematical model of a physical problem is selected and then FEA techniques are utilized to solve that model. The physical problem typically involves an actual structure or structural component subjected to certain loads. The idealization of the physical problem to a mathematical model requires certain assumptions that together lead to integral equations governing the mathematical model. The FEA solves this mathematical model.

In the FEA, a mathematical model is generated by subdividing the actual domain into a finite number of small sub-domains, called elements. The displacements and stresses are approximated using polynomial shape functions for each element. Adjacent elements are connected with each other through nodes, and interaction among them is given by the forces they exert through nodes only. Element material properties and geometry are used to generate the stiffness matrix of the whole structure. The solution requires the known loads, boundary conditions, and stiffness matrix to solve for the unknown displacements. The displacements are then used to find element results such as stress, strain and reactions etc. Since the finite element solution technique is a numerical procedure, it is necessary to assess the solution accuracy. If the accuracy criteria are not met, the numerical (i.e. finite element) solution has to be repeated with refined solution parameters (such as finer meshes) until a sufficient accuracy is reached.

The present work employs linear as well as non-linear static finite element analysis using *ADINA AUI 8.3.3* [42-43]. The background for this software is presented

by Bathe [44]. A general overview of static linear and non-linear finite element analysis as used by *ADINA* is presented in this chapter.

3.2 Static linear analysis

For the FEA of pressure vessels, commonly static linear analysis is used. In the static linear analysis, the problem is reduced to the solution of the matrix equilibrium equation.

$$KU = R \tag{3.1}$$

where K is the system stiffness matrix, U is the displacement vector, and R is the vector of applied forces.

In *ADINA*, a direct solution scheme or an iterative solution scheme is used. The equation solvers assume that the system stiffness matrix is symmetric and positive definite. This requirement can be summarized based on the assumption that the Rayleigh Quotient must be greater than zero for any displacement vector ϕ:

$$\rho(\phi) = \frac{\phi^T K \phi}{\phi^T \phi} \tag{3.2}$$

Since $\rho(\phi)$ is equal to twice the strain energy stored in the system for $\phi^T \phi = 1$, this is equivalent to the requirement that the strain energy stored in the finite element system when subjected to any displacement vector ϕ must be greater than zero. Hence, the finite element system must be properly supported, so that the system cannot undergo any rigid body displacements or rotations. It also follows that no part of the total finite element system nodal point degrees of freedom for which there is no stiffness must have been deleted. A degree of freedom does not carry any stiffness if none of the elements connected to the nodal point carry stiffness into that degree of freedom. In such a case, the degree of freedom must be deleted using any one of the boundary conditions.

3.3 Non-linear (elastic-plastic) analysis

In ADINA, generally the recommended most convenient incremental method for non-linear analysis is to use a reasonable number of load steps with the default iteration scheme (full Newton iteration method), with default tolerances and the automatic time stepping method. The algorithm of this method consists of the following two basic steps:

$$^{t+\Delta t}K^{(i-1)}\Delta U^{(i)} = {}^{t+\Delta t}R - {}^{t+\Delta t}F^{(i-1)} \tag{3.3}$$

$$^{t+\Delta t}U^{(i)} = {}^{t+\Delta t}U^{(i-1)} + \Delta U^{(i)} \tag{3.4}$$

where $^{t+\Delta t}K^{(i-1)}$ is the tangent stiffness matrix based on the solution calculated at the end of iteration $(i-1)$ at time $t+\Delta t$.

$^{t+\Delta t}F^{(i-1)}$ is the consistent nodal force vector corresponding to the element stresses due to the displacement vector $^{t+\Delta t}U^{(i-1)}$.

$\Delta U^{(i)}$ is the incremental displacement vector in iteration (i).

3.4 Selection of elements group

The FEA is the most popular numerical method used to check how the pressure vessels under design will behave in the real-life environment under specific working conditions. The quality of the idealised model, which is also known as the mesh model, directly affects the quality of the results. Despite the fact that designers have at their disposal a wide range of modern computer software for FEA, the preparation of the idealised model is still based mostly on user's experience and some rules of thumb.

The preparation of the mesh model is often the most time-consuming and costly part of undertaking the FEA. Many FEA pre-processors will automatically create the mesh like the one used in this study. However, the "automatic" pre-processors still require input data, such as type of the elements, density of the mesh, and position and type of boundary conditions to be applied. Selection of the adequate finite elements is strongly related with the meshing task. The use of an inadequate type of finite elements leads to poor quality of the results, which therefore cannot serve as a reliable basis for further design decisions.

In the present analysis using FEA code ADINA 8.3.3, 2-D solid axisymmetric elements were used for the analysis of sphere-nozzle intersections with nine nodes per element as per recommendation given in this code. The kinematic formulation for 2-D solid elements can be used with small displacement/small strain, large displacement/small strain or large displacement/large strain formulation. To find the

maximum stress values these options were set to default (small displacement/small strain) and for fatigue analysis large displacement and large strain were considered.

For the cylinder-nozzle intersection 3-D solid brick elements with 8-nodes per element were used. A 27-node element was also available, which could give a little more accuracy (less than 0.5%) than 8-nodes. Analysts have to compromise between analysis time and accuracy level to complete the parametric study. In the present case the duration for analysis was about three times less with 8-nodes than with 27-nodes per element.

3.5 Modeling of elastic material model

In ADINA, this model can be employed using the small displacement or large displacement formulations. The total stress is uniquely determined by the total strain but the strains are assumed small. When the elastic-isotropic and elastic-orthotropic materials are used with the small displacement formulation, the formulation is linear. If the material models are employed in a large displacement analysis, the Total Lagrangian (TL) or the Updated Lagrangian (UL) formulation is automatically selected by the program depending on which formulation is numerically more effective.

In the small displacement formulation, the stress-strain relationship is:

$$ {}_0^t\sigma = C_0^t e \tag{3.5} $$

where ${}_0^t\sigma$ is the engineering stress, C_0^t is the constitutive matrix, and ${}_0^t e$ is strain.

In the TL formulation, the stress-strain relationship is:

$$ {}_0^t S = C_0^t \varepsilon \tag{3.6} $$

where ${}_0^t S$ is the second Piola-Kirchhoff stress and ${}_0^t\varepsilon$ is the Green-Lagrange strain.

In the UL formulation, the stress-strain relationship is:

$$ {}^t\tau = C_0^t \varepsilon^a \tag{3.7} $$

where ${}^t\tau$ is the Cauchy stress and ${}_0^t\varepsilon^a$ the Almansi strains.

The same matrix C is employed in all of these formulations. As long as the strains are small (with large displacements), the difference in the response predictions

obtained with the TL and UL formulations is negligible. However, if the strains are large, the difference in the response predictions is very significant. The elastic-isotropic material model is available in ADINA for the various shell and solid elements used in this study.

CHAPTER 4: STRESS ANALYSIS OF SPHERE-NOZZLE INTERSECTION

4.1 The problem

The sphere-nozzle intersection (Fig. 4.1) is used in the pressure vessel and piping systems of chemical plants, refineries and power generation plants. These vessels often carry fluids under high temperatures and pressures. The extensive use of vessels for storage and industrial processing has provided motivation to develop better and cost effective design through analytical, numerical and experimental approaches. Since 1960s research has been carried out to determine the linear and non-linear behaviour of undamaged intersections under pressure loading. Recently, interest has turned to the determination of the characteristics of such structures damaged by local area wall thinning (LTA). The aim is to determine the structural integrity of damaged vessels and their suitability for continued service.

In this chapter a linear elastic finite element analysis (FEA) based on 2D solid axi-symetric ring elements is discussed to predict the stress concentration factor (SCF) in pressurized sphere-nozzle intersection without and with LTA. One aim of the study is to determine with maximum accuracy the SCF of the intersection using current FEA software. In a validation study it is shown that for undamaged intersections the results obtained using the current method show good agreement with experimental and other results given in the literature. The effect of the extent of the wall thinning damage on the SCF is assessed through the analysis of specific sphere-nozzle intersections with varying extents of wall thinning. Then, a parametric study is conducted covering sphere-nozzle intersections with a broad range of diameter and thickness ratios, and various depths of thinning. Finally, conclusions are drawn about the effect of LTA on SCF values.

4.2 Finite element modeling

The SCF is defined as the ratio of the maximum stress to the nominal stress. For internal pressure loading the nominal stress is calculated as $\sigma_n = pD/2T$, where p is the internal pressure, and T and D are respectively the thickness and mean diameter of the vessel. The maximum stress is variously defined as the largest normal stress, largest equivalent

stress (von Mises stress, used for current results), or largest Tresca stress. The value of SCF is a direct measure of the level of weakness at a location in the vessel because of stress concentration. The ASME Code, Section VIII, Division 2 uses the Tresca criterion as a framework for the design by analysis procedure as it is more conservative, and as it is considered easier to apply. The von Mises stress criterion is however considered better suited for the determination of the SCF for pressure vessels, since it deals with a continuous function. Thus in the current work the von Mises definition of the SCF is used. For the nominal stress, the value of the hoop stress in the sphere is taken.

The weld shape and quality affect the value of the SCF at the junction. A sharp corner at the intersection of the outer surfaces will lead to a mathematical singularity. In this analysis, to accommodate the effect of weld, a circular fillet is modeled at the outside of the junction. The radius of the fillet is taken as the larger of the thicknesses of either the sphere or nozzle.

The material chosen for the analysis was carbon steel (STS410) which corresponds to ASTM A106B and A333 Gr. The mechanical properties for this material are:

Young modulus	= 207GPa
Poisson's ratio	= 0.3
Initial yield strength	= 424 MPa
Strain hardening modulus	= 900MPa.

The analysis presented in this chapter is based on the assumption of axisymmety, and an internal pressure p is applied on the inner surface of the vessel. The magnitude of p is chosen to give a unit nominal stress in the sphere. Since the model is linear, the numerical value of the maximum stress (σ_{max}) at the junction is then the SCF. The nozzle is considered closed at the outlet, leading to a tensile stress σ_t at the top (Fig. 4.1). This axial tension is taken as $\sigma_t = pr_i^2/ (r_o^2 - r_i^2)$, where r_i and r_o are the internal and external radii of the nozzle.

In the present work the FEA code ADINA 8.3.3 [42] was used for the sphere-nozzle analysis. All models were constructed using 9-noded 2D axisymmetric (ring)

elements. In these elements each node has 2 translational degrees of freedom, giving eighteen degrees of freedom per element. For the SCF analysis a linear elastic material was assumed.

4.3 Convergence study

A convergence study was carried out in order to quantify the finite element error due to discretization. Two specific models were analyzed (Table 4.1). For the first model the geometry was defined by d=47mm, D=362mm, t=12mm, T=16mm, where d, D are the mean diameters of the nozzle and sphere, and t, T are the respective wall thicknesses. For the second model the geometry was defined by d=1890mm, D=5000mm, t=10mm, T=10mm. For both models results were obtained for five different mesh densities, as shown in Table 4.1. Steady convergence of the SCF is indicated, and for a mesh of density 16 (elements per unit length) the SCF value obtained differs only by 0.01% to 0.05% from the values obtained for a mesh of density 64. It must be kept in mind that numerical accuracy is achieved at the expense of increased computational cost. In view of these considerations a mesh of density 16 was selected for further work on the SCF. In Figure 4.2, a view of the vicinity of the junction of a sample mesh for an undamaged intersection is shown.

4.4 Validation study

A total of 32 models, as described in Table 4.2, were analyzed to validate the current process for the determination of the SCF. Results for these models were taken from six previous studies. The prior determination of the SCF was by means of analytical, experimental, and numerical methods.

Results for the SCF for models 1-4 were reported in 1965 by Lind [4]. These models have relatively low diameter ratios (d/D), and have relatively thick spheres. The experimental work was based on the photo-elastic technique. The current FEA results show good agreement with the experimental results, with a maximum difference of 5.7%. Models 5-7 were reported in 1967 by Lind [6]. He developed an empirical formula to find the maximum stress at the discontinuity of cylinder-cylinder and sphere-cylinder intersections based on the "area method" and photo-elastic results. The current FEA

results for these models are compared with the "area method" formula, and the maximum difference is found to be 11.9%. Models 8-17 contain relatively thin nozzle and sphere components. The SCF values were earlier determined by Leckie and Penny [3]. Their results are based on thin shell assumptions, and plots based on their work are available for the design of sphere-nozzle intersections in the BS 5500 Code. In their work, Leckie and Penny have referred to the experimental work of Taylor, Lind and Schweiker [1], and Rose [2]. Their work suggested that the maximum stress occurs in the sphere and not in the nozzle. Later experimental work completed by Taylor and Lind [5] indicated that as the thickness ratio (t/T) decreases, the maximum stress point moves from a position in the sphere at the outside surface to the inside base of the nozzle. The present FEA study has confirmed the fact that the maximum stress point is not necessarily always on the spherical side of the junction, but can be near the base of the nozzle (see Figs. 4.3-4.4).

In the present work it was observed that if the maximum stress remains on the spherical side of the junction (most of the cases when $t/T \geq 0.75$), then there is close agreement (within 5%) between the shell theory and the current FEA results. On the contrary when the maximum stress is at the base of the nozzle (most of the cases when $t/T \leq 0.5$), there is a large difference between the shell theory and the current FEA results (exceeding 40% in some cases for large diameter ratios).

For models 18-22 the sphere components are quite thin, and the nozzle thickness equals or exceeds that of the sphere. Numerical results for these models were reported earlier by Weisz and Rudolph [10]. These researchers also used the axisymmetric 2D finite element approach, and presented extensive charts for the SCF. The meshes used in their study generally contained fewer elements than those of the current study. The current FEA results are within 11% of the previous values, except for one case involving a large diameter ratio.

Models 23-28 were discussed earlier by Dekker and Brink [11]. These models all have a D/T ratio of 79, and a diameter ratio varying from 0.2 to 0.5. Results for the SCF for these models were given by Dekker and Brink [11] based on a single and double discontinuity analysis, as well as on a shell-theory and an axisymmetric 2D ring finite

element analysis. Agreement between the previous and the current FEA results is within 12%, except for one case.

Models 29-32 have d/D ratios of 0.35 or 0.4, and various thickness and diameter ratios. Results for the SCF for these models were given by Gurumurthy [23]. An empirical formula was developed by these authors, which was based on a parametric study of sphere-nozzle junctions, using the shell-theory finite element method. The formula is expected to give close agreement with the FEA work for the particular ranges of geometry used in their parametric study. Agreement between the formula values and the current FEA results is within 12%, except for one case.

In summarizing results, it should be noted that there were slight differences between the geometric models in the past and current studies. For eight of the thirty-two models of Table 4.2 the difference for the SCF between the previous and current results exceeded 20%, while in seventeen cases the difference was below 10%. For all of the eight cases involving large differences the previous results were based on shell-theory analysis. In five of these cases, the assumption that the maximum stress occurs in the sphere was implicit. Furthermore, shell theory results account only for membrane and bending stresses, not peak stresses. The smallest difference in results was obtained for the cases where the previous results stemmed from photo-elastic experimental work. It is concluded from this validation study that the current axisymmetric 2D FEA analysis gives reliable results, for the full range of geometries studied.

4.5 Parametric study

A parametric study was next conducted, using the linear axisymmetric (2D) FEA approach, covering a wide range of geometric parameters. The analysis served to extend the previously available plots for the SCF of sphere-nozzle intersections to cover cases with inner-wall thinning. In planning the parametric study (Tables 4.3-4.4) choices were first made for the main geometric parameters. Five thickness ratios were selected; t/T = 0.25, 0.5, 0.75, 1.0 and 1.25. The resulting range in the nozzle-sphere diameter ratio was $0.017 \leq d/D \leq 0.5$, and the range for the sphere diameter-thickness ratio was $18 \leq D/T \leq 555$.

To help define the parameters of the LTA, a preliminary study was first carried out to determine the sensitivity of the SCF on the size of the LTA. In the preliminary thinning study, the intention was to make a rational selection for the overall configuration of the LTA, and the axial extent of thinning in each component (Figs. 4.5-4.6). Three configurations of LTA were considered; (1) thinning in the nozzle only, (2) thinning in the sphere only, and (3) thinning in both the nozzle and sphere. Three axial lengths were also considered, giving a total of nine possible preliminary cases. The lengths were: L_c, $2L_c$, $3L_c$ (both in sphere and nozzle), where $L_c = 2.45\sqrt{rt}$, is the critical length of the nozzle given in the code at which discontinuity stresses become negligible. For the models of the preliminary LTA study the percentage thinning was set as 30%. This percentage was defined as $[(T_u-T_d)/T_u] \times 100\%$, where T_d is the reduced wall thickness after damage, and T_u is the original or undamaged wall thickness (Fig. 4.6). It is clear that the value represents the percentage reduction in the diagonal line AB of the cross-section at the junction. Four models, as described in Table 4.5, were analyzed for each of the nine possible cases of thinning. The SCF was determined in the preliminary thinning study also for the undamaged geometries. For all models, an axisymmetric thinning was assumed, reducing linearly in depth away from the junction.

The results for the preliminary LTA study are given in Table 4.5 for the three configurations, i.e. (1) LTA in the nozzle only (N), (2) LTA in the sphere only (S), and (3) LTA in both the nozzle and sphere (B). The results indicate that the effect of thinning on the SCF values for small d/D ratios (models 1-N, 1-S, and 1-B) is not severe. In a comparison between the three cases of thinning considered, it is seen that the configuration (3) experiences the most serious effect. The length of the LTA in the nozzle/sphere away from the junction is another important parameter affecting the SCF value. It is seen from Table 4.5 that an increase in the length of the LTA generally leads to an increase in the SCF. However, the percentage rise in SCF values is considerable only for one critical length (L_c). Beyond the length L_c, i.e. for lengths $2L_c$ and $3L_c$, the percentage rise in the SCF is comparatively low. In the light of the above observations, an axisymmetric thinning model comprising of the case (3) configuration (thinning in both components), and a thinning length of L_c in both components, was selected. This form of thinning was applied to all models of the main parametric study.

4.6 Results for SCF without and with wall thinning

In the main parametric study calculations were carried out for undamaged geometries, and for two sets of geometries with LTA. The damaged geometries had a wall thinning configuration as discussed in the previous section and two depths; 20% and 40%. Stress contour plots for model 3-S of Table 4.5 shown in Fig. 4.7, indicate an increase in stress level as the depth of LTA increases. The overall view (Fig. 4.7-a) shows the locations of maximum and minimum stress. Figure 4.7 (b-d) shows that the stress level at the inside and outside of sphere and nozzle near the junction increases with the size of LTA.

To define the main geometry of the parametric models (Table 4.3-4.4) there are three main parameters, *t/T*, *d/D* and *D/T*. The graphical representation of the SCF results in terms of three parameters however is difficult, as is explained in the studies [31-35]. Therefore a representation of the SCF results is given in terms of *t/T*, and a non-dimensional parameter ρ defined as: $\rho = (d/D)\,(D/2T)^{1/2} = r / (RT)^{1/2}$.

In Table 4.6, the results for the undamaged and damaged models are presented. In this table the percentage rise in SCF values due to 20% and 40% thinning at the intersection is compared with undamaged models. The percentage increase of SCF values with 20% LTA and 40% LTA is 2.6%-29.3% and 1.3%-79.5% respectively. For same t/T ratio the percentage rise in SCF values due to LTA increases as d/D ratio increases. For all t/T ratios a general trend is the increase in SCF values due to LTA and is more significant when d/D>0.2.The greatest increase was found when nozzle thickness is greater than the vessel's thickness i.e t/T>1.

Plots of the SCF against ρ are shown in Figs. 4.8-4.10, for five different thickness ratios. The first of these figures is for models without thinning, whereas the other two are for 20% and 40% thinning respectively. In Fig. 4.8 values from the BS 5500 Code (shell-theory results from the Leckie and Penny theory [3]) are compared with the current FEA values. It is seen that for thin nozzle cases ($t/T \leq 0.5$) the current FEA results are up to 40% greater than the code results. As noted in the preceding, for $t/T \leq 0.75$, the maximum stress may be in the nozzle, and this possibility is not provided for by BS 5500. However, for $t/T \geq 1$, the location of maximum stress remains on the

sphere side at the outside of the junction, and the difference in SCF value from the BS 5500 code is small.

Figures 4.9 and 4.10 give comparisons of the SCF for undamaged models with models having 20% and 40% thinning. Plots of the SCF versus ρ are given for five different thickness ratios in each figure. It is observed that an increase of the thinning percentage increases the SCF. The increase in the SCF value becomes larger with an increase in the ρ value. For $d/D \leq 0.04$, thinning does not lead to a significant change of the SCF value. For in-service pressure vessels which have LTA at the junction, the SCF-ρ curves of Figures 4.9-4.10 can help to find the increase in SCF due to thinning.

4.7 Conclusion

A two dimensions axisymmetric linear finite element analysis was carried out using FEA Code ADINA 8.3.3, to find SCF for sphere-nozzle intersection over a range of dimensional parameters like vessel, nozzle thickness and their mean diameters (T, t, d, and D). First SCF values were found for undamaged components and results were validated with the data available in the literature. A good agreement was found with the work of previous researchers along with new findings for the location of maximum stress. The study was then extended to simulate the damaged sphere-nozzle intersections. Important results were found for the change in SCF values arising from local area thinning. The results are presented in chart form for the convenience of designers.

CHAPTER 5: STRESS ANALYSIS OF CYLINDER-NOZZLE INTERSECTION (TEE-JOINT)

5.1 The problem

Carbon steel piping has been widely used in gas processing plants, oil refineries, chemical plants, and nuclear power plants. The vessel with attached nozzles, also known as two intersecting cylinders or tee-junctions (Fig. 5.1), is one of the principal components of piping and pipelines. Some of the examples of vessel with attached nozzles are heat exchangers, process columns, pressure vessels, fluid storage tanks, and the simplest of all is two intersecting pipes in any piping system. The aging of piping of nuclear power plants and refineries has raised concerns about the integrity and remaining functionality of existing piping and its components. Thus, an understanding of the behaviour of these types of structures is essential in modifying design rules and safety criteria.

In this chapter a linear elastic finite element analysis (FEA) based on three-dimensional (3D) solid elements is performed to predict the stress concentration factor (SCF) in pressurized tee joints without and with local wall thinning damage (LTA). One aim of the study is to determine with maximum accuracy the SCF of tee-joints using current FEA software. In a validation study it is shown that for undamaged tees the results obtained using the current method show good agreement with experimental and other results given in the literature. The effect of the extent of the wall thinning damage on the SCF is assessed through the analysis of specific tee-joints. Then, a parametric study is conducted covering tee joints with a broad range of diameter and thickness ratios, and various depths of thinning. Finally, conclusions are drawn about the effect of wall thinning damage on the stress state of tees.

5.2 Finite element modeling

The commercial package ADINA 8.3.3 [42-43] was used for the current numerical analysis. The elements available for three-dimensional analysis in this software include both hexahedral (brick) and tetrahedral elements, and both types were considered in the convergence-validation part of this study. The analysis was for a quarter tee model,

accounting for the symmetry that exists in a pressurized tee joint about the longitudinal YZ plane, and the transverse XZ plane (Fig. 5.1). The nodes on the planes of symmetry were constrained against motion in the direction perpendicular to the plane, as well as against out-of-plane rotations. The end of the vessel was subject to an axial pressure loading corresponding to closed end conditions. A similar pressure loading was applied in the axial direction on the nozzle.

In order to represent the presence of a weld, a fillet radius was inserted at the outer surface of junction of the two components (position C of Fig. 5.1-b). The size of the fillet was adjusted for each model to a value that would closely approximate the weld size used in industry for tee joints. A small rounding (about 2-3 mm radius) at the inner surfaces of the intersection (position A of Fig. 5.1-b) is provided to eliminate the sharp corner at the inside of the junction. A typical FEA mesh illustrating the outer fillet radius and inner rounding at the junction is shown in Figure 5.2.

The material considered in the analysis was carbon steel (STS410) which corresponds to ASTM A106B. The mechanical properties for this material are: Young's modulus = 210,000 MPa, Poisson's ratio = 0.3. A linear elastic analysis was carried out throughout in the tee SCF study.

5.3 Convergence study

A convergence study was carried out in order to describe the variation in FEA results due to mesh refinement. Three convergence models, C1, C2, and C3 were considered, covering tees of various diameter and thickness ratio. Geometric details of the models are given in Table 5.1. Some sample meshes from the convergence study for model C2 are given in Fig. 5.3.

Results were obtained for selected mesh densities for the three models as shown in Table 5.2. For model C1, meshes consisting of both 10-node tetrahedral and 8-node brick elements were used. With mesh refinement, convergence of the SCF is clearly observed for the series of models of both types of elements. The numerical stability in the analysis of models with tetrahedral elements was in general less than with brick elements. For models C2 and C3, meshes consisting only of 8-node brick elements were used. For both of these models, convergence is clearly observed as the mesh is refined. A set of

results using 27-node brick elements was also obtained, showing a difference of less than 0.05% relative to the results using 8-node brick elements. The increase in computational time and file size though was by a factor as large as 10. In consideration of these results, meshes consisting of 8-node brick elements, having density of about four elements over the run pipe thickness, were selected for further work in the study.

5.4 Validation study

Twelve models (V1-V12), as described in Table 5.1, were studied to validate the current FEA process for determining the SCF. Each of these models has been featured in a previous FEA or experimental study (a summary is given by Moffat et al [22]). For these models the ranges in the geometric parameters are as d/D: 0.09 to 1.00, t/T: 0.2 to 1.5, and D/T: 8.0 to 156. A comparison of the SCF results from the previous experimental and FEA studies and the current study (FEA) is given in the Table 5.1. The range in the differences of the current values from the previous ones is from –9.0% to +17.9%, with an average difference of +5.2%. A positive average difference was expected, in view of the better capability of the 3D FEA to predict stress peaks. In evaluating the results, it should be noted that there were inevitably slight geometric differences in the models of the past and current studies.

In Table 5.3 a comparison is given of the SCF results obtained by the approximate formulas of equations (2.1-2.5) and the current FEA approach. The previous experimental-numerical [3-4, 6, 19-23] values are repeated for convenience. For each of the approximate formulas and for the FEA, the minimum, maximum, and average differences relative to the reference values are stated. It is noted that the formula values relative to the reference value are significantly higher for model V7, and significantly lower for model V12.

The current FEA values agree much more closely with the reference values than do the formula values. The FEA is more independent of the range of geometric parameters, and can give dependable results provided there is correct usage of element type and mesh density, and accurate modeling of the domain, material, loading, and boundary conditions. For the present validation models, the Money [19] and Moffat et al [22] correlation equations (2.2) and (2.5) respectively, gave the most satisfactory results.

The formulas given by Lind [6] and Decock [20] generally gave conservative results. The Gurumurthy formula [23] gave results which were significantly conservative on the average, and which also showed a greater fluctuation than the other formulae.

In a further evaluation of the current approach, special attention will be given to a comparison of the current results with the results for the experimental models of Table 5.1. In Fig. 5.4, plots of the SCF versus the diameter ratio are presented for these experimental models. Generally there is good agreement between the two sets of results. Some differences though arise in the range d/D=0.3 to d/D=0.6, and these may partially be explained by limitations in the experimental procedures. Finite-length strain gauges used in experimental studies cannot exactly represent peak stresses in areas of high stress gradient. A reported maximum stress value may then be lower than that which actually occurs in the physical model. Using elements that are finite, the FEA also has this difficulty, but the difficulty can be controlled by refining the mesh or increasing the order of interpolation. Thus, it is considered that the current 3D FEA gives reliable predictions for the SCF over the full range of the geometries studied.

5.5 Parametric study

The American National Standards Institute (ANSI) assigns "schedule numbers" to classify wall thicknesses for different pressure. The ANSI schedule numbers cover all pipe sizes from NPS 1/8" through NPS 48" identified as Standard (STD), Extra Strong (XS) and Double Extra Strong (XXS). The wall thicknesses of the parametric models were considered according to ANSI B36.19-B36.10 schedule number [44], and a 10 inch nominal pipe size (NPS) was selected for the vessel or run pipe. For the nozzle, sizes varying from NPS ½", 1", 3", 6", to 8" are selected, to represent a range in the d/D ratio (Table 5.4).

A total of twenty models were selected for the parametric study, with geometric properties as given in Tables 5.4-5.5. In these tables the d and D represent the mean nozzle and pipe diameters respectively. The models are grouped together in four categories, based on the run pipe (vessel) schedule. Models 1-5 are according to schedule XXS, models 6-10 according to schedule XS, models 11-16 according to schedule S40S (STD), and models 16-20 according to schedule S10S (relatively thinnest). The ranges in

the geometric parameters were as follows; nozzle-vessel diameter ratio: $0.05 \leq d/D \leq 0.8$, nozzle-vessel thickness ratio: $0.2 \leq t/T \leq 1.0$ and vessel diameter-thickness ratio: $10.75 \leq D/T \leq 65.14$.

A study of the parametric tees in undamaged conditions was first carried out. Fig. 5.5 describes the spatial change in the von Mises stress level arising in a set of tees having solely a change in thickness of the run pipe and nozzle. In viewing Figs. 5.5 a-d in an increasing sequence, the effect on the von Mises stress of decreasing the thickness is observed. The high stress zone in the junction area consistently increases as the thickness decreases, with the highest stress occurring at the crotch corner in all four cases. In the axial directions of both the vessel and nozzle the region of high stress intensity steadily widens as the model thickness decreases.

In Table 5.6, a comparison of FEA values with empirical formulae (2.1-2.5) values for parametric models is given. On the average, the values from the formulae by Lind [6], Decock [3] and Moffat et al [21-22] show good agreement with FEA results, with few exceptions. Though the Moffat formula shows closest agreement for most of the parametric ratios, for large d/D (0.6, 0.8) and comparatively smaller t/T ratios the formula results are conservative. The Money [19] formula gives lower results for all parametric ratios. The Gurumurthy [23] formula gives lower results for $d/D<0.6$, but for $d/D>0.6$ the results are considerably higher than the FEA values. These formulae give a quick way to find SCF value for a tee-joint, but each formula is restricted in the valid range of parameters. The FEA results are independent of the geometry's parameters. If an analyst makes proper use of the FEA, the results can be more reliable.

To define the main geometry of a tee joint, three main parameters are required; t/T, d/D and D/T. Plots of the SCF versus the d/D ratio of the undamaged parametric models for different D/T ratio are shown in Fig. 5.6 for each of the four main groups. The t/T ratio is proportional to the d/D ratio as per dimensions given in the ANSI standard. The plots presented may be used to find the dimensions of both components (vessel and nozzle) corresponding to a certain admissible value of the SCF in the design of tee-joint. Conversely, the SCF values can be estimated for existing tee geometry.

5.6 Modeling of wall thinning

In modeling the wall thinning, the assumption was made that the damaged model would also satisfy two-ply symmetry, allowing consideration of ¼ of the structure. In the present study the wall thinning was assumed to be the result of depth corrosion from the inside, around the crotch position A. The original thickness along the diagonal line AC is represented as T_u, and the remaining thickness after corrosion by T_d (Fig. 5.7). The percentage thinning is then obtained as $[(T_u-T_d)/T_u]$ x 100%. A localized corrosion surrounding the junction was assumed, extending for a distance L_N into the nozzle, and L_V into the vessel (Fig. 5.7-b).

For the damaged nozzle, tapering of the thinning was assumed in the axial direction. The inner limiting surface of the removed material was modeled by a cone defined by a circle at the upper position and a spatial line along the junction surface. For the damaged run pipe, tapering of the thinning was assumed in both the axial and circumferential directions relative to the junction. The inner limiting surface of the removed material was modeled by a spatial surface which was described by a circle at the distant end of the pipe and an ellipse around the junction as shown in Fig. 5.8. In this figure part (a) and (b) showing the solid blocks that was removed from the nozzle and cylinder to produce required thinning respectively.

An effort was made to model the thinning so as to closely represent the expected industrial experience. It is expected that the extent (mid-surface distance) of thinning away from the junction for a small nozzle is less than for a large nozzle. As well, it is expected that the depth of thinning decreases with the distance away from the junction. Thus in this study, the depth of thinning is assumed to follow a linear taper away from the junction (Fig. 5.7) and the extent of the thinning area is taken as a function of the inside radius of the nozzle (Fig.5.9). A preliminary study was carried out to determine the sensitivity of the SCF on the extent of the wall thinning area. In this preliminary study, the intention was to determine the overall configuration of the wall thinning, i.e. the axial extent of thinning in each component (L_v and L_n of Fig. 5.7-b), and the circumferential extent in the vessel. As well, the difference in the results for tapered and uniform thinning was studied.

Four configurations of wall thinning were considered in detail; (1) tapered thinning to a distance from the junction in the components of r_i (inner radius of nozzle), (2) tapered thinning to a distance of $2r_i$, (3) tapered thinning to the end of the components (90^o circumferentially in the vessel), and (4) full depth thinning to the end of the components. For each of the configurations a maximum thinning of 30% was assumed at the junction. Results for the four damaged configurations are given in Table 5.7.

From these four LTA cases one was selected to apply for all parametric models. The last case (4) mentioned was not considered as it does not closely represent industrial experience, but was included only for comparative purposes. In case of full length tapered thinning, for all models (PT1-PT5) the SCF values are higher than for the case of undamaged components. However, configuration (3), full length tapered thinning, was not considered for the parametric study because this is an extreme case of thinning which is unlikely to occur in the working life of a tee.

For two cases of partial length tapered thinning (extent r_i and $2r_i$), the changes in SCF values with increasing extent is not always positive, rather the SCF values decrease with thinning for smaller d/D ratios (models PT1 and PT2). This indicates that for smaller d\D ratio, the stress level may fall with thinning of some extent. But a problem was experienced in drawing a specific rule for the extent of thinning at which stress level falls due to thinning. For models PT3-PT5 ($d/D \geq 0.3$) a monotonic increase in SCF values with extent of thinning was found. The configuration (1) was also not considered for parametric study because the thinning extent r_i for smaller d/D ratio (i.e for smaller nozzles) just gives a triangular prism cut out at the junction, leading to an unlikely kind of thinning. The configuration (2) with thinning extent $2r_i$ represents a more realistic thinning for all d/D ratios. Furthermore, the thinning extent $2r_i$ gave both a positive and negative change in the SCF values owing to the fact of damage in the structure. Based on these considerations, configuration (2), i.e. thinning to an extent of $2r_i$ was selected for further use in the parametric study.

5.7 Results for SCF without and with wall thinning

In the main thinning study results were determined for all twenty parametric models for three different conditions of the geometry; (1) undamaged, (2) 20% thinning, and (3)

40% thinning. For the latter two conditions the wall thinning extent was of the configuration (2) as discussed in the previous section. The results for parametric study are given in Table 5.8. In this table the SCF values for undamaged models and those with 20% and 40% LTA are presented. The percentage differences for SCF values of damaged models from undamaged ones are also given. As a general trend in this table the value of SCF increases with percentage LTA but for smaller diameter ratios and relatively thick models there can be a decrease in SCF value.

In Fig. 5.10 are shown the mesh and stress contour plot for parametric model 3 with 40% thinning. The enlarged view of the mesh clearly shows the thinning profile in the vessel and nozzle. The enlarged view of the contour plot shows the concentration of the von Mises stress on the inside surface at the crotch area of the tee. In Figs. 5.11-5.14, the intensity and distribution of the von Mises stress for tees of different diameters and schedules is shown for three different thinning percentages. As the thinning percentage is increased from 0%-40% the stress level at the junction and crotch corner increases, and the extent of high stress areas clearly shows a continuous spreading. But the inside curved surface of the run pipe (vessel) experiences a reduction in stress as the thinning percentage increases.

In studying these figures, one should keep in mind that each model has its own color scheme to present stresses level, i.e a particular color in the different models does not show same level of stress. In Fig. 5.15, stress contours are shown on the inside and outside surfaces of the parametric model 10 with 40% thinning. It is observed that the distribution and intensity of the von Mises stress is different for the inside and outside surfaces. The highest stresses are at the junction, for both the inside and outside surfaces, with the globally largest values lying on the inside surface. The overall maximum stress is again at the crotch corner (position A of Fig. 5.1b).

The change in SCF with d/D and D/T ratios are shown in Fig. 5.16. The figure is divided into four sections to indicate the changes in SCF values for the different pipe schedules as XXS, XS, STD and S10S (or D/T = 10.75, 21.50, 29.45 and 65.14). In this figure, a comparison of SCF values from thinner to thicker models for some particular value of the d/D ratio can be made for both undamaged and damaged components. The

first section of this figure (top left) shows that the effect of thinning is not significant for thicker models, especially when the d/D ratio is small. The other three sections show that as the models become thinner, i.e the D/T ratio increases, the effect of the LTA on the SCF values is more significant. All four sections of this figure indicate that the effect of LTA on the tee-joint's safe functioning is more severe for large diameter ratio and comparatively thinner models.

5.8 Conclusion

A three dimensional, linear finite element analysis was carried out using the FEA code ADINA 8.3.3 to find the SCF of cylinder-nozzle intersections. The FEA results for the SCF values were compared with empirical formulae, FEA, and experimental results available in the literature for undamaged components, and good agreement was found with few exceptions. The same parametric study was extended to simulate the damaged tee-joint having metal loss at the junction. To understand the level of risk with the size of thinning (or metal loss due to erosion and corrosion) at the intersection, the SCF values for undamaged intersections are compared with those having local area thinning. The results for undamaged and damaged tee-joints are compared in the charts provided. The thicker and thinner models show different levels of risk (after studying their SCF values) for certain levels of cylinder to nozzle diameter ratio. The effect of LTA on thicker models with small d/D ratio is not significant. The comparatively thin models with greater d/D ratio, experience a considerable percentage increase in SCF values due to LTA.

CHAPTER 6: SEISMIC FATIGUE ANALYSIS

6.1 Introduction

Corrosion is the primary means by which metals deteriorate. Metals corrode on contact with water or moisture in air, acids, bases, salts, oils, aggressive metal polishes, and other solid and liquid chemicals. Most of the pressure vessels and piping systems in nuclear power plant, petroleum, chemical and processing industries are made of steel which is the metal most likely to suffer from corrosion. Aged steel structures in industry can have defects such as stress corrosion cracking or local wall thinning. To maintain the nuclear power plants in safe conditions even in high amplitude and destructive earthquakes, it is necessary to study the dynamic behaviour of pressure vessels and piping. The study of dynamic behaviour then can be applied to estimate the safety margin of degraded pipes against seismic loading. Seismic safety is one of the major issues for nuclear power plant safety especially in geographic regions where earthquakes are most prevalent. In Canada, the greatest risk is known to be on the west coast.

Carbon steel pipe is widely used in power plants, and in the chemical and gas industries. Erosion/corrosion can occur in piping due to high-temperature, high pressure, and high speed water or vapour flow. The vessel-nozzle intersection in piping system experiences converging or diverging fluid flow. The corrosion/erosion effect or loss of material is most likely to occur at the sharpest edge or joint. It is important to clarify the dynamic response characteristics and seismic integrity of the locally thinned junctions of the aged structures. It is considered that the failure mode of piping system undergoing excessive seismic load is one of or combination of collapse, buckling and fatigue with ratchetting.

In this study, collapse of intersections, i.e. excessive progressive deformation due to cyclic loading, is determined. A series of finite element analysis (FEA) using ADINA 8.3.3 were performed. Information is provided on the following topics.

1) Elastic-plastic and failure response due to cyclic loading of pressurized vessel-nozzle junctions with metal loss/wall thinning near the junction,

2) The degree of reduction in strength due to thinning against cyclic loading of the vessel-nozzle junction,

3) The effect of d/D, t/T and D/T ratios on the cyclic response of the junction.

6.2 Literature review

A number of recent studies [34-35, and 37-40] have focused on the failure modes of ratchetting fatigue or collapse, seismic design margins against such failures, and allowable stress rules. These studies indicate that, according to current seismic design codes, nuclear piping possesses large safety margins, leading to streamlining of the piping design. But there are still some technical issues related to the understanding of piping behaviour with plasticity. The American Society of Mechanical Engineers (ASME) codes [45] and American Petroleum Institute (API 570 – Piping) Construction codes do not provide complete guidelines to evaluate a component containing a flaw or damage after initial commissioning. Fitness-For-Service (FFS) assessments are quantitative engineering evaluations that are performed to demonstrate the structural integrity of an in-service component containing a flaw or damage. API 579 was developed to evaluate flaws and damage associated with in-service operation. Several studies [27-40] have been conducted to determine seismic fatigue behaviour and the effect of local thinning area (LTA) in pipe cases.

A recent study by Shiratori et al [27] and then by Balan and Redekop [28] have provided detailed theoretical information about the fatigue characteristics of a carbon steel piping elbow with wall thinning subject to pressure and in plane bending due to seismic action. Yahiaoui, Moffat, Moreton, [40] performed a series of experimental works for the fatigue analysis of tee-joint with local thinning under the effect of internal pressure and simulated seismic loadings. The use of FEA in solving pressure vessel and piping problems has been reviewed by Mackerle [41].

The present chapter deals with the cyclic fatigue of sphere-nozzle junctions and tee-joints with LTA under the effect of pressure and simulated seismic loading. The primary objective is to determine the sensitivity of intersections, subjected to seismic fatigue action, to different sizes of LTA. The intention is not to define precisely the

fatigue life, but to attempt to compare the effect of different levels of LTA on the factors affecting fatigue life.

6.3 Methods and laws for fatigue analysis

Fatigue has been recognized as a major failure mode in pressure vessels and specific rules for its prevention appear in design codes. The fatigue process consists of crack initiation, crack propagation, and eventually fracture after a number of cycles. In many design situations expected number of cycles is in millions or infinity by setting the design within endurance limit. However, designing within the endurance limit is not the ultimate safe design because fatigue failure typical occurs at high stress zone. The high stress zones are due to abrupt change in geometry, temperature differential, and or residual stresses. Fatigue has been classified as of high and low cycle. To provide relevant data, a linear FEA approach can be used for the first method and a non-linear FEA approach for the second.

High cycle fatigue involves very little plastic action. Stress intensity-fatigue life is based on S-N curve provided in the ASME code [45]. In this method a linear analysis is needed to find peak stress or SCF.

The low cycle fatigue failure involves a few thousands cycles and involves strains in excess of yield strain. In this method a non-linear elastic plastic analysis is used, which identifies a plastic strain state that accounts for plastic action and ratcheting in the progressive failure that arises from cyclic action.

In order to estimate the low cycle fatigue lives with ratchet, there have been two approaches proposed, one is based upon the Miner's rule [46], and the other is based upon Asada's experimental formula [47]. In the present fatigue study using FEA, the same material properties are used as in references [27-28] and the low cycle fatigue can be characterized by Asada's Formula:

$$\Delta\varepsilon_t = 0.6158N_f^{-0.0746} + 89.08N_f^{-0.5414} \qquad (6.1)$$

where, $\Delta\varepsilon_t$ is the applied total strain amplitude and N_f is the number of cycles to failure at this amplitude. If the applied strain amplitude changes, the fatigue damage η is defined by $\eta = \Sigma N_i / N_{fi}$, where N_i and N_{fi} are the number of cycles actually applied and cycles

$\eta = \Sigma N_i / N_{fi}$, where N_i and N_{fi} are the number of cycles actually applied and cycles to failure, respectively. Then the Miner's rule is described such that the low cycle fatigue life can be estimated by taking $\eta = 1$.

Alternatively, from ADINA, the effective accumulative strain (elastic plus plastic) can be taken and thus for the multi-axial stress condition, the Coffin-Manson relation can be used in the following form:

$$\Delta\varepsilon^{t}_{eq} / 2 = \Delta\varepsilon^{e}_{eq} / 2 + \Delta\varepsilon^{p}_{eq} / 2 = \rho_f^{/} / E\,(2N_f)^{b} + \varepsilon^{/}_{f}(2N_f)^{c} \qquad (6.2)$$

where,

b, c, $\rho^{/}_{f}$ and $\varepsilon^{/}_{f}$ are Coffin-Mansion coefficients,

$\Delta\varepsilon^{t}_{eq} / 2$, total equivalent Von-Mises strain amplitude,

$\Delta\varepsilon^{e}_{eq} / 2$, elastic strain amplitude,

$\Delta\varepsilon^{p}_{eq} / 2$, plastic strain amplitude,

N_f, number of cycle to failure.

The Asada formula and Coffin-Manson Law can be used to determine the fatigue life to failure (N_f) from the total strain amplitude ($\Delta\varepsilon$). A detailed fatigue analysis of the intersections with and without LTA could be planned using either of the two methods mentioned.

6.4 Seismic fatigue analysis of sphere-nozzle intersection

The primary objective in this section is to determine the sensitivity of sphere-nozzle intersections, subjected to cyclic loading action, to different levels of LTA. The intention is not to define precisely the fatigue life, but to compare the effect of different levels of LTA on the factors affecting fatigue life, particularly the strain amplitudes. A non-linear elastic-plastic FEA analysis is carried out; using again the same material (STS410), the same element type, and the FEA Code ADINA 8.3.3 as considered in chapter 4.

In the SCF analysis of chapter 4, the internal pressure was the sole loading parameter. In the seismic fatigue analysis, a cyclical axial displacement of the nozzle tip is added, as described in the studies [27-28]. A total of 33 cycles was applied on the

nozzle in the vertical direction (z-axis). The loading was described in 1160 time steps, with an increment of 3mm displacement at each time step. Maximum amplitude of ± 35mm was taken as shown in Fig. 6.1. A total of four geometric seismic models were analyzed. All models had a diameter ratio of d/D=0.2, and a sphere diameter-thickness ratio of D/T=200. The models differed in the thickness ratios, which were taken respectively as t/T=0.5, 0.75, 1.0, 1.25 for the four cases. Each model was analyzed without thinning, and with 20% and 40% thinning.

Three responses to the seismic action are considered here, reaction range ΔR, cumulative effective plastic strain ε, and strain amplitude $\Delta\varepsilon$. The reaction was defined as the nodal axial force at a specific node at the tip of the nozzle, and the strain value and range were taken at the point having the maximum effective stress. The SCF values for internal pressure loading, as well as the results for the three responses for the pressure-seismic action analysis are given in Table 6.1. Sample hysteresis plots (node reaction-displacement plots for model SF-4) are shown in Figs. 6.2-6.4. In comparing the results of Table 6.1, it is clear that the range of reaction is significantly affected by the amount of the thinning, owing to the increase in flexibility at the sphere-nozzle junction. The cumulative effective plastic strain ε at the point of highest stress concentration near the junction decreases as the t/T ratio increases. With an increase of percentage thinning at the junction, for a specific geometry, the ε values increases. The trend in the strain amplitude $\Delta\varepsilon$ is the same.

The present seismic study gives an indication only of the effect of the wall thinning on the factors influencing fatigue life, so it remains for a further study to specify the difference of the effect of thinning on SCF and fatigue life. The present displacement cycle is of constant amplitude, but the approach presented can be applied to simulate actual dynamic cases of seismic loading, with varying amplitudes of displacement. This study could be a useful tool in the planning of a rational fatigue experimental plan, serving to save time and cost.

6.5 Seismic fatigue analysis of cylinder-nozzle intersection (tee-joint)

A three dimensional elastic-plastic finite element analysis has been carried out to study the effect of LTA on the factors affecting fatigue life of a pressurized tee-joint under seismic loading. All the models are loaded with 10 MPa inside pressure and a sinusoidal seismic load applied in vertical (z-axis) direction. A total of 33 cycles was applied on the nozzle in the vertical direction (z-axis). The loading was described in 1160 time steps, with an increment of 2.14mm displacement at each time step. Maximum amplitude of ± 25mm was taken.

The sensitivity of the intersections to such parameters like depth and extent of thinning are considered. A total of five (parametric models 11-15 of chapter 5) geometric seismic models were analyzed. All models are of schedule 40 (STD). Further the models are divided into three groups as undamaged, with 20% LTA, and 40% LTA respectively.

Three responses to the seismic action are considered here, reaction range ΔR, cumulative effective plastic strain ε, and strain amplitude $\Delta\varepsilon$. The reaction was defined as the nodal axial force at a specific node at the tip of the nozzle, and the strain value and range were taken at the point having the maximum effective stress. The SCF values for internal pressure loading, as well as the results for the three responses for the pressure-seismic loading analysis are given in Table 6.2. In comparing the results of this table, it is clear that the range of reaction is affected significantly by the amount of the thinning, owing to the increase in flexibility at the cylinder-nozzle junction. The cumulative effective plastic strain ε at the point of highest stress concentration near the junction decreases as the t/T ratio increases. With an increase of percentage thinning at the junction, for a specific geometry, the ε values increases. The trend in the strain amplitude $\Delta\varepsilon$ is the same.

Sample hysteresis plots representing the load variation with the prescribed displacement (node reaction-displacement plot for model TF-5) are shown in Figs. 6.5-6.7. The range of reaction force (Table 6.2) for all models considered are showing that the flexibility of the junction decreases as the size of the LTA increases. For model TF-5 with 20% and 40% thinning the values of SCF increased by 21.7% and 51% respectively

due to LTA. For the same model with 20% and 40% LTA, the reaction force decreased by 3.1% and 15.6% respectively, showing that flexibility is affected by size of LTA.

6.6 Conclusion

A series of non-linear elastic-plastic finite element analyses using the FEA code ADINA 8.3.3 was carried out to study the cyclic fatigue behaviour of pressurized sphere-nozzle and cylinder-nozzle intersections. Three responses, reaction range ΔR, cumulative effective plastic strain ε, and strain amplitude $\Delta\varepsilon$, were determined, and a comparison was made for these responses to study the effect of different sizes of LTA in the vicinity of the junction. The results indicate the damaging affect of LTA on the main factors affecting fatigue life of the two intersections.

CHAPTER 7: CONCLUSIONS

7.1 Sphere-nozzle intersection

The present study confirms that finite element analysis (FEA) based on axisymmetric 2D ring elements gives reliable results for stresses in pressurized sphere-nozzle intersections. To overcome the difficulty of a singularity, a smooth transition must be inserted in the geometric model at the outside surface of the junction between the two components. Such a transition approximates a fillet weld. It is clear that for non-symmetrical loadings, such as a moment on the nozzle, 3D solid elements must be used, increasing the computational time and data storage required. The effects of micro-structural notches due to welding defects are not considered in the FEA modeling, but adjustments can be made using factors available in engineering codes.

The parametric study in this work indicates that for $t/T \leq 0.75$, the stress concentration factor (SCF) values at or near the junction are 10% to 40% higher than those provided by the BS 5500 code (see Figure 4.8). The difference in the SCF values between the BS 5500 (shell theory) and the present FEA study is greater for smaller t/T ratios, and for larger d/D ratios. For such cases the highest stress is at the base of the nozzle, rather than in the sphere, as is assumed in the code. High peak stresses in the nozzle are expected when the nozzle is thin ($t/T \leq 0.5$) and the diameter to thickness ratio of the vessel is large ($D/T \geq 200$).

The results of this study indicate that inner wall thinning at the sphere-nozzle junction leads generally to a significant increase in the SCF. Quantitative information supporting this fact is provided in the Figs. 4.9-4.10. A preliminary seismic fatigue study indicates that thinning also produces a damaging effect on the factors influencing fatigue life. Further work is needed to provide more detailed information on this latter topic.

7.2 Cylinder-nozzle intersection

The present study shows that the 3-D FEA is a reliable technique for finding the SCF for pressurized tee joints. To overcome the difficulty of a mathematical singularity, and to accurately represent the weld area at the junction, a smooth transition (fillet radius) should be inserted at the intersection of the outer surfaces of the two components.

Formulating this three-dimensional surface is relatively simple using professional modeling software. It is observed that there is a systematic rise in the SCF values with an increase in the diameter ratio d/D, for a specified vessel diameter-thickness ratio D/T. It is also observed that for a specified d/D ratio, the SCF value increases as the D/T ratio increases. These two latter observations hold for tee joints without and with wall thinning damage.

Important results are found from the wall thinning study. In general, the value of the SCF increases as the wall thinning percentage increases (see Fig. 5.16). For relatively thick components having small d/D ratios (d/D<0.2), the effect of wall thinning is not significant. Instead, with an increase of wall thinning the SCF values may decrease, or increases very slightly. For relatively thin components having relatively large d/D ratios (d/D>0.3), the percentage increase in SCF is proportional to the extent of the wall thinning area. However, with an increase in depth and extent of thinning the components which were relatively thick experience less percentage rise in SCF than those which were relatively thinner. For tees, without and with wall thinning damage, the largest stress is always found at the crotch corner.

7.3 Suggestion for future study

Suggested future work includes further determination of low cyclic fatigue life of the tee joints and sphere-nozzle intersections without and with wall thinning damage. It is suggested that simulations should include non-uniform cyclic displacements (random, sinusoidal), to provide realistic information on the dynamic response of piping and pressure vessels structure to seismic events.

REFERENCES

[1] Taylor, C.E., Lind, N.C., Schweiker, J.W., 1959, "A Three-dimensional Photo-Elastic Study of Stresses around Reinforced Outlets in Pressure Vessels," WRC Bulletin 51.

[2] Rose, R.T., 1962, "A New Design for Pressure Vessel Nozzles," Engineer, London.

[3] Leckie, F.A., Penny, R.K., 1963, "Stress Concentration Factors for the Stresses at Nozzle Intersections in Pressure Vessels," WRC Bulletin 90, pp. 19-26.

[4] Lind, N.C., 1965, "A Rapid Method to Estimate the Elastic Stress Concentration of a Nozzle in a Spherical Pressure Vessel," Nucl. Struct. Eng., Vol. 2, pp. 159-168.

[5] Taylor, C.E., Lind, N.C., 1966, "A Photo-Elastic Study of the Stresses near the Opening in Pressure Vessels," WRC Bulletin 113.

[6] Lind, N.C., 1967, "Approximate Stress-Concentration Analysis for Pressurized Branch Pipe Connections," ASME Paper 67-WA/PVP-7, pp. 952-958.

[7] Wood, J., 1984, "Observations on Shell Intersections," 4th World Congr. Finite Element Methods, Interlaken, Switzerland.

[8] Primm, A. H., Stoneking, J. E., 1989, "Accuracy of the Finite Element Method for Pressure Vessel/Nozzle Design," ASME PVP-Vol. 175, pp. 3-9.

[9] Attwater, I.J.S., Anderson, J., Dindlay, G.E., 1994, "Three-dimensional Finite Element Analysis of Sphere/Cylinder Intersections under Axisymmetric Loading," Int. J. Pres. Ves. Piping, Vol. 57, pp. 231-235.

[10] Weisz, E., Rudolph, J., 1995, "Finite Element Analyses Concerning the Fatigue Strength of Nozzle-to-Spherical Shell Intersections," Int. J. Pres. Ves. Piping, Vol. 64, pp. 101-109.

[11] Dekker, C.J., Brink, H.J., 2000, "Nozzle on Sphere with Outward Weld Area under Internal Pressure Analyzed by FEM and Thin Shell Theory," Int. J. Pres. Ves. Piping, Vol. 77, pp. 399-415.

[12] Schindler, S., Zeman, J.L., 2003, "Stress Concentration Factors of Nozzle-Sphere Connections," Int. J. Pres. Ves. Piping, Vol. 80, pp. 87-95.

[13] Makaraci, M., 2005, "A Parametric Finite Element Geometric Analysis of a Pressurized Sphere with Cylindrical Flush Nozzle Outlet," J. Pres. Ves. Techn., Vol. 127, pp. 369-372.

[14] Xue, M.D., Chen, W., Hwang, K.C., 1995, "Stresses at the intersection of two cylindrical shells," Nucl. Eng. Des., Vol. 154, pp. 231-238.

[15] Moini, H., Mitchell, T.P., 1991, "Stress analysis of a thick-walled pressure vessel nozzle junction," Int. J. Pres. Ves. Piping, Vol. 46, pp. 67-74.

[16] Dekker, C.J., Stikvoort, W.J., 1997, "Pressure stress intensity at nozzles on cylindrical vessels a comparison of calculation methods," Int. J. Pres. Ves. Piping, Vol. 74, pp. 121-128.

[17] Finlayson, J.P., Rothwell, G., English R., Montgomery R.K., 2003, "Effective stress factors for reinforced butt-welded branch outlets subjected to internal pressure or external moment loads," Int. J. Pres. Ves. Piping, Vol. 80, pp. 311-331.

[18] Diamantoudis, A.T., Kermanidis, T., 2005, "Design by analysis versus design by formula of high strength steel pressure vessel a comparative study," Int. J. Pres. Ves. Piping, Vol. 82, pp. 43-50.

[19] Money, H.A., 1968, "Designing flush cylinder-to-cylinder intersections to withstand pressure," ASME PVP-17.

[20] Decock, J., "Reinforcement method of openings in cylindrical pressure vessels subjected to internal pressure," Report No. MT 104, Centre de Recherches

Scientifiques et Techniques de L'Industrie des Fabrications Metalliques.

[21] Moffat, D.G., Mwenifumbo, J.A.M., Xu, S.H., Mistry, J., 1991, "Effective stress factor for piping branch junction due to internal pressure and external moment loads," J. Strain Analysis, Vol. 26, pp 84-101.

[22] Moffat, D.G., Mistry, J., Moore S.E., 1999, "Effective stress factor correlation equations for piping branch junction under internal pressure loading," J. Press. Ves. Techn., Vol. 121, pp. 121-126.

[23] Gurumurthy, K., Jain, R., Salpekar, V.Y., 2001, "Simplified Formula for Stress Concentration Factor in Radial Nozzle Shell Junctions under Internal Pressure Loading," ASME PVP-Vol. 442, pp. 3-6.

[24] Finlay, J. P., Rothwell, G., English, R., and Montgomery, R. K., 2003, "Effective Stress Factors for Reinforced Butt-welded Branch Outlets Subjected to Internal Pressure or External Moment Loads," Int. J. Press. Ves. Piping, Vol. 80, pp. 311-331.

[25] Netto, T.A., Ferraz, U.S., Estefen, S.F., 2005, "The Effect of Corrosion Defects on the Burst Pressure of Pipelines," J. Const. Steel Res., Vol. 61, pp. 1185-1204.

[26] Dooley, R.B., Chexal, V.K., 2000, "Flow-Accelerated Corrosion of Pressure Vessels in Fossil Plants," Int. J. Pres. Ves. Piping, Vol. 77, pp. 85-90.

[27] Shiratori, M., Nakamura, I., Ochi, Y., Otani, A., 2002, "Failure Analysis of Thinned Wall Elbows under Excessive Seismic Loading," ASME PVP-Vol. 445-1, pp. 7-17.

[28] Balan, C., Redekop, D., 2005, "The Effect of Bi-directional Loading on Fatigue Assessment of Pressurized Piping Elbows with Local Thinned Areas," Int. J. Press. Ves. Piping, Vol. 82, pp. 235-242.

[29] Namita, Y., 2002, "Seismic Proving Test of Eroded Piping (Program and Preliminary Analysis of Eroded Piping Tests)," ASME PVP-Vol. 445-1, pp. 91-97.

[30] Ahmad, T., Khan, M.A., Redekop, D., 2007, "Pressurized Shell Intersections with Local Area Wall Thinning," Proc. SMiRT 19, Toronto, 8 pages.

[31] Hwang, K.M., Woo, L., Jin, T.E., Kim, K.H., 2008, "A Study on the Shell Wall Thinning Causes Identified through Experiment, Numerical Analysis and Ultrasonic Test of High-Pressure Feed Water Heater," Nucl. Eng. Des., Vol. 238, pp. 25-32.

[32] Park, J.H., Shin, K.I., Park, C.Y., Lee, S.H., 2007, "Allowable Local Thickness of Wall-Thinned Straight Pipes in ASME code case N-597-2," Int. J. Pres. Ves. Piping, doi:10.1016/j.ijpvp.2007.08.003.

[33] Kim, J.W., Na, M.G., Park, C.Y., 2008, "Effect of Local Wall Thinning on the Collapse behaviour of Pipe Elbows Subjected to a Combined Internal Pressure and In-Plane Bending Load," Nucl. Eng. Des., doi:10.1016/j.ijpvp.2007.10.017.

[34] Namita, Y., Suzuki, K., Abe, H., 2003, "Seismic proving Test of Eroded Piping," Trans SMiRT17, Prague, Paper K15-3, PP. 1-8.

[35] Akahashi, K., Kato, A., Ando, K., Hisasune, M., Hasegawa, K., 2007, "Fracture and Deformation Behaviors of Tee Pipe With Local Wall Thinning," Nucl. Eng. Des., Vol. 237, pp. 137-142.

[36] Ahmad, T., 2006, "Finite Element Stress and Collapse Analysis of a Pressurised Vessel-Nozzle Intersection with Locally Thinned Area," M. Eng. Report, U. of Ottawa, Canada.

[37] Kim, T., Moon, C., Kim, B., 2007, "Development of the Three-dimensional Fatigue Analysis Procedure for Major Components of the New Advanced Power Reactor," Trans. SMiRT 19, Toronto, August 2007, Paper S02/3, 6 pages.

[38] Giglio, M., 2003, "Fatigue Analysis of Different Types of Pressure Vessel Nozzle," Int. J. Pres.Ves. Piping, Vol. 80, pp. 1-8.

[39] Weisz, E., Rauth, M., Rudolph, J., 1998, "Fatigue Behaviour of Oblique Nozzles on Cylindrical Shells Submitted to Internal Pressure and Axial Forces," Int. J. Press. Ves. Piping, Vol. 75, pp. 473-481.

[40] Yahiaoui, K., Moffat, D.G., Moreton, D.N., 1995, "Cumulative Damage Assessment of Pressurized Piping Branch Junctions Under In-Plane Run Pipe Simulated Seismic Bending," Int. J. Pres. Ves. Piping, Vol. 63, pp. 119-128.

[41] Mackerle, J., 2005, "Finite Elements in the Analysis of Pressure Vessels and Piping," Addendum: A Bibliography (2001-2004)," Int. J. Pres. Ves. Piping, Vol. 82, pp. 571-592.

[42] ADINA AUI 8.3.3 - User Interface Primer and AUI Command Reference Manual, ADINA R & D Inc., Watertown, M.A., 2003.

[43] Bathe, K. J., 1996, "Finite Element Procedures," Prentice Hall, New Jersey, USA.

[44] ASME/ANSI B36.10/19 (Carbon, Alloy and Stainless Steel Pipes).

[45] ASME Boiler & Pressure Vessel Code, Section VIII, Division 1-3.

[46] Miner, M.A., 1945, "Cumulative Damage in Fatigue," J. Appl. Mech., Vol. 12, A-159.

[47] Asada, Y., "Fatigue Criterion on Low-Cycle Fatigue with Excessive Progressive Deformation," Proceeding of Third German-Japanese Joint Seminar, 2.2, pp. 3-11.

BIBLIOGRAPHY

[1] Biron, A., Courchesne, A., 1976, "On Limit Analysis of Cylinder-Cylinder Intersections Subjected to Internal Pressure," Nucl. Eng. Des., Vol. 36, pp. 68-80.

[2] Ellenberger, J. P., Chuse, R., Carson, B. E., 2004, "Pressure Vessels – ASME Code Simplified," McGraw-Hill Companies, Inc., New York, USA.

[3] Ellyin, F., Turkkan, N., 1971, "Lower Bound to Limit Pressure of Nozzle-to-Cylindrical Shell Attachment," ASME Paper 71, PVP-38.

[4] Gill, S. S., 1970, "The Stress Analysis of Pressure Vessels and Pressure Vessel Components," Pergamon Press, Oxford, UK.

[5] Kutz, M., 1998, "Mechanical Engineer's Handbook," John Wiley & Sons, Inc., New York, USA.

[6] Lekkerkerker, J. G., 1972, "The Determination of Elastic Stresses Near Cylinder-to-Cylinder Intersections," Nucl. Eng. Des., Vol. 20, pp. 57-84.

[7] Lynch, M. A., Moffat, D. G., Moreton, D. N., 2000, Limit Loads for Cracked Piping Branch Junctions under Pressure and Branch Out-of-Plane Bending," Int. J. Pres. Ves. Piping, Vol. 77, pp. 185-194.

[8] Nichols, R.W., 1977, "Development in Stress Analysis for Pressurized Components," Applied Science Publishers Ltd., London, UK.

[9] Weiss, E., and Joost, H., 1997, "Local and Global Flexibility of Nozzle-to-Vessel Intersection under Local as Boundary Conditions for Piping System Design," Int. J. Pres. Ves. Piping, Vol. 73, pp. 241-247.

[10] Wheat, S., Jandu, C. S., Bramley, D. N., and Liu, J. H., 2002, "Fitness-for-Purpose Assessment of Encirclement Split Tees," ASME PVP, Vol. 442, pp. 23-30.

[11] Williams, D. K., Clark, J. R., 1996, "Development of Flexibility Factors for Fabricated Tee Branch Connections," ASME PVP, Vol. 331, pp. 55-64.

[12] Xue, M. D., Hwang, K. C., Lu, W., and Chen, W., 1996, "A Reinforcement Design Method Based on Analysis of Large Openings in Cylindrical Pressure Vessels," ASME PVP, Vol. 2, pp. 197-205.

[13] Mackerle, J., 1996, "Finite Elements in the Analysis of Pressure Vessels and Piping, A Bibliography, 1976–1996," Int. J. Pres. Ves. Piping, Vol. 69, pp. 279-339.

[14] Mackerle, J., 1999, "Finite Elements in the Analysis of Pressure Vessels and Piping, An Addendum, 1996 – 1998," Int. J. Pres. Ves. Piping, Vol. 76, pp. 461-485.

[15] Mackerle, J., 2002, "Finite Elements in the Analysis of Pressure Vessels and Piping, A Bibliography 1998 – 2001," Int. J. Pres. Ves. Piping, Vol. 79, pp. 1-26.

[16] Van Dyke, P., 1965, "Stresses About a Circular Hole in a Cylindrical Shell," AIAA Journal, Vol. 9, pp. 1733-1742.

[17] Eringen, A. C., and Suhubi, E. S., 1965, "Stress Distribution at Two Normally Intersecting Cylindrical Shells," Nucl. Eng. Des., Vol. 2, pp. 253-270.

[18] Dyke, P. V., 1967, "Stresses in a Cylindrical Shell with a Rigid Inclusion," AIAA Journal, Vol. 5, pp. 125-137.

[19] Steel, C. R., and Steele, M. L., 1983, "Stress Analysis of Nozzle in Cylindrical Vessels with External Load," Int. J. Pres. Ves. Piping, Vol. 105, pp. 191-200.

[20] Xue, M. D., Chen, W., and Hwang, K. C., 1995, "Stresses at the Intersection of Two Cylindrical Shells," Nucl. Eng. Des., Vol. 154, pp. 231-238.

[21] Xue, M. D., Li, D. F., and Hwang, K. C., 2005, "A Thin Shell Theoretical Solution for Two Intersecting Cylindrical Shells due to External Branch Pipe Moment," Int. J. Pres. Ves. Piping, Vol. 127, pp. 357-368.

[22] Goodell, R. A., 1974, "An Analytical and Experimental Investigation of A Nozzle-to-Cylindrical Shell Junction," Published under Contract No. AT (10-1)-1375, U.S. Atomic Energy Commission, Idaho.

[23] Lock, J. D., Carmichael, G. D. T., and Moffat, D. G., 1985, "Finite Element Stress Analysis of an Equal Diameter Branch Pipe Intersection Subjected to Internal Pressure and In-Plane Moment Loading," Pipe Works Design and Operation, Institute of Mechanical Engineers, London.

[24] Kirkwood, M. G., Carmichael, G. D. T., Moffat, D. G., 1986, "Finite Element Stress Analysis of an Equal Diameter Branch Pipe Intersection Subjected to Out-of-Plane and Twisting Moments," Journal of Strain Analysis, Vol. 21, No. 1, pp. 9-16.

[25] Natarajan, R., Widera, G. E. O., Afshari, P., 1987, "A Finite Element Model to Analyze Cylinder-Cylinder Intersections," Int. J. Pres. Ves. Piping, Vol. 109, pp 411-420.

[26] Bryson, J. W., Johnson, W. G., Bass, B. R., 1977, "Stresses in Reinforced Nozzle-Cylinder Attachments Under Internal Pressure Loading Analysed by the Finite Element Method," A Parametric Study, Oak Ridge National Laboratory Reprint No. ORNL/NUREG-4.

[27] Berak, E. G., Gerdeen, J. C., 1990, "A Finite Element Technique for Limit Analysis of Structure," Int. J. Pres. Ves. Piping, Vol. 112, pp 138-144.

[28] Antaki, George, A., 2003, "Piping and Pipeline Engineering–Design, Construction, Maintenance, Integrity, and Repair, Marcel Dekker Inc., New York, USA.

[29] Rodabaugh, E. C., 1998, "A Review of Area Replacement Rules for Pipe Connection in Pressure Vessels and Piping," Welding Research Council Bulletin 335, Pressure Vessel Research Council, New York.

PUBLICATIONS ARISING FROM THIS STUDY

[1] Qadir, M., Redekop, D., 2008, "SCF and Fatigue Analysis of Sphere-Nozzle Intersection with LTA," Proceedings of ASME Pressure Vessels and Piping Division Conference PVP2008-61176, July 27-31, 2008, Chicago, Illinois, USA.

[2] Ahmad, T., Qadir, M., Redekop, D., 2008, "FEM Stress and Fatigue Analysis of Tee Intersection with LTA," Proceedings of ASME Pressure Vessels and Piping Division Conference PVP2008-61177, July 27-31, 2008, Chicago, Illinois, USA.

[3] Qadir, M., Redekop, D., "SCF Analysis of a Pressurized Vessel-Nozzle Intersection with Wall Thinning Damage," (Submitted to Int. J. Pres. Ves. Piping).

TABLES

Table 4.1 Convergence study of sphere-nozzle intersection

Model	Elements per unit length	No. of nodes	No. of elements	SCF (K)
1	4	1637	352	2.003
	8	5861	1351	2.006
	16	22.7k	5456	2.007
	32	88.7k	21.7k	2.008
	64	355k	87.3k	2.008
2	4	38.0k	8450	8.425
	8	144k	33.8k	8.521
	16	557k	135k	8.592
	32	2,117k	527k	8.593
	64	8,253k	2,112k	8.593

Table 4.2 Validation study of sphere-nozzle intersection

Model #	d/D	D/T	t/T	SCF from reference		FEA value	% Difference
				Ref.	Value		
1	0.13	23.9	0.26	[4]	2.12	2.24	5.7
2	0.13	23.9	0.26		3.24	3.34	3.1
3	0.39	23.9	0.78		4.08	3.95	-3.2
4	0.13	23.9	0.26		2.78	2.75	-1.1
5	0.5	23.9	0.67	[6]	5.04	5.18	2.8
6	0.41	23.9	0.89		4.14	3.81	-8
7	0.4	19.7	0.33		4.2	4.7	11.9
8	0.15	160	0.7	[3]	3.3	4.6	39.4
9	0.15	133	0.5		3.4	4.3	26.5
10	0.15	160	0.7		3.2	3.78	18.1
11	0.15	200	0.49		4	5.5	37.5
12	0.39	79	1		4.4	4.42	0.5
13	0.45	79	1		4.75	4.88	2.7
14	0.2	79	1		2.7	2.84	5.2
15	0.39	79	0.5		5.4	7.83	45
16	0.3	79	0.5		4.9	6	22.4
17	0.5	79	0.5		6.4	8.9	39.1
18	0.02	317	1.2	[10]	2.25	2.08	-7.6
19	0.06	385	1.2		2.3	2.23	-3
20	0.38	500	1		7.9	8.59	8.7
21	0.51	500	1		9.2	10.2	10.9
22	0.63	500	1		9.5	11.2	17.9
23	0.39	79	1	[11]	4.2	4.42	5.2
24	0.39	79	0.5		8.82	7.83	-11.2
25	0.45	79	1		4.42	4.88	10.4
26	0.3	79	0.5		7.53	6	-20.3
27	0.5	79	0.5		9.71	8.9	-8.3
28	0.2	79	1		2.88	2.84	-1.4
29	0.35	19.7	0.25	[23]	4.3	4.8	11.6
30	0.4	85.7	0.2		7.8	11.5	47.4
31	0.35	133	0.5		5.7	6	5.3
32	0.4	50	0.2		6.6	6.7	1.5

Table 4.3 Dimensions of the parametric models without LTA

Model #	d_i	d_o	D_i	D_o	t	T	Fillet radius	ρ/T	s/S
1	0.05	0.08	2	2.13	0.02	0.06	0.06	1	0.2
2	0.06	0.08	1.5	1.56	0.01	0.03	0.03	1	0.32
3	0.24	0.25	2	2.03	0	0.01	0.01	1	0.96
4	0.8	0.81	4	4.04	0.01	0.02	0.02	1	1.6
5	2	2.02	7.41	7.47	0.01	0.03	0.03	1	2.16
6	0.8	0.81	2	2.04	0.005	0.02	0.02	1	3.2
7	1.5	1.51	3	3.03	0	0.02	0.02	1	4
8	0.05	0.22	3	3.33	0.08	0.17	0.17	1	0.07
9	0.06	0.08	3	3.03	0.01	0.02	0.02	1	0.08
10	0.24	0.25	2	2.03	0.01	0.01	0.01	1	0.48
11	0.8	0.82	4	4.04	0.01	0.02	0.02	1	0.8
12	2	2.03	7.41	7.47	0.02	0.03	0.03	1	1.08
13	3	3.02	10	10.04	0.01	0.02	0.02	1	1.2
14	3	3.04	7	7.08	0.02	0.04	0.04	1	1.71
15	2	2.1	4	4.2	0.05	0.1	0.1	1	2
16	0.06	0.08	3	3.03	0.01	0.02	0.02	1	0.05
17	0.12	0.15	1.6	1.64	0.01	0.02	0.02	1	0.2
18	0.24	0.26	2	2.03	0.01	0.01	0.01	1	0.32
19	0.8	0.83	4	4.04	0.02	0.02	0.02	1	0.53
20	2	2.05	7.41	7.47	0.02	0.03	0.03	1	0.72
21	3	3.03	10	10.04	0.01	0.02	0.02	1	0.8
22	3	3.04	7.5	7.56	0.02	0.03	0.03	1	1.07
23	3	3.05	6	6.06	0.02	0.03	0.03	1	1.33
24	0.06	0.09	3	3.03	0.02	0.02	0.02	1	0.04
25	0.12	0.15	2	2.03	0.01	0.01	0.01	1	0.12
26	0.24	0.27	2	2.03	0.01	0.01	0.01	1	0.24
27	0.8	0.84	4	4.04	0.02	0.02	0.02	1	0.4
28	2	2.06	7.41	7.47	0.03	0.03	0.03	1	0.54
29	3	3.04	10	10.04	0.02	0.02	0.02	1	0.6
30	1.6	1.63	4	4.03	0.01	0.01	0.01	1	0.8
31	3	3.06	6	6.06	0.03	0.03	0.03	1	1
32	0.06	0.1	3	3.03	0.02	0.02	0.02	1	0.03
33	0.12	0.16	2	2.03	0.02	0.01	0.01	1	0.1
34	0.24	0.28	2	2.03	0.02	0.01	0.01	1	0.19
35	0.8	0.85	4	4.04	0.03	0.02	0.02	1	0.32
36	2	2.08	7.41	7.47	0.04	0.03	0.03	1	0.43
37	3	3.05	10	10.04	0.02	0.02	0.02	1	0.48
38	0.8	0.85	2	2.04	0.03	0.02	0.02	1	0.64
39	3	3.06	6	6.05	0.03	0.02	0.02	1	0.8

Table 4.4 Parametric study for sphere-nozzle intersection without LTA

Model #	t/T	d/D	D/T	ρ	K Ref. BS-5500	K FEA	% difference
1	0.25	0.03	32.00	0.10	1.80	2.33	22.9
2	0.25	0.04	50.00	0.20	2.10	2.34	10.4
3	0.25	0.12	138.89	1.00	4.20	4.41	4.7
4	0.25	0.20	200.00	2.00	6.50	10.01	35.1
5	0.25	0.27	246.90	3.00	8.50	14.09	39.7
6	0.25	0.40	100.00	2.83	8.25	10.91	24.4
7	0.25	0.50	200.00	5.00	11.90	19.03	37.5
8	0.50	0.02	18.07	0.05	1.75	2.78	37.1
9	0.50	0.02	200.00	0.20	1.90	2.30	17.5
10	0.50	0.12	138.89	1.00	3.10	2.87	-7.9
11	0.50	0.20	200.00	2.00	5.00	5.91	15.3
12	0.50	0.27	246.90	3.00	6.40	8.90	28.1
13	0.50	0.30	555.56	5.00	8.70	15.95	45.5
14	0.50	0.43	175.00	4.01	7.60	10.62	28.4
15	0.50	0.50	40.00	2.24	5.25	5.18	-1.4
16	0.75	0.02	200.00	0.20	1.90	2.27	16.2
17	0.75	0.08	88.89	0.50	1.95	2.16	9.6
18	0.75	0.12	138.89	1.00	2.80	2.33	-20.2
19	0.75	0.20	200.00	2.00	4.50	3.99	-12.9
20	0.75	0.27	246.90	3.00	5.60	5.85	4.3
21	0.75	0.30	555.56	5.00	7.50	10.18	26.3
22	0.75	0.40	253.38	4.50	7.30	8.24	11.4
23	0.75	0.50	200.00	5.00	7.60	8.57	11.3
24	1.00	0.02	200.00	0.20	1.80	2.20	18.1
25	1.00	0.06	138.89	0.50	1.95	2.11	7.4
26	1.00	0.12	138.89	1.00	2.30	2.27	-1.5
27	1.00	0.20	200.00	2.00	3.75	3.59	-4.6
28	1.00	0.27	246.90	3.00	4.95	4.87	-1.7
29	1.00	0.30	555.56	5.00	6.85	7.73	11.4
30	1.00	0.40	312.50	5.00	6.90	7.11	2.9
31	1.00	0.50	200.00	5.00	6.80	6.55	-3.8
32	1.25	0.02	200.00	0.20	N.A	3.28	N.A
33	1.25	0.06	138.89	0.50		2.03	
34	1.25	0.12	138.89	1.00		2.18	
35	1.25	0.20	200.00	2.00		3.48	
36	1.25	0.27	246.90	3.00		4.73	
37	1.25	0.30	555.56	5.00		6.76	
38	1.25	0.40	100.00	2.83		4.00	
39	1.25	0.50	241.94	5.50		10.78	

Table 4.5 Preliminary LTA study of sphere-nozzle intersection

Model #	d/D	t/T	SCF			
			Meridional length of LTA			
			0	L_c	$2L_c$	$3L_c$
Thinning in nozzle only						
1-N	0.02	0.50	2.30	2.19	2.27	2.27
2-N	0.30	0.75	10.18	15.09	15.68	15.63
3-N	0.30	1.00	7.72	11.50	11.48	11.47
4-N	0.43	1.25	10.78	12.00	12.06	12.08
Thinning in sphere only						
1-S	0.02	0.50	2.30	2.42	2.52	2.53
2-S	0.30	0.75	10.18	11.80	12.30	12.56
3-S	0.30	1.00	7.72	11.19	10.06	10.19
4-S	0.43	1.25	10.78	15.3	15.28	15.26
Thinning in nozzle and sphere						
1-B	0.02	0.50	2.30	2.41	2.47	2.47
2-B	0.30	0.75	10.18	15.95	16.48	16.65
3-B	0.30	1.00	7.72	10.79	11.09	11.18
4-B	0.43	1.25	10.78	15.60	15.80	15.86

Table 4.6 Parametric study for sphere-nozzle intersection with LTA

Model No.	d/D	ρ	t/T	SCF Value With Thinning Length = Lc				
				Depth of thinning (0%)	Depth of thinning (20%)	Depth of thinning (40%)	% differ. with 20% thinning	% differ. with 40% thinning
1	0.03	0.10	0.25	2.33	2.75	2.64	17.7	13.0
2	0.04	0.20	0.25	2.34	2.48	2.45	5.8	4.7
3	0.12	1.00	0.25	4.41	5.06	5.45	14.9	23.6
4	0.20	2.00	0.25	10.01	10.68	12.68	6.7	26.7
5	0.27	3.00	0.25	14.09	14.55	18.55	3.3	31.7
6	0.40	2.83	0.25	10.91	12.70	15.88	16.4	45.6
7	0.50	5.00	0.25	19.03	23.89	30.92	25.5	62.5
8	0.02	0.05	0.50	2.78	3.04	2.56	9.2	-7.8
9	0.02	0.20	0.50	2.30	2.41	2.39	4.4	3.6
10	0.12	1.00	0.50	2.87	3.11	4.12	8.2	43.5
11	0.20	2.00	0.50	5.91	6.78	8.83	14.7	49.5
12	0.27	3.00	0.50	8.90	10.31	14.10	15.8	58.4
13	0.38	5.00	0.50	14.60	17.19	23.35	17.7	59.9
14	0.43	4.01	0.50	10.62	13.08	18.11	23.2	70.5
15	0.50	2.24	0.50	5.18	6.32	8.10	22.0	56.6
16	0.02	0.20	0.75	2.27	2.33	2.30	2.8	1.3
17	0.08	0.50	0.75	2.16	2.30	2.44	6.7	13.0
18	0.12	1.00	0.75	2.60	2.83	3.47	8.7	33.4
19	0.20	2.00	0.75	4.20	4.89	6.38	16.4	52.0
20	0.27	3.00	0.75	5.85	7.28	9.65	24.4	64.9
21	0.38	4.95	0.75	9.39	12.11	16.45	28.9	75.1
22	0.40	4.50	0.75	8.24	10.55	14.85	28.0	80.2
23	0.50	5.00	0.75	8.57	10.81	14.69	26.1	71.4
24	0.02	0.20	1.00	2.20	2.26	2.25	2.6	2.2
25	0.06	0.50	1.00	2.11	2.36	2.46	12.3	16.8
26	0.12	1.00	1.00	2.27	2.69	3.29	18.6	45.3
27	0.20	2.00	1.00	3.59	4.09	5.58	14.0	55.5
28	0.27	3.00	1.00	4.87	5.86	7.52	20.4	54.5
29	0.30	5.00	1.00	7.73	9.66	13.25	25.0	71.4
30	0.40	5.00	1.00	7.11	8.83	11.98	24.2	68.6
31	0.50	5.00	1.00	6.55	8.14	11.13	24.2	69.8
32	0.02	0.20	1.25	1.90	2.14	2.17	12.4	14.2
33	0.06	0.50	1.25	2.03	2.19	2.40	8.3	18.5
34	0.12	1.00	1.25	2.18	2.56	3.28	17.7	50.5
35	0.20	2.00	1.25	3.48	4.13	4.77	18.9	37.2
36	0.27	3.00	1.25	4.73	5.75	7.90	21.7	67.2
37	0.30	5.00	1.25	6.76	8.73	12.13	29.3	79.5
38	0.40	2.83	1.25	4.00	4.91	6.67	22.8	66.9
39	0.50	5.50	1.25	6.91	8.55	12.01	23.8	73.9

Table 5.1 Geometric description and partial results for the validation-convergence models of cylinder-nozzle intersection

Model #	Ref., Table, Model	Geometric parameters				SCF		
		d/D	t/T	D/T	Type	Ref.	FEA	Diff. %
V1	[41] T5, M1	0.09	1.13	36.1	FEA	2.55	2.339	-8.3
V2 (C1)	[41] T5, M4	0.2	0.2	8	Expt.	3.25	3.242	-0.2
V3	[41] T4, M7	0.25	0.57	16.5	Expt.	3.4	3.215	-5.4
V4	[41] T4, M2	0.31	0.4	17.9	Expt.	3.4	3.853	13.3
V5 (C2)	[21] T5, M12	0.5	0.5	11	FEA	4.23	4.304	1.7
V6	[41] T4, M14	0.55	0.91	57.6	Expt.	4.9	5.775	17.9
V7	[41] T5, M14	0.62	1	15.1	Expt	3.7	4.225	14.2
V8	[41] T5, M13	0.62	0.62	10	FEA	4.24	4.783	12.8
V9	[41] T4, Craw.	0.66	0.64	18.9	Expt.	4.53	4.376	-3.4
V10	[41] T4, M3	0.69	0.63	156	FEA	4.08	4.789	17.4
V11	[41] T4, M5	0.76	1.5	10.3	Expt.	3.5	3.186	-9
V12 (C3)	[41] T4, M10	1	1	19	Expt.	5.4	6.013	11.4

Table 5.2 Comparison of results for SCF in convergence study

Model No.	Element type	Nodes per element	Elements per unit length	Max. element size (mm)	Total elements (k)	SCF
C1 (V2)	Tetra	10	1	19.00	3.00	3.286
			2	9.50	14.40	3.717
			3	6.33	69.80	3.364
			4	4.75	94.90	3.484
	Brick	8	1	19.00	2.30	2.621
			2	9.50	6.20	2.973
			3	6.33	15.00	3.092
			4	4.75	29.90	3.215
			5	3.80	53.10	3.227
C2 (V5)	Brick	8	1	21.00	2.40	3.862
			2	10.50	7.70	4.162
			3	7.00	17.30	4.217
			4*	5.25	33.90	4.225
C3 (V12)	Brick	8	1	4.20	6.50	1.932
			2	2.10	31.90	2.108
			3	1.40	42.60	2.316
			4	1.05	107.30	2.339

* mesh type and size used in the parametric study

Table 5.3 SCF - comparison of reference and FEA values with formula values for validation study

Model	Lind [6]	Money [19]	Decock [20]	Gurum. [23]	Moffat [22]	Ref.	FEA
V1	2.710	3.325	2.680	2.154	3.228	2.55	2.339
V2	2.587	2.725	2.846	2.462	3.193	3.25	3.242
V3	3.195	3.519	3.381	3.622	3.681	3.40	3.215
V4	5.446	4.029	4.864	7.913	4.568	3.40	3.853
V5	3.485	3.101	3.349	4.359	3.800	4.23	4.304
V6	4.894	4.094	4.549	6.397	4.631	4.90	5.775
V7	10.156	3.653	9.667	7.764	6.288	3.70	4.225
V8	2.715	2.657	2.565	3.663	3.085	4.24	4.783
V9	5.113	3.963	4.724	7.646	4.725	4.53	4.376
V10	3.657	3.548	3.658	4.045	4.239	4.08	4.789
V11	3.855	3.684	3.769	4.308	4.455	3.50	3.186
V12	1.778	1.478	2.009	1.096	2.255	5.40	6.013
Min. %	-67.1	-72.6	-62.8	-79.7	-58.2	-	-9.0
Max. %	174.5	30.4	161.3	132.7	69.9	-	17.9
Ave. %	8.8	-11.5	5.6	20.1	6.0	-	5.2

Table 5.4 Dimensional detail of parametric models for cylinder-nozzle intersection

Model No.	Vessel NPS (inches)	D_o (mm)	Mean D(mm)	Schedule	T (mm)	Nozzle NPS (inches)	d_o (mm)	Mean d(mm)	t (mm)	d/D	t/T	D/T
1	10.00	273.00	247.60	XXS	25.40	0.50	21.34	13.93	7.41	0.05	0.29	10.75
2	10.00	273.00	247.60	XXS	25.40	1.00	33.40	24.31	9.09	0.10	0.36	10.75
3	10.00	273.00	247.60	XXS	25.40	3.00	88.90	73.66	15.24	0.30	0.60	10.75
4	10.00	273.00	247.60	XXS	25.40	6.00	168.28	146.34	21.94	0.60	0.86	10.75
5	10.00	273.00	247.60	XXS	25.40	8.00	219.08	196.85	22.23	0.80	0.88	10.75
6	10.00	273.00	260.30	S80S(XS)	12.70	0.50	21.34	17.60	3.73	0.05	0.29	21.50
7	10.00	273.00	260.30	S80S(XS)	12.70	1.00	33.40	28.85	4.55	0.10	0.36	21.50
8	10.00	273.00	260.30	S80S(XS)	12.70	3.00	88.90	81.28	7.62	0.30	0.60	21.50
9	10.00	273.00	260.30	S80S(XS)	12.70	6.00	168.28	157.30	10.97	0.60	0.86	21.50
10	10.00	273.00	260.30	S80S(XS)	12.70	8.00	219.08	206.38	12.70	0.80	1.00	21.50
11	10.00	273.00	263.73	S40S(STD)	9.27	0.50	21.34	18.58	2.76	0.05	0.30	29.45
12	10.00	273.00	263.73	S40S(STD)	9.27	1.00	33.40	30.02	3.38	0.10	0.36	29.45
13	10.00	273.00	263.73	S40S(STD)	9.27	3.00	88.90	83.41	5.49	0.30	0.59	29.45
14	10.00	273.00	263.73	S40S(STD)	9.27	6.00	168.28	161.16	7.11	0.60	0.77	29.45
15	10.00	273.00	263.73	S40S(STD)	9.27	8.00	219.08	210.90	8.18	0.80	0.88	29.45
16	10.00	273.00	268.81	S10S	4.19	0.50	21.34	19.23	2.11	0.05	0.50	65.14
17	10.00	273.00	268.81	S10S	4.19	1.00	33.40	30.63	2.77	0.10	0.66	65.14
18	10.00	273.00	268.81	S10S	4.19	3.00	88.90	85.85	3.05	0.30	0.73	65.14
19	10.00	273.00	268.81	S10S	4.19	6.00	168.28	164.87	3.40	0.60	0.81	65.14
20	10.00	273.00	268.81	S10S	4.19	8.00	219.08	215.32	3.76	0.80	0.90	65.14

Table 5.5 Geometric description of the parametric models

Model #	D(mm)	T(mm)	d(mm)	t(mm)	d/D	t/T	D/T
1	247.6	25.4	13.93	7.41	0.05	0.29	10.75
2			24.31	9.09	0.1	0.36	
3			73.66	15.24	0.3	0.6	
4			146.34	21.94	0.6	0.86	
5			196.85	22.23	0.8	0.88	
6	260.3	12.7	17.6	3.73	0.05	0.29	21.5
7			28.85	4.55	0.1	0.36	
8			81.28	7.62	0.3	0.6	
9			157.3	10.97	0.6	0.86	
10			206.38	12.7	0.8	1	
11	263.73	9.27	18.58	2.76	0.05	0.3	29.45
12			30.02	3.38	0.1	0.36	
13			83.41	5.49	0.3	0.59	
14			161.16	7.11	0.6	0.77	
15			210.9	8.18	0.8	0.88	
16	268.81	4.19	19.23	2.11	0.05	0.5	65.14
17			30.63	2.77	0.1	0.66	
18			85.85	3.05	0.3	0.73	
19			164.87	3.4	0.6	0.81	
20			215.32	3.76	0.8	0.9	

Table 5.6 SCF - comparison of formulae and FEA values for parametric study

Model #	Lind Formula [6]	Money equations [19]	Decock formula [20]	Gurum. Formula [23]	Moffat correlation eq. [22]	Present FEA results
1	2.653	1.764	2.142	0.639	2.538	2.437
2	2.539	2.037	2.292	0.973	2.692	2.469
3	2.582	2.594	2.777	2.196	3.27	2.978
4	3.343	2.959	3.282	3.567	3.93	3.666
5	3.985	3.499	3.82	4.665	4.47	4.213
6	2.545	2.206	2.223	1.111	2.602	2.311
7	2.475	2.491	2.451	1.592	2.802	2.513
8	3.08	3.079	3.183	3.342	3.443	3.133
9	4.152	3.475	3.909	5.288	4.092	3.898
10	4.572	3.92	4.259	6.395	4.376	4.856
11	2.514	2.386	2.269	1.356	2.652	2.33
12	2.455	2.673	2.54	1.913	2.887	2.511
13	3.406	3.329	3.432	4.01	3.595	3.452
14	4.938	3.918	4.528	6.606	4.377	4.562
15	5.564	4.526	5.037	7.989	4.682	6.919
16	2.377	2.288	2.334	1.677	2.747	2.461
17	2.278	2.476	2.616	2.266	3.014	2.585
18	4.237	3.627	3.961	5.598	4.107	4.184
19	6.562	4.526	5.674	9.732	4.936	7.078
20	7.575	5.468	6.493	11.937	5.193	9.566

Table 5.7 SCF values for the preliminary wall thinning study (30% thinning)

	Model properties		**Wall thinning extent**				
Model#	**d/D**	**t/T**	**0**	**r_i**	**2 r_i^***	**Full-length tapered**	**Full-length uniform**
PT1	0.05	0.30	2.33	2.65	2.13	3.26	2.92
PT2	0.10	0.36	2.51	2.34	2.76	3.55	2.78
PT3	0.30	0.59	3.45	3.53	5.01	5.73	3.55
PT4	0.60	0.77	4.56	6.47	6.51	6.76	7.31
PT5	0.80	0.88	6.92	8.39	8.44	8.47	11.5

*extent used for the parametric models

Table 5.8 Parametric study for cylinder-nozzle intersection with LTA

Model #	SCF values			% Difference	
	No thinning	20% thinning	40% thinning	20% thinning	40% thinning
1	2.44	1.95	2.01	-19.94	-17.48
2	2.47	2.07	2.3	-16.08	-6.68
3	2.98	3.33	3.35	11.79	12.63
4	3.67	4.03	4.18	9.96	13.88
5	4.21	4.92	6.04	16.71	43.27
6	2.31	2.23	2.48	-3.55	7.4
7	2.51	2.6	2.78	3.46	10.58
8	3.13	3.54	4.71	13.02	50.43
9	3.9	4.68	6.31	19.98	61.98
10	4.86	6.2	9.49	27.68	95.47
11	2.33	2.42	2.61	3.78	11.93
12	2.51	2.76	2.96	9.76	18.04
13	3.45	3.85	4.41	11.47	27.81
14	4.56	5.22	8.31	14.42	82.16
15	6.92	8.41	10.45	21.48	51.03
16	2.46	2.72	3.24	10.65	31.78
17	2.59	2.75	3.51	6.38	35.94
18	4.18	5	5.89	19.43	40.73
19	7.08	8.21	9.57	16.01	35.26
20	9.57	11.3	15.27	18.13	59.63

Table 6.1 Results for the seismic fatigue study of sphere-nozzle intersection

Model	t/T	% Thin.	SCF	ΔR (KN)	ε	Δε
SF-1	0.50	0	5.91	60	0.160	0.0033
		20	6.78	54	0.175	0.0043
		40	8.83	44	0.200	0.005
SF-2	0.75	0	4.20	65	0.110	0.003
		20	4.89	57	0.135	0.0033
		40	6.38	48	0.145	0.004
SF-3	1.00	0	3.59	85	0.053	0.0013
		20	4.09	76	0.083	0.002
		40	5.58	65	0.102	0.003
SF-4	1.25	0	3.48	145	0.019	0.0004
		20	4.13	125	0.043	0.001
		40	4.77	105	0.045	0.0015

Table 6.2 Results for the seismic fatigue study of cylinder-nozzle intersection

Model	d/D	t/T	% Thinning	SCF	ΔR (KN)	ε	Δε
TF-1	0.05	0.30	0	2.330	41	0.016	0.0025
			20	2.418	35	0.019	0.0034
			40	2.608	27	0.030	0.0048
TF-2	0.10	0.36	0	2.511	79	0.063	0.0022
			20	2.756	71	0.077	0.0031
			40	2.964	64	0.096	0.0042
TF-3	0.30	0.59	0	3.452	174	0.074	0.0017
			20	3.848	161	0.098	0.0023
			40	4.412	142	0.113	0.0037
TF-4	0.60	0.77	0	4.562	270	0.055	0.0013
			20	5.220	255	0.092	0.0017
			40	8.310	205	0.163	0.0028
TF-5	0.80	0.88	0	6.919	320	0.075	0.0008
			20	8.405	310	0.130	0.0010
			40	10.450	270	0.172	0.0017

FIGURES

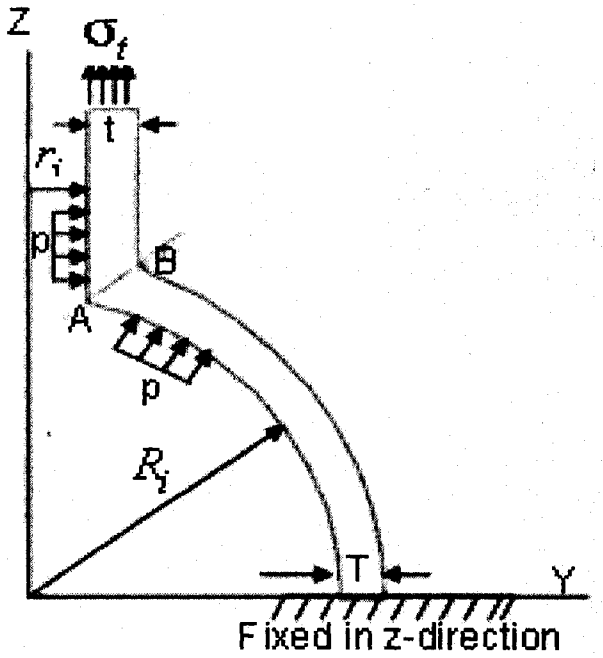

Fig. 4.1 Radial section of sphere-nozzle intersection.

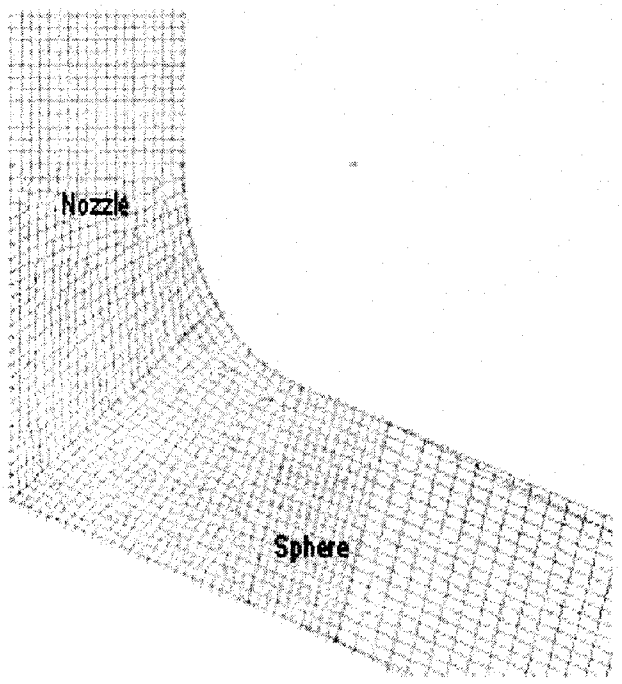

Fig. 4.2 Mesh showing axisymmetric 2D ring elements.

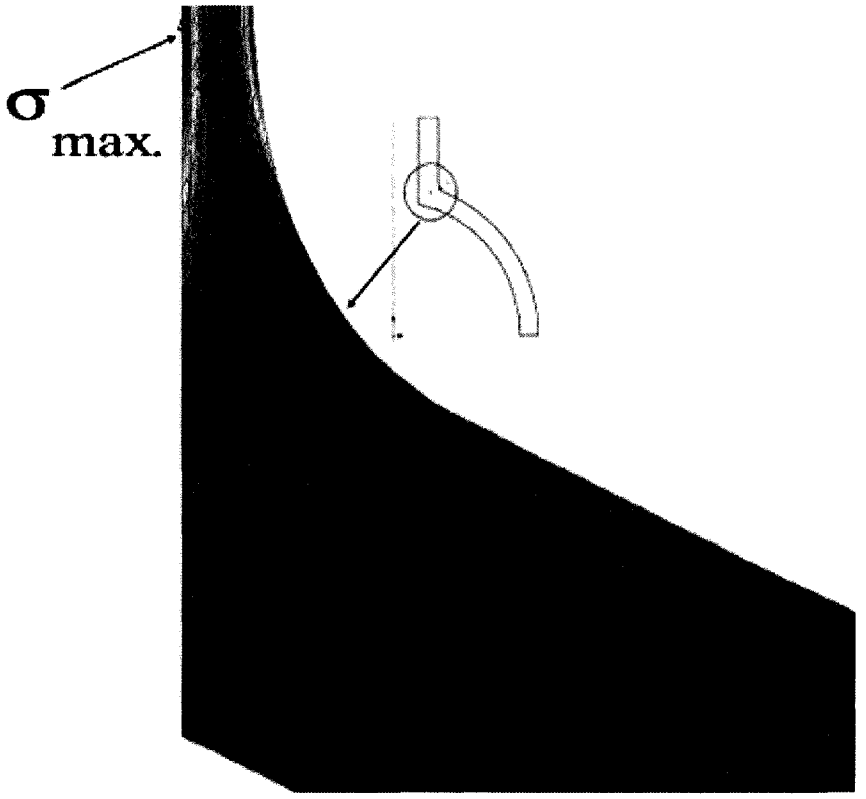

Fig. 4.3 Stress contour plot (t/T=0.25), max. stress in nozzle.

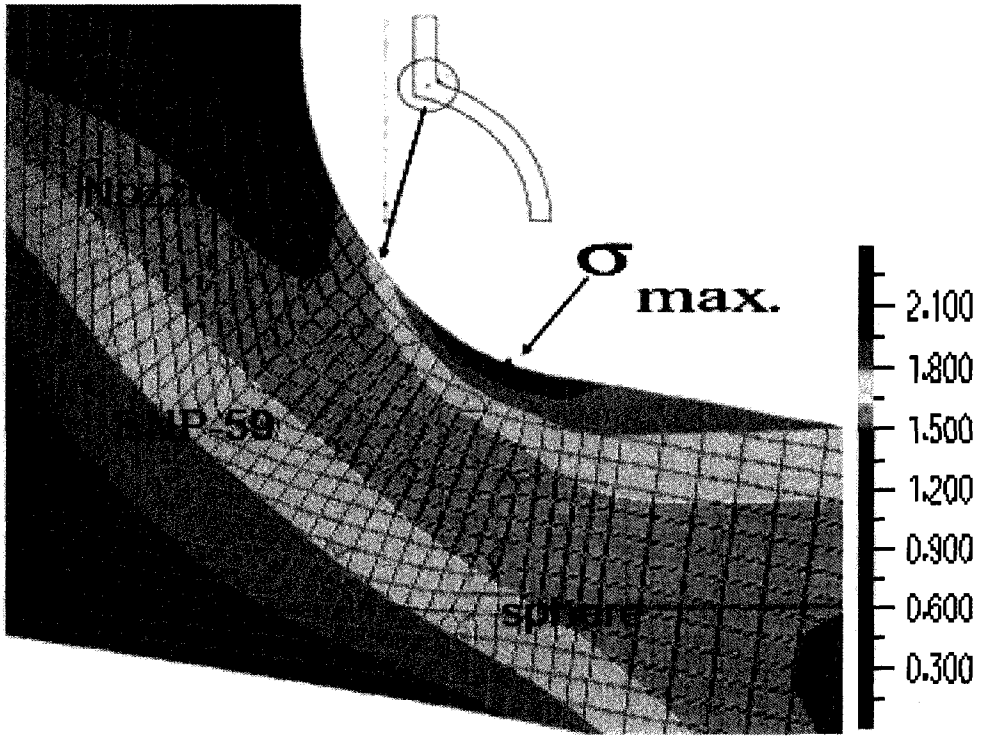

Fig. 4.4 Stress contour plot (t/T=1.0), max. stress in sphere.

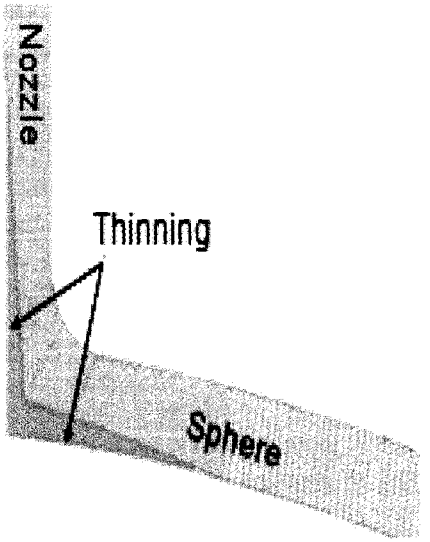

Fig. 4.5 Mesh showing inner wall LTA in both components.

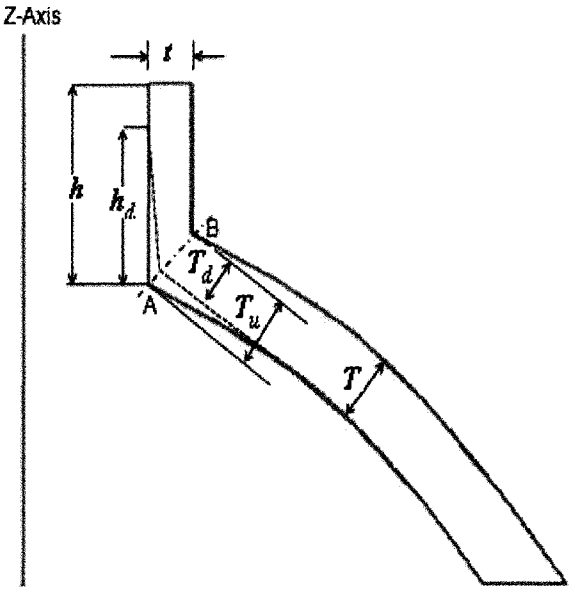

Fig. 4.6 Model with inner wall LTA in both nozzle and sphere.

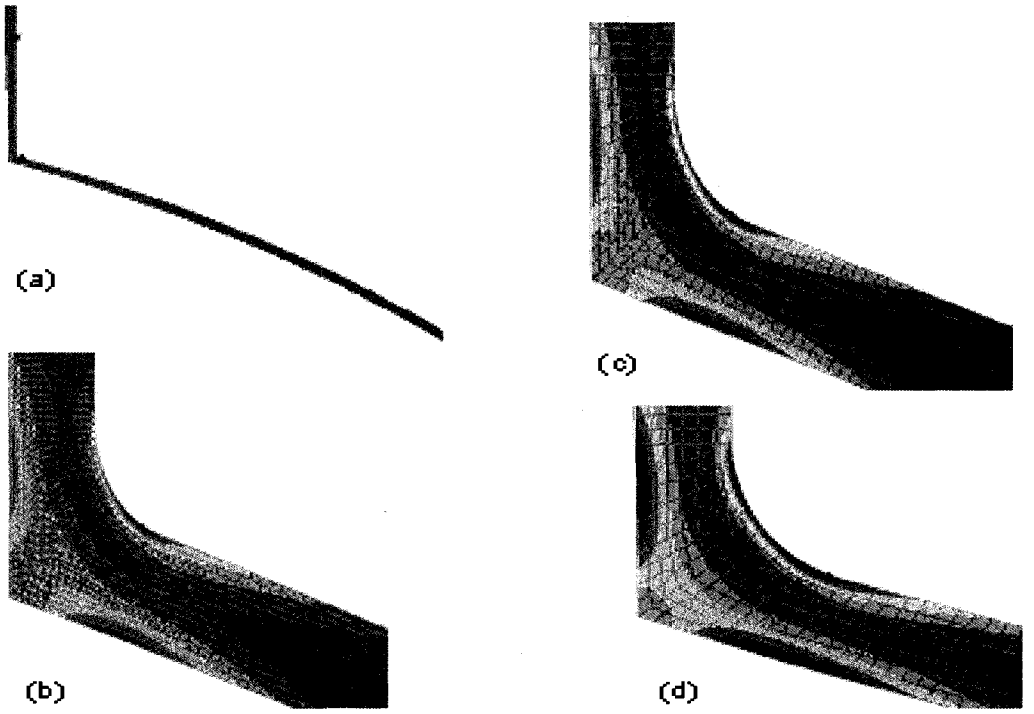

Figure 4.7 Stress contour plots for model 3-S (d =2.0, D=7.407, t=T=0.03m), (a) overall view, (b) 0% LTA, (c) 20% LTA, (d) 40% LTA.

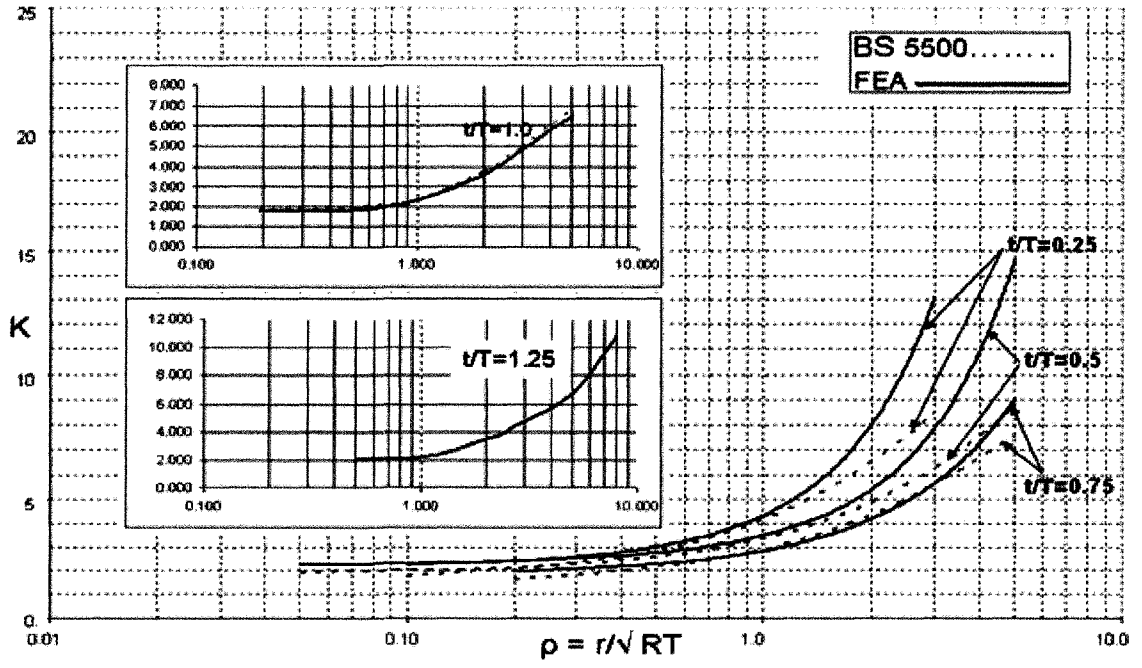

Figure 4.8 Comparison of FEA results for SCF with values from BS5500 (t/T= 0.25, 0.5, 0.75, 1.0, 1.25).

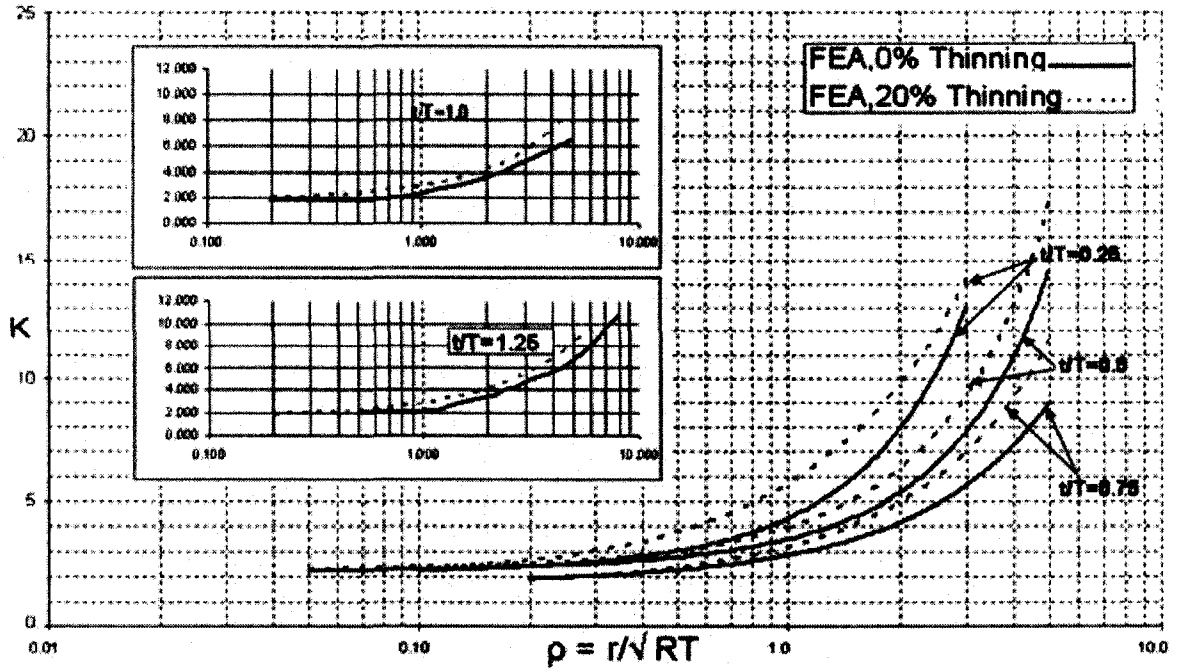

Figure 4.9 Comparison of FEA results for SCF for 0% and 20% LTA (t/T= 0.25, 0.5, 0.75, 1.0, 1.25).

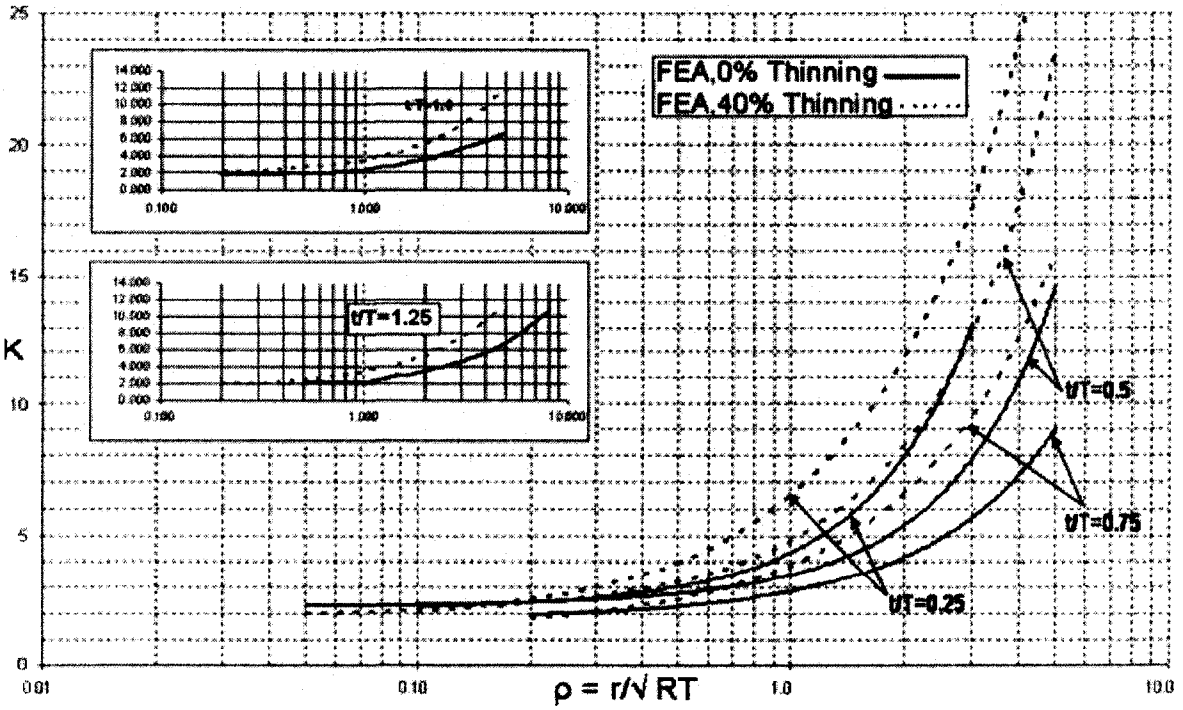

Figure 4.10 Comparison of FEA results for SCF for 0% and 40% LTA (t/T= 0.25, 0.5, 0.75, 1.0, 1.25).

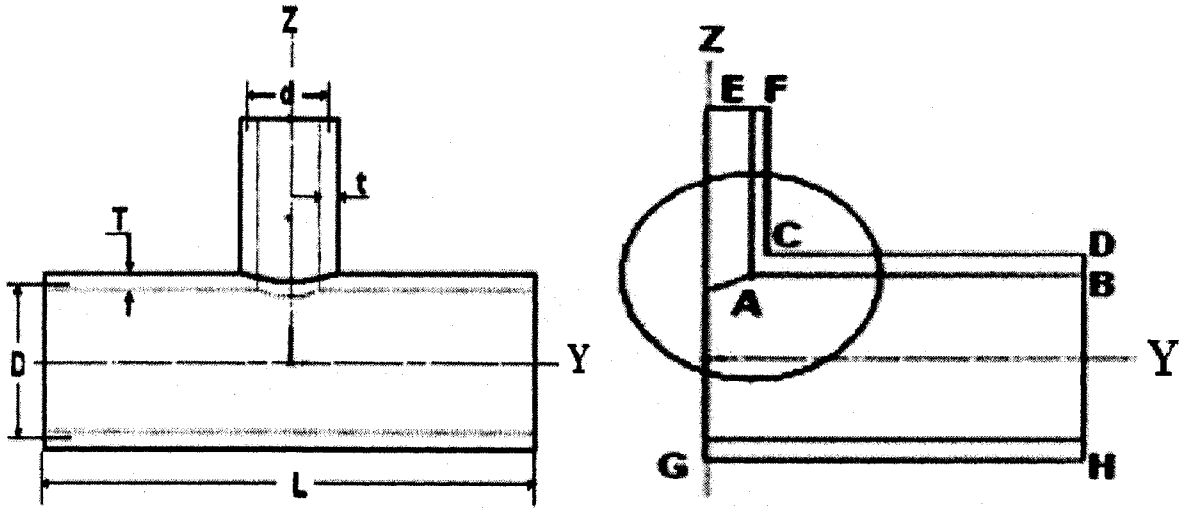

(a) (b)

Figure 5.1 Geometric details of a tee intersection, without wall thinning (a) full geometry, (b) half-section of YZ plane.

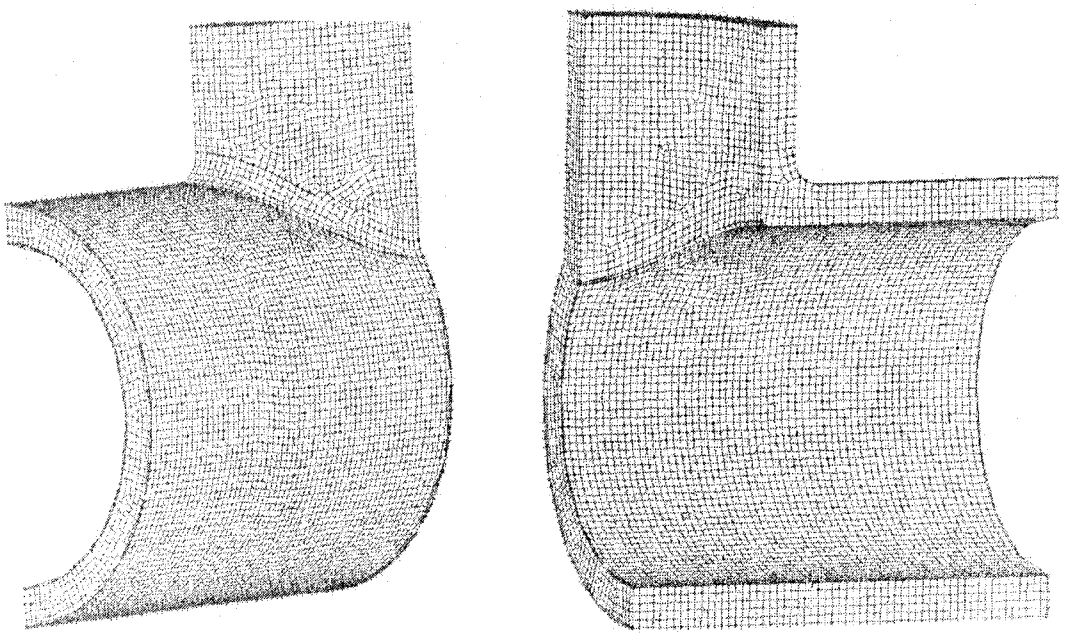

Figure 5.2 View of the details of the outside fillet weld and the inside rounding at the junction.

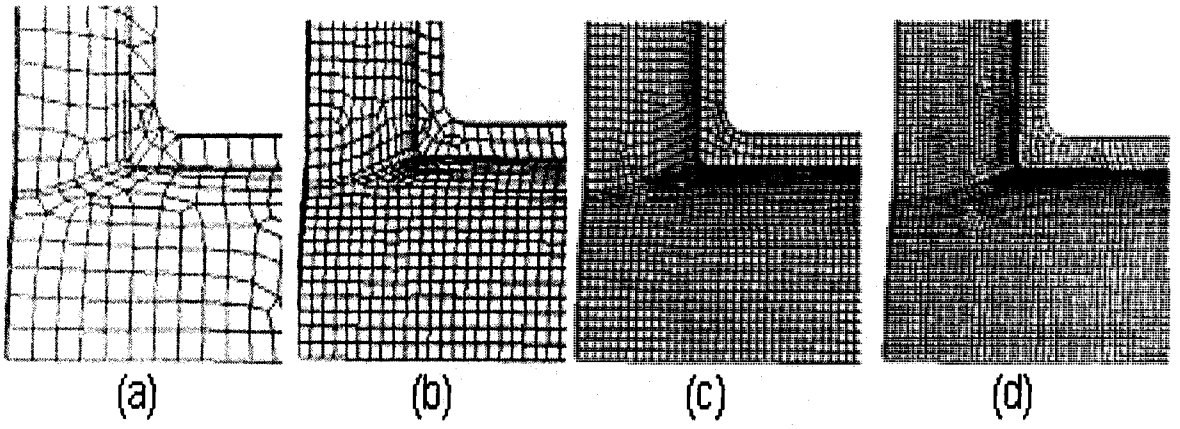

Figure 5.3 (a)-(d) Partial mesh plots for convergence model C2 showing 1-4 elements over the thickness.

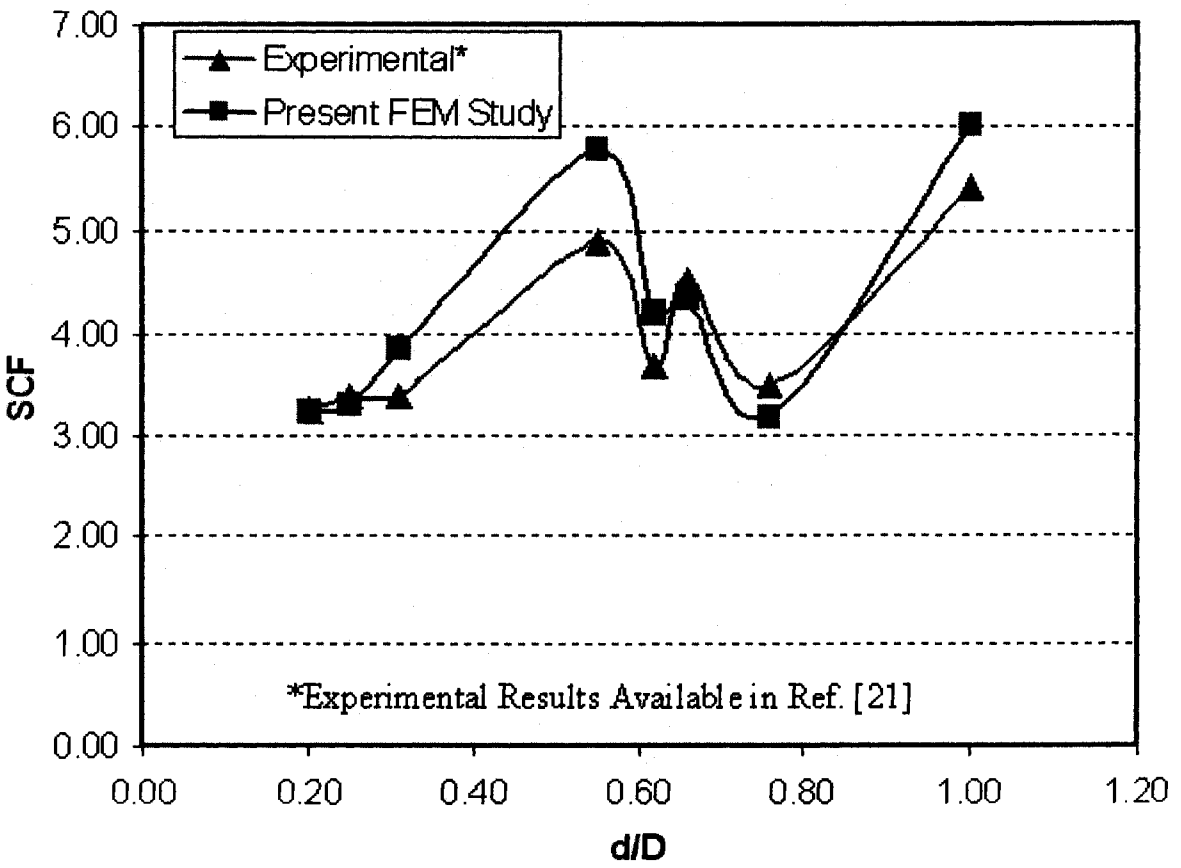

Figure 5.4 Validation study – comparison of experimental results with present FE results, (models have various t/T ratios).

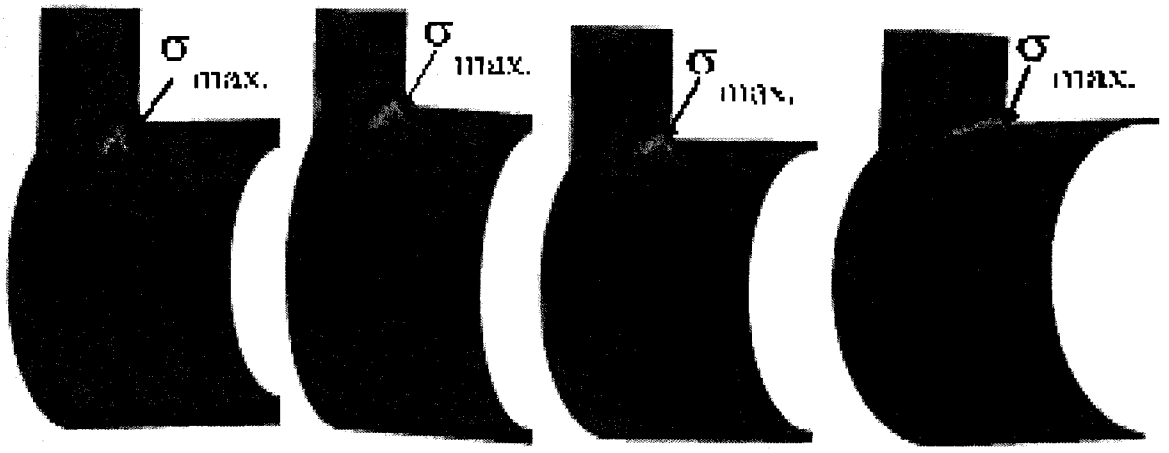

(a) (b) (c) (d)

Figure 5.5 Contours of von Mises stress of parametric models having the same diameter ratio, d/D = 0.6, (a) model 4 (schedule XXS), (b) model 9 (schedule S80S(XS)), (c) model 14 (schedule S40S (STD)), (d) model 19 (schedule S10S).

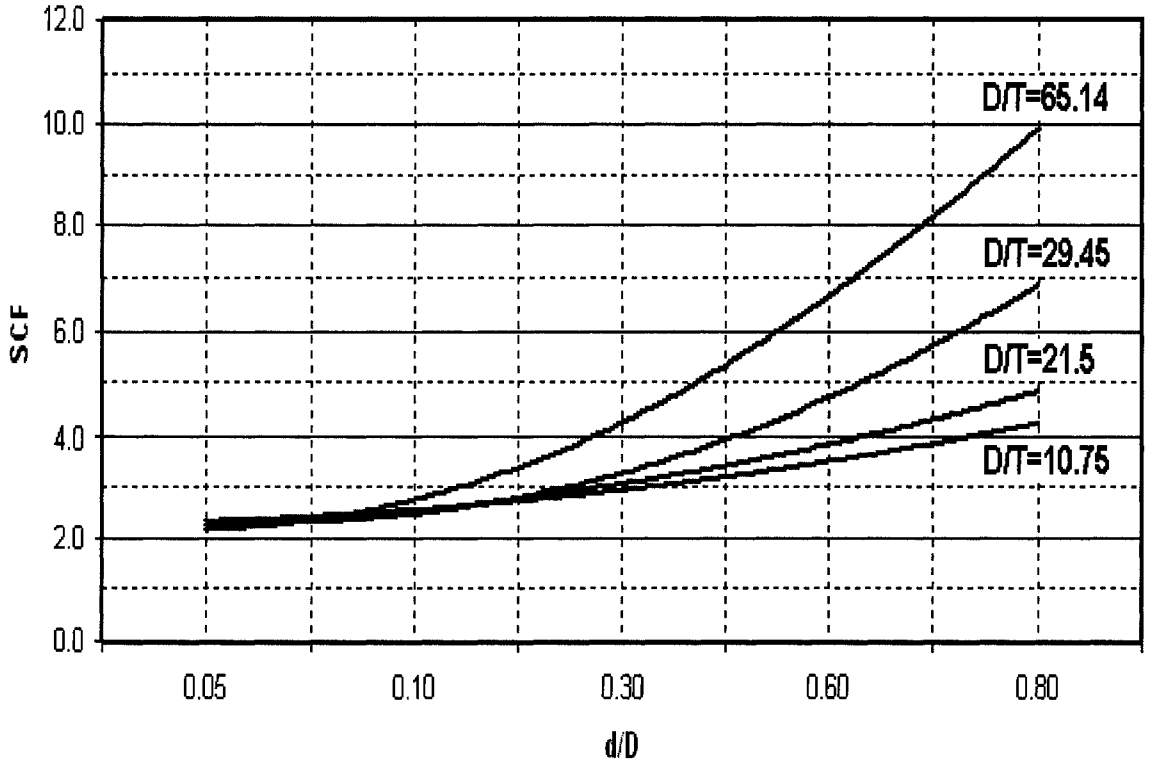

Figure 5.6 Variation in undamaged tees of the SCF with the d/D ratio for different D/T ratios (results apply to tees with nozzle thickness and fillet welds as discussed in section 5.6).

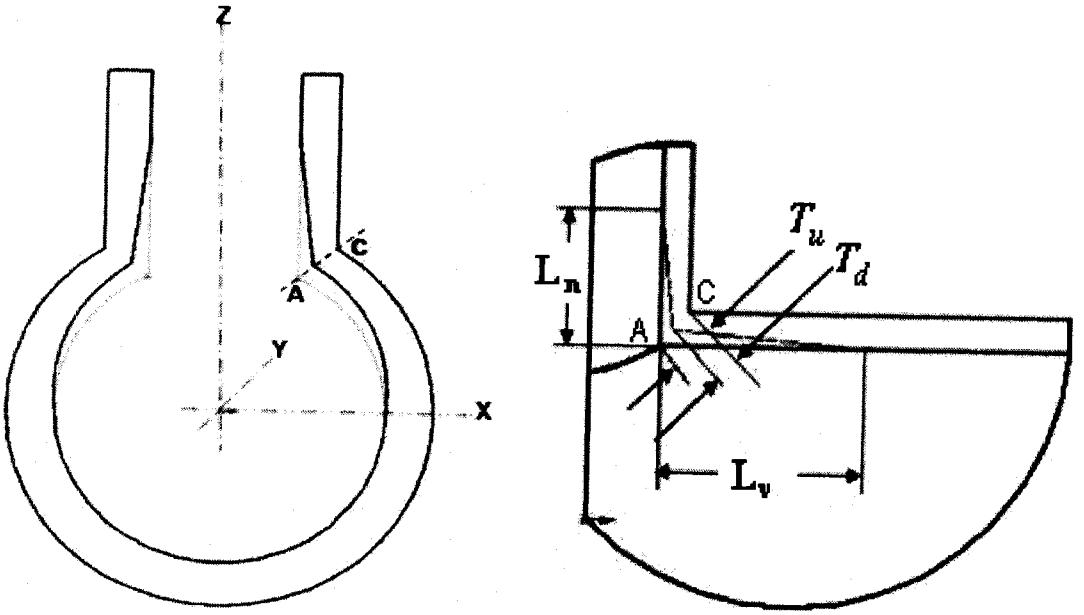

(a) (b)

Figure 5.7 Details of the assumed wall thinning; (a) full cross-sectional view in the XZ plane, (b) part cross-sectional view in the YZ plane showing enlargement of the crotch area.

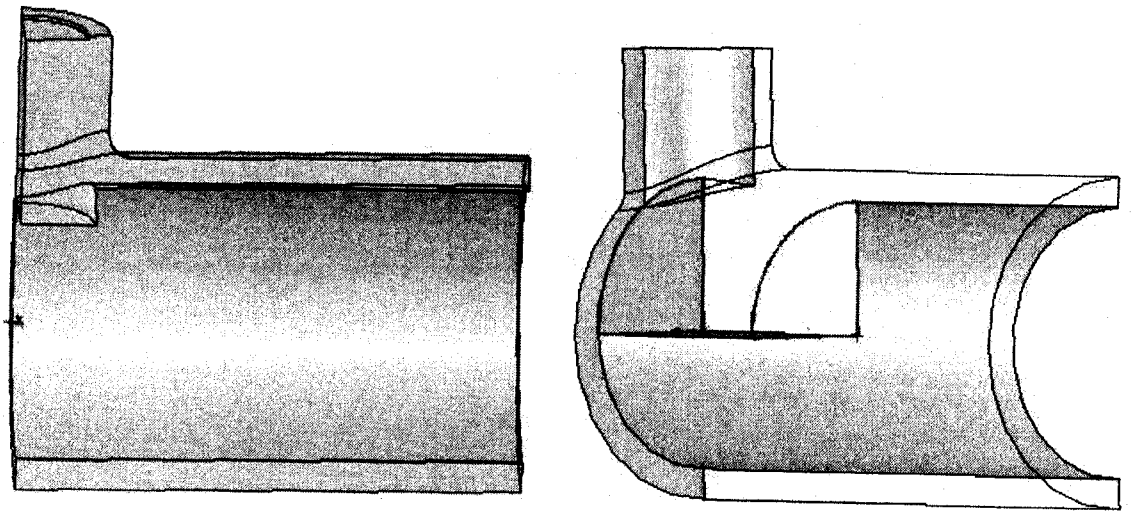

(a) (b)

Figure 5.8 Isometric views for thinning detail, (a) thinning in nozzle, (b) thinning in vessel.

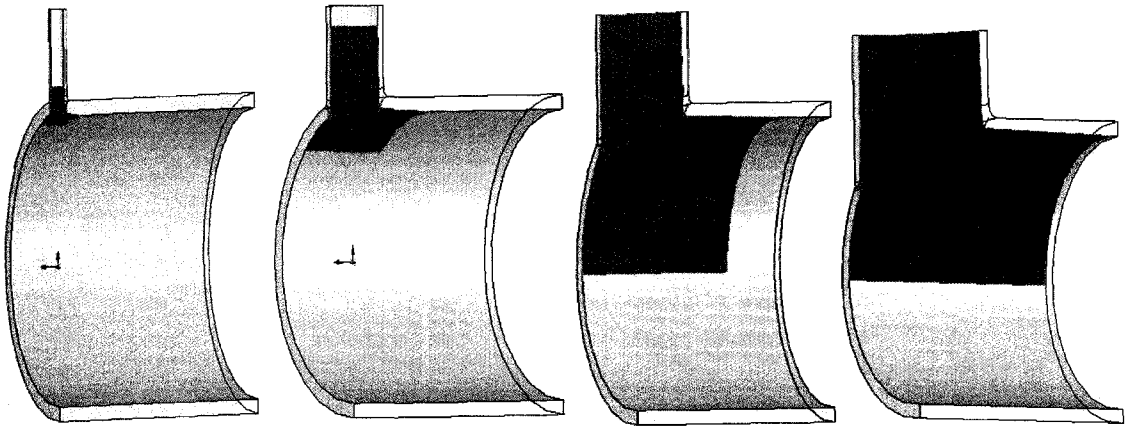

Figure 5.9 View of the assumed extent of the thinning areas (dark shading) for a tee having nozzles of different size.

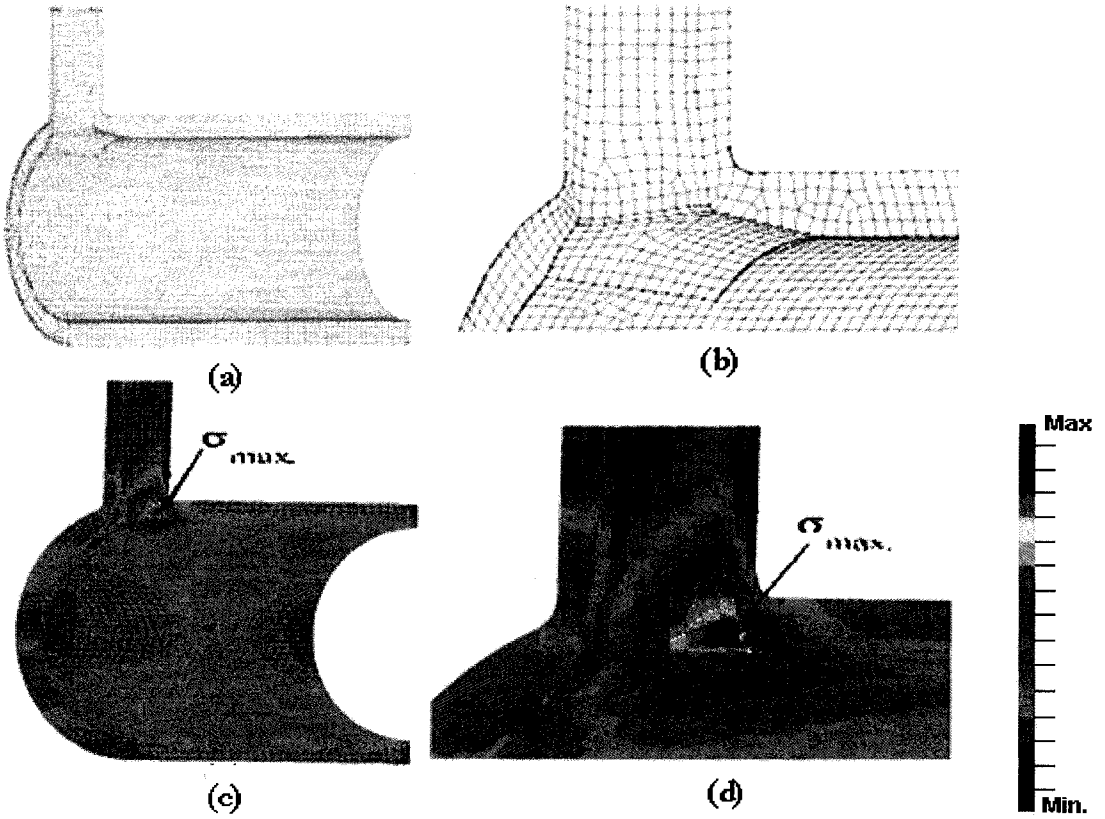

Figure 5.10 Parametric model 3 with 40% thinning: (a) mesh with thinning extent, (b) magnified view of mesh near junction, (c) contour plot of whole model, (d) magnified view of contour near junction.

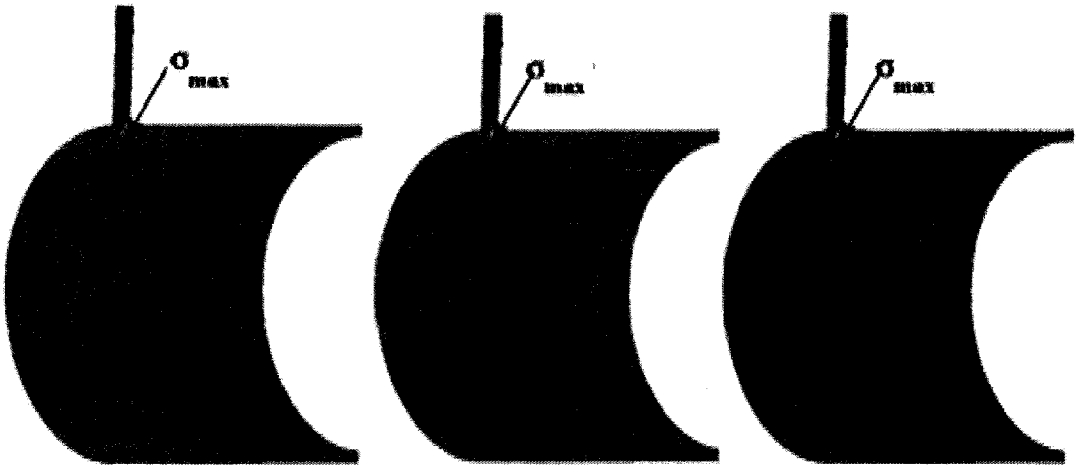

(a) (b) (c)

Figure 5.11 Contours of von Mises stress for parametric model 11 (schedule STD, d/D=0.05) with different thinning percentages; (a) 0%, (b) 20%, (c) 40%.

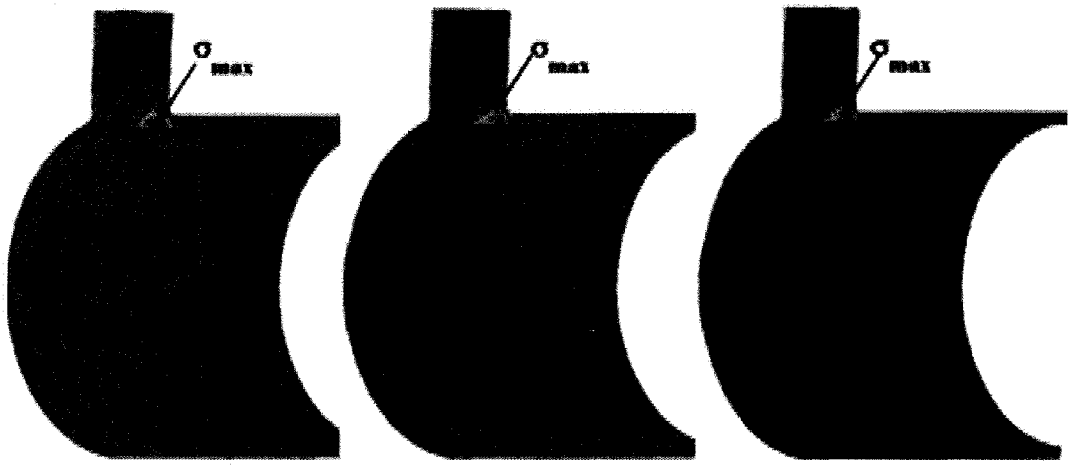

(a) (b) (c)

Figure 5.12 Contours of von Mises stress for parametric model 13 (schedule STD, d/D=0.3) with different thinning percentages; (a) 0%, (b) 20%, (c) 40%.

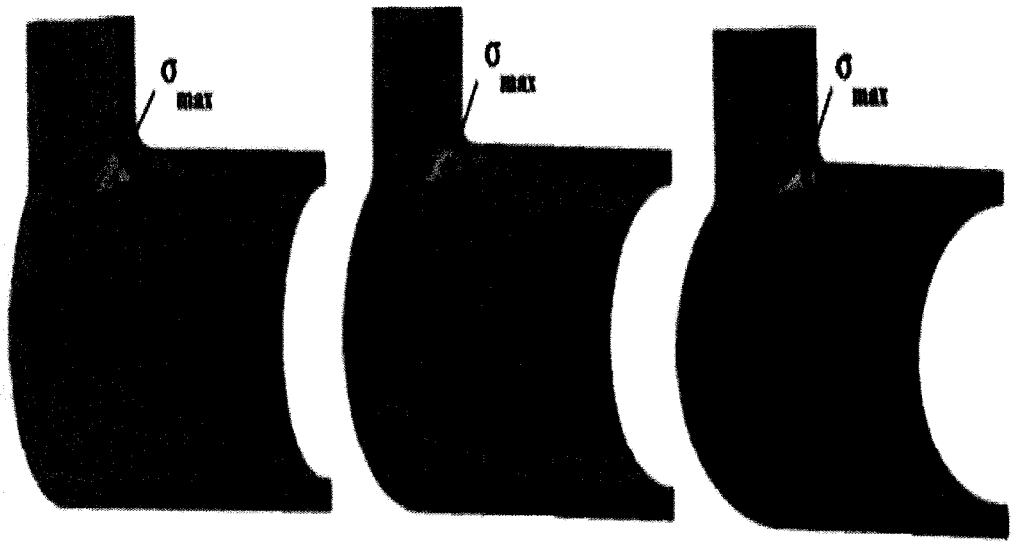

(a) (b) (c)

Figure 5.13 Contours of von Mises stress for parametric model 4 (schedule XXS, d/D=0.6) with different thinning percentages; (a) 0%, (b) 20%, (c) 40%.

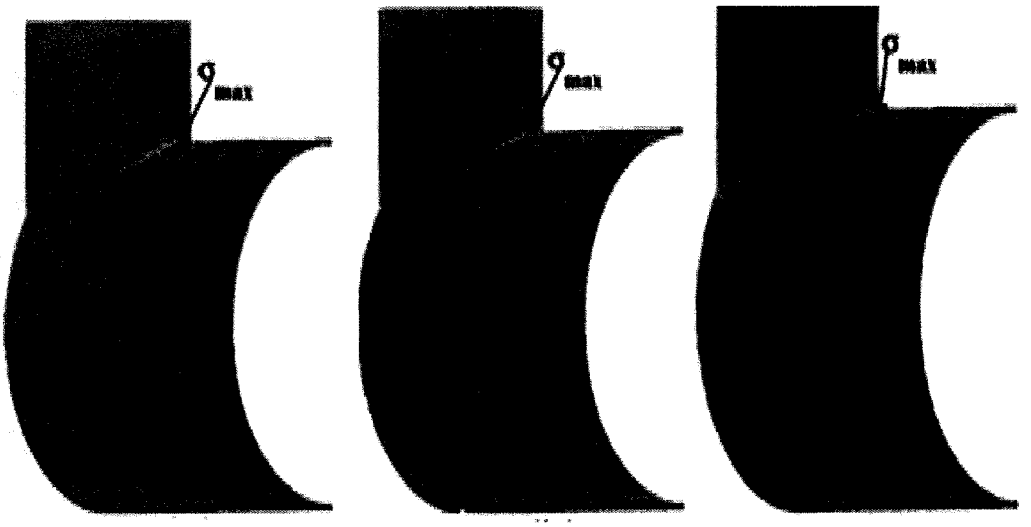

(a) (b) (c)

Figure 5.14 Contours of von Mises stress for parametric model 20 (schedule S10S, d/D=0.8) with different thinning percentages; (a) 0%, (b) 20%, (c) 40%.

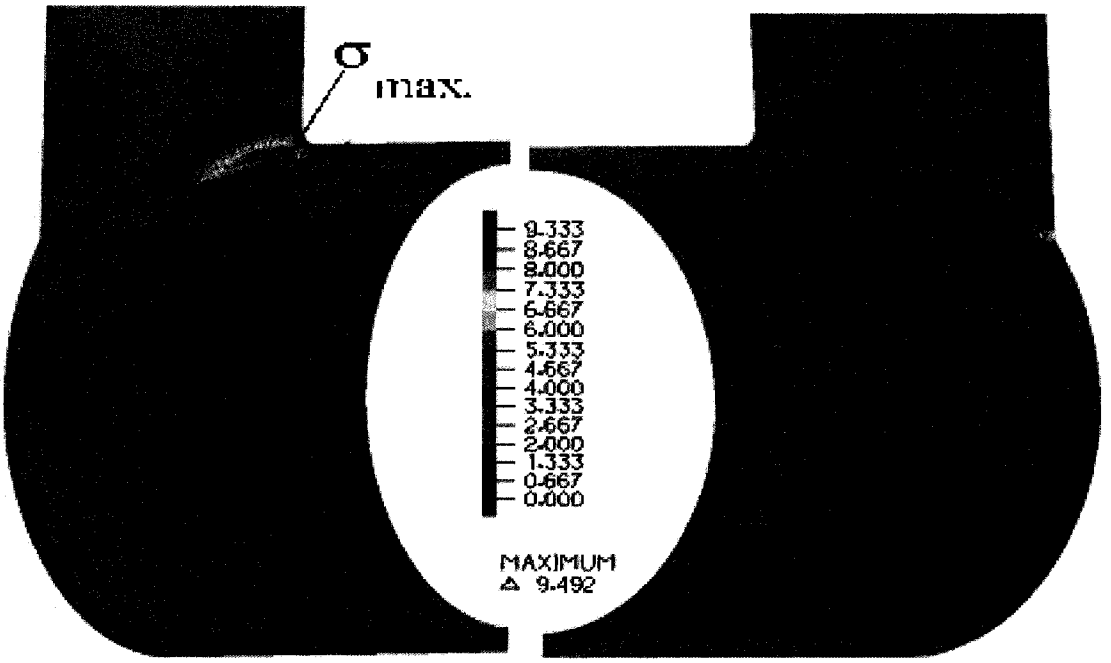

(a) (b)

Figure 5.15 Contours of von Mises stress for parametric model 10 with 40% thinning; (a) inside surface (b) outside surface.

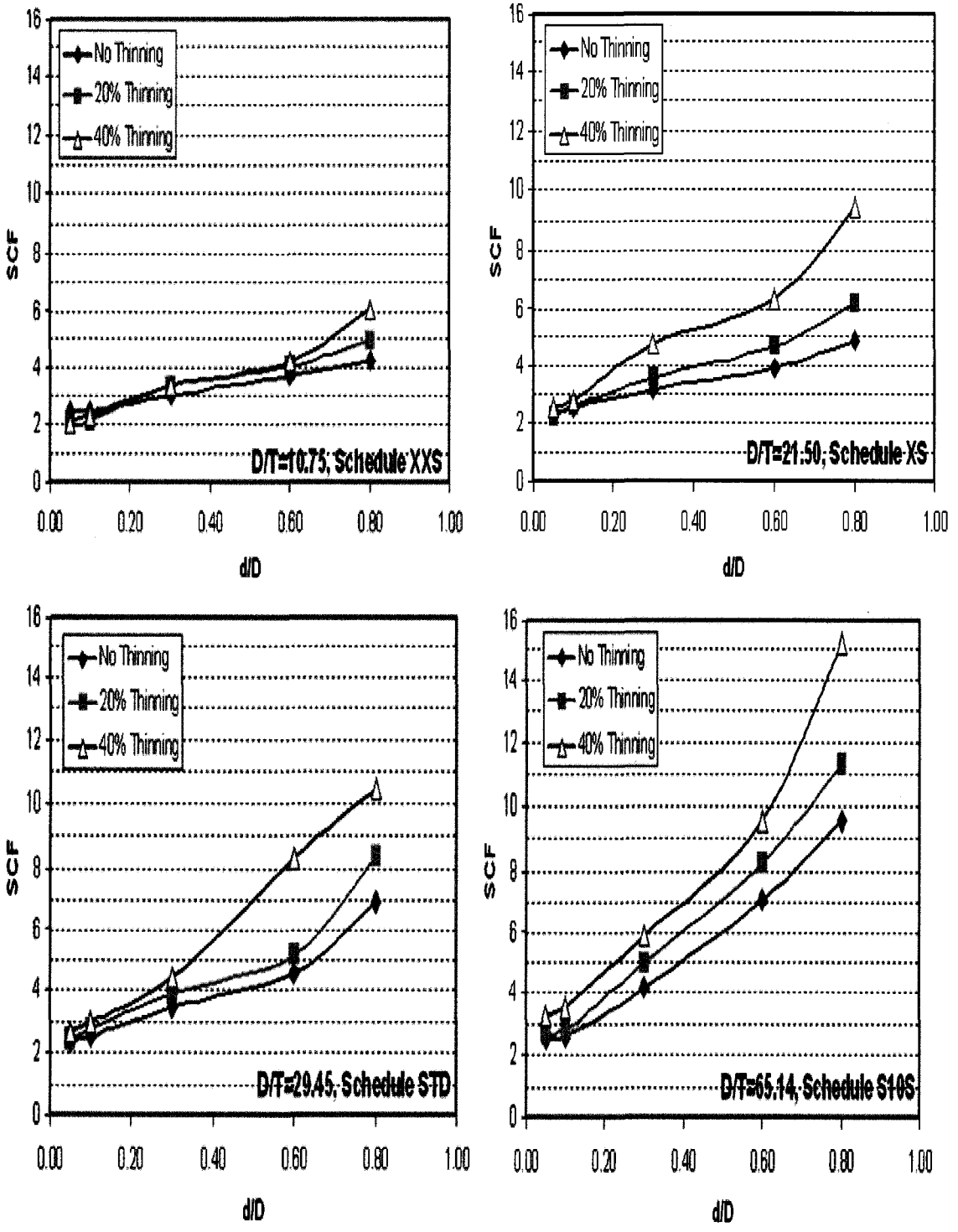

Figure 5.16 Effect on SCF of the wall thinning percentage for different pipe schedules.

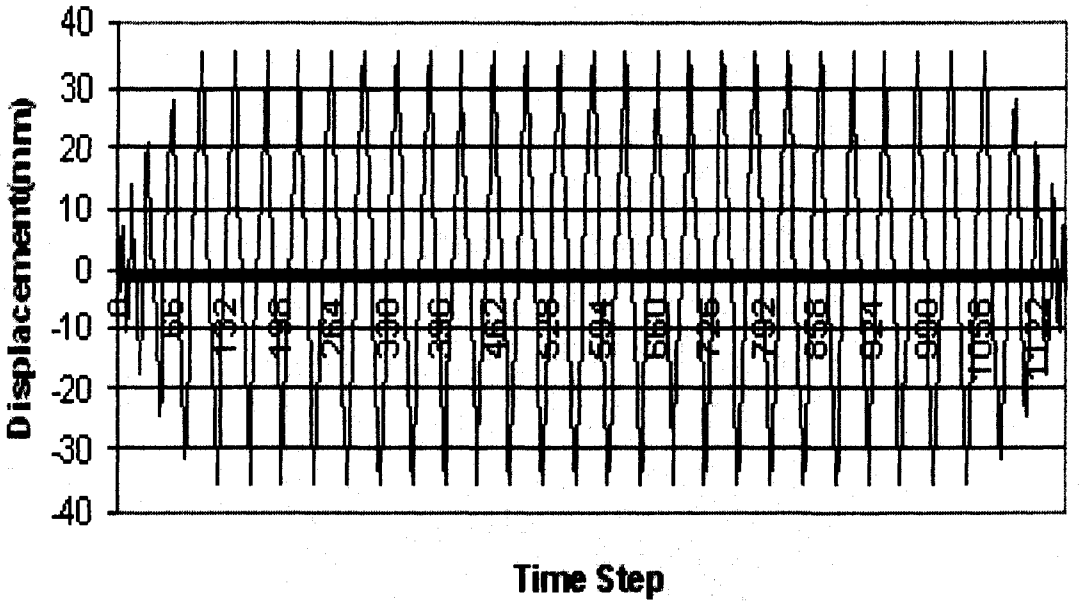

Figure 6.1 Time-displacement graph for cyclic loading.

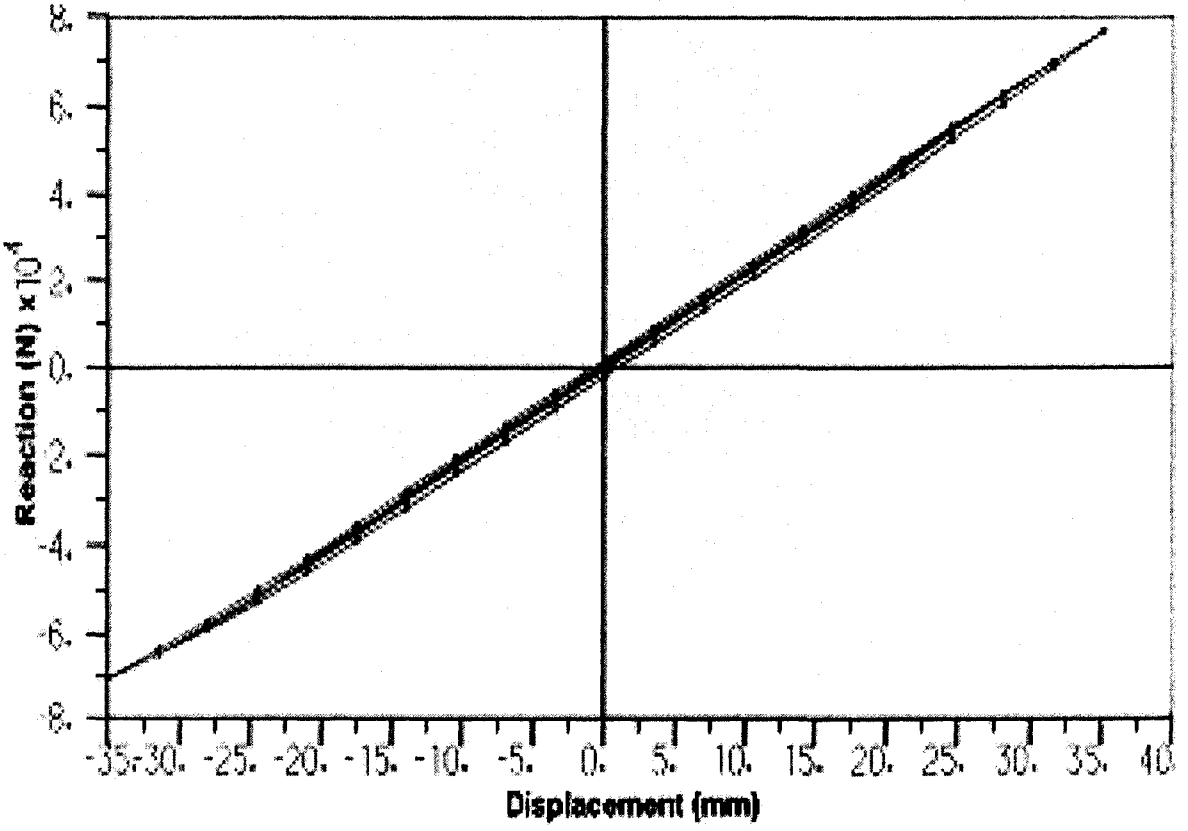

Fig. 6.2 Sphere-nozzle intersection, hysteresis plot for model SF-4, 0% LTA.

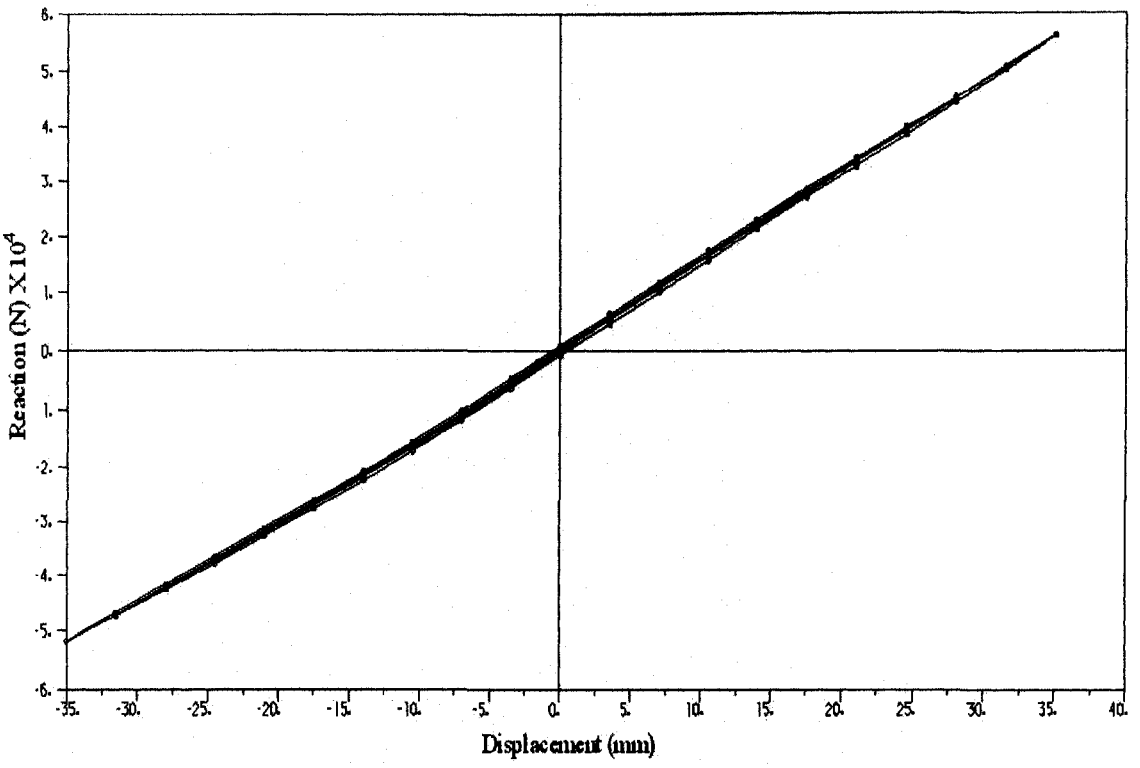

Fig. 6.3 Sphere-nozzle intersection, hysteresis plot for model SF-4, 20% LTA.

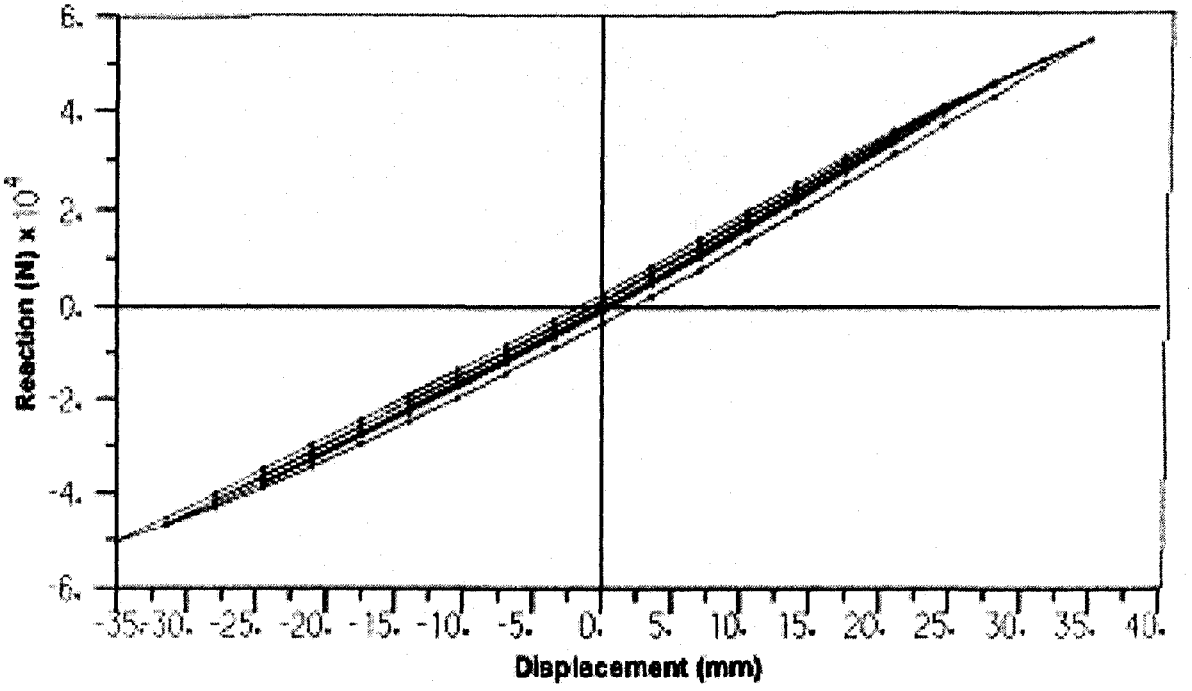

Fig. 6.4 Sphere-nozzle intersection, hysteresis plot for model SF-4, 40% LTA

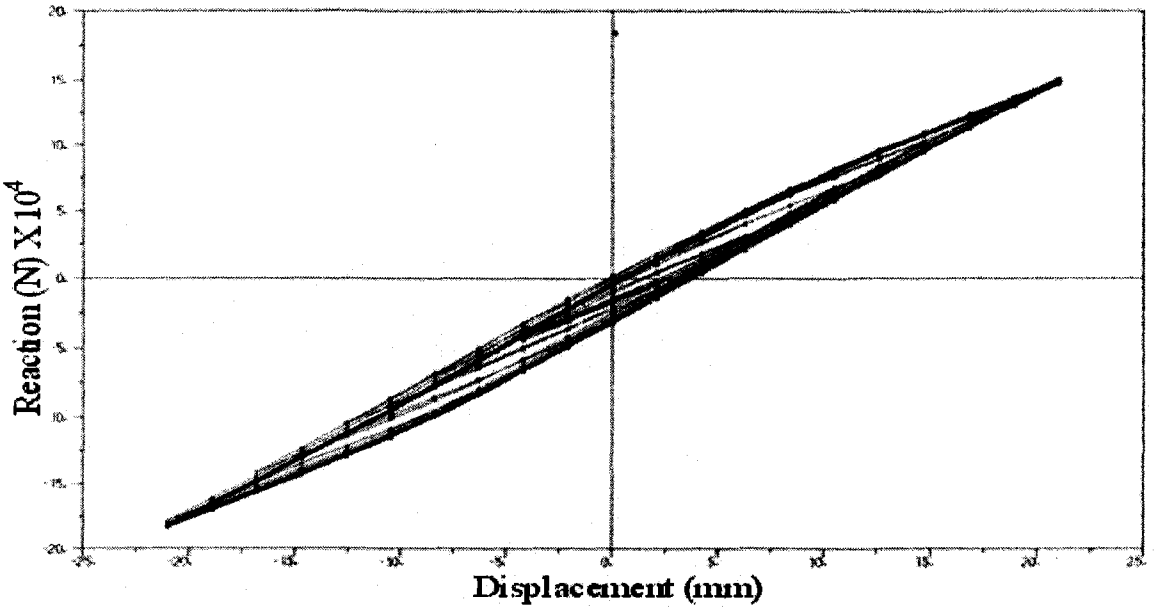

Figure 6.5 Cylinder-nozzle intersection, hysteresis plot for model TF-5, 0% LTA.

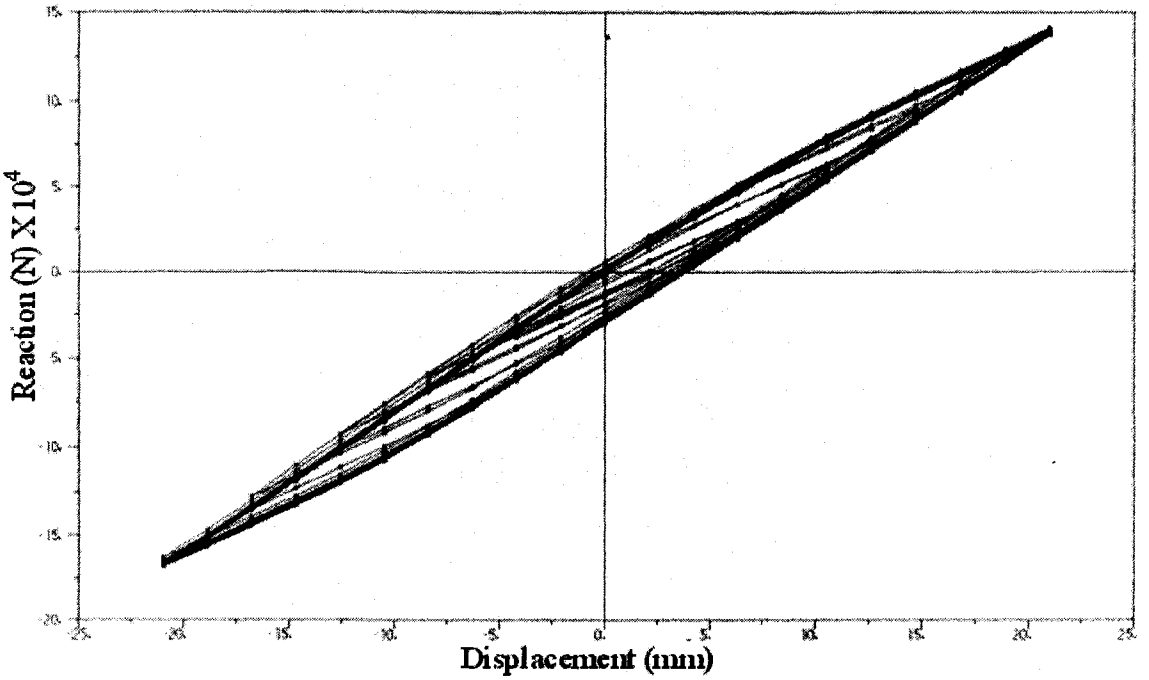

Figure 6.6 Cylinder-nozzle intersection, hysteresis plot for model TF-5, 20% LTA.

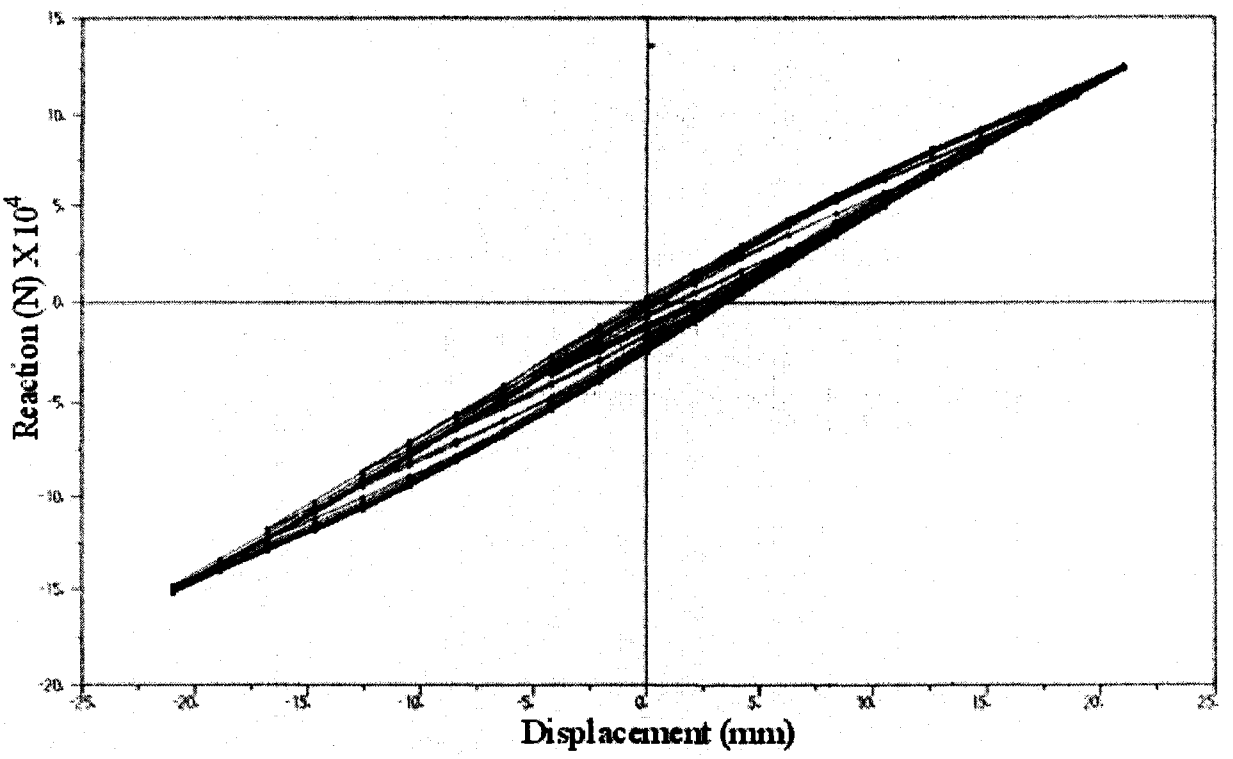

Figure 6.7 Cylinder-nozzle intersection, hysteresis plot for model TF-5, 40% LTA.

APPENDICES

Appendix-A: FEA software modeling instructions for sphere-nozzle intersection

STEP-1 Development of geometry

For the sphere-nozzle models a program was written to generate the geometric points for all models used in the validation and parametric studies. The input data for this program was r, R, t, T (Fig. 4.1) fillet radius, length of nozzle and percentage thinning at the junction. The out put for this program was the set of geometric points which were imported into FE software ADINA 8.3.3. Using these points the ADINA platform was used for the development of lines and arcs. Finally different surfaces were made from these lines and arcs to develop 2-D geometry for the analysis as shown in the following Fig. A-1

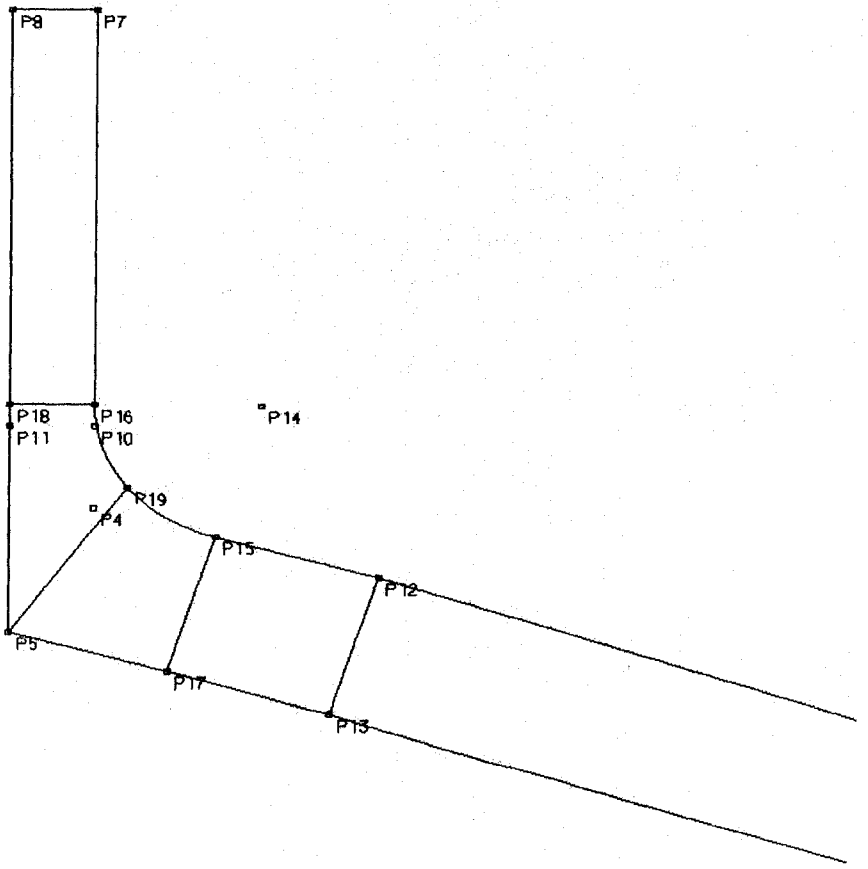

Fig. A-1 Partial view of 2D models showing points, lines and surfaces.

Table A-1 Sample output for SNP-66 Model points

Point #	X-Axis	Y-Axis	Z-Axis
1	0	1	0
2	0	1.014	0
3	0	0.9794	0.2624
4	0	0.078	1.011
5	0	0.0672	1.0033
6	0	0.9659	0.2588
7	0	0.078	1.2482
8	0	0.06	1.2482
9	0	0	0
10	0	0.078	1.0787
11	0	0.06	1.0787
12	0	0.1421	1.004
13	0	0.1401	0.9901
14	0	0.092	1.0239
15	0	0.0907	1.0099
16	0	0.078	1.0239
17	0	0.0895	0.996
18	0	0.0618	1.0239
19	0	0.0817	1.0144
20	0	0.06	0.9982
21	0	0	0
22	0	0	0
23	0	0.0817	0.9998
24	0	0.0787	1.0192

Step-2 Use of FEM pre-processor and processor

Invoke ADINA AUI 8.3.3

1-Select from the drop down boxes of "Program Module" and "Analysis Type":

ADINA – Static Analysis – No FSI

From the "Menu Bar"

1) Control – Heading – Type the problem heading (e.g.; SNP-66)

Control – Degree of Freedom – uncheck x, y and z rotation-uncheck x translation-OK

2- Defining Geometry of the Model

Defining Geometry-Points

A window will open for feeding geometry points manually or can be imported directly from note pad file as practised in this study.

From the "Menu Bar"

Geometry-points-Import-*give the path of the file and press open, all points will be imported in the ADINA system.*

Defining geometry-lines and arcs

From the "Menu Bar"

Geometry-lines-define, add line 1, 2, 3.....n, type-straight *(For each line give starting point as point 1 and ending point as point 2 of the line, for arc give end points and centre point of the arc)*

Defining Geometry-surfaces

From the "Menu Bar"

Geometry-surface-Define, add surface 1, 2, 3.....n, Type-patch *(For each surface give four lines/arcs as 1,2,3,4 bounding the respective surface)*

3-Defining the material

From the "Menu Bar"

Model-Material-Elastic-Isotropic *(A window will open for mechanical properties of the material)*

Add-material # 1

Young's Modulus 207000000000

Poisson's Ratio 0.3

Click OK.

4-Defining element group

From the "Menu Bar"

Meshing-element group *(A window will open to define the group)*

Add-Group no. 1, Type 2-D solid, element sub-type -axisymmetric, all other option left to default.

5- Defining the mesh

From the "Menu Bar"

Meshing-Mesh density-Surface *(A window will open for selecting different option for meshing).*

Select method-Use length put element edge length 0.0045(say)

Meshing type-ruled base

Nodes per Element 9

OK

6-Applying the boundary conditions

From the "Menu Bar"

Model- boundary conditions-define Fixity

(A window will open to define different fixity)

Add-Fixity name, new name e.g X-Fixed, check the x-translation box, same way define all the fixities needed.

From the "Menu Bar"

Model-boundary conditions-apply fixity *(A window will open)*

In this window

Apply to-line

Put Line # 1

Fixity, Z-Fixed

7-Applying the load

From the "Menu Bar"

Model- loading-apply *(A window will open to define loads)*

Load type-pressure

Apply to-Line

Load no.1, define (*A window will open for defining the load*)

Add- pressure # 1

Magnitude= 0.0072(say)

Add- pressure # 2

Magnitude = -0.0081(say)

Apply the load #1 (say) on line no. 1, 3, 5, 7, 5,8 etc.

Apply the load #2 (say) on line no. 9 traction on the nozzle

8- Running the analysis

From the "Menu Bar"

Solution-data file/run *(A window will open to create the ADINA input file)*

Give file name SNP-66RUN etc and click OK.

ADINA analysis window will open and take some time for the solution. You will get a message that the solution is successfully completed. Close the entire windows.

Step-3 Post processing and results:

Invoke ADINA AUI 8.3.3

From the dropdown list given in the top-left corner

Select post-processing (*A new window will open for the analysis results*).

Click open give the path of the file as SNP-66RUN and press open.

As the file open, the structure of the geometry will appear on the screen.

From the Menu bar click the button for Quick band plot, the whole model will show the stress contour in different colours.

The value and location of maximum and minimum stress can also be seen.

The value of maximum stress can be used to find the stress concentration factor.

Step-4 Fatigue analysis

1) Repeat 1-9 steps

2) *From the "Menu Bar"*

Control-Time function *(A window for defining time function will open)*

Add-Time function number1

Function multiplier as constant

Time Value

1 1

1.0000e20 1

Add-Time function number2

Function multiplier as constant

Import-give the path of the note pad files to load the Time ~ Displacement values given in Table A-2.

Table A-2 Time ➨Displacement values

Time	value	Time	value	Time	value
0	0	72	0	.....	.....
1	-3.5	73	-3.5	458	28
2	0	74	-7	459	31.5
3	3.5	75	-10.5	460	35
4	7	76	-14	461	31.5
5	3.5	77	-17.5	.....	.....
6	0	78	-21	.....	
7	-3.5	79	-24.5	1136	-14
8	-7	80	-28	1137	-10.5
9	-10.5	81	-31.5	1138	-7
10	-7	82	-28	1139	-3.5
11	-3.5	83	-24.5	1140	0
12	0	84	-21	1141	3.5
13	3.5	85	-17.5	1142	7
14	7	86	-14	1143	10.5

15	10.5	87	-10.5	1144	14
16	14	88	-7	1145	10.5
17	10.5	89	-3.5	1146	7
18	7	90	0	1147	3.5
19	3.5	91	3.5	1148	0
20	0	92	7	1149	-3.5
21	-3.5	93	10.5	1150	-7
22	-7	94	14	1151	-10.5
23	-10.5	95	17.5	1152	-7
24	-14	96	21	1153	-3.5
25	-17.5	97	24.5	1154	0
26	-14	98	28	1155	3.5
27	-10.5	99	31.5	1156	7
28	-7	100	35	1157	3.5
29	-3.5	101	31.5	1158	0
30	0	102	28	1159	-3.5
.....	.....	103	24.5	1160	0

Graphical presentation of the load step can be seen by pressing "Graph" button and is given in Fig. 6.1

Fig. A-2 Time-Displacement graph for cyclic loading.

Applying Time Step

From the "Menu Bar"

Control-time step *(A window will open for time steps)*

Time step name as "default"

Number of Steps Constant Magnitude

1160 1

3) Applying seismic wave on the model

From the "Menu Bar"

Model-Load-Apply *(A window will open to apply the load)*

Load Type-Displacement

Apply to-Surface

Site # *5 (should be top face of the nozzle)*, Select Time function #2

Click define button (*A window will open for defining the load*)

Add- Displacement # 1

Prescribed value of translation

X-Free, Y-Free, Z= -0.001

Prescribed value of rotation

X-Free, Y-Free, Z= Free

4) Running the analysis

From the "Menu Bar"

Solution-Data file/run *(A window will open to create the ADINA input file)*

Give file name SNP-66Fatigue etc. and click OK.

ADINA analysis window will open and will take some time for the solution to be completed. You will get a message that the solution is successfully completed. Close the entire windows.

5) Post processing and results:

From the dropdown list given in the top-left corner

Select Post-processing

A new window will open for the analysis results.

Click open give the path of the file as SNP-66Fatigue and press open.

It will take about half an hour to open the Porthole file

As the file open, the structure of the geometry will appear on the screen.

From the menu bar click the button for quick band plot, the whole model will show the stress contour in different colours.

The required graph for stress, strain and reaction can be obtained by defining the nodes and elements at which these results are needed.

Appendix-B: FEA software modeling instructions for cylinder-nozzle intersection

Step-1 Development of geometry

All the models for cylinder-nozzle intersection were developed in CAD software (Solidworks). For undamaged Tee-joints, the models are developed from two cylinder/pipes intersecting each other. A fillet was provided outside at the junction equivalent to the weld area. A fillet with small radius of the order of 2-3 mm was also provided inside at the junction. The damaged models/locally thinned were also made in Solidworks and detail is provided in Fig.5.8. Then parasolid of the models were imported into ADINA 8.3.3 for FEA analysis.

Step-2 Use of FEM pre-processor and processor

Invoke ADINA AUI 8.3.3

1) Select from the drop down boxes of "Program Module" and "Analysis Type":

ADINA – Static Analysis – No FSI

From the "Menu Bar"

On left side Click button "import Para solid model" beside Define Body button and give the path of the file for Para solid model. Model will be imported into ADINA with all its geometric properties.

2) Control-Heading-type the problem heading (e.g. T-18)

Control-Degree of freedom – uncheck x, y and z rotation-OK

3) Control-Time function *(A window for defining time function will open)*

Add-Time function number1

Function multiplier as constant

Time	Value
1	1

1.0000e20 1

Add-Time function number 2

Function multiplier as constant

Import-give the path of the note pad files to load the time step given in Table A-2

4) Model-Material-Elastic-Isotropic *(A window will open to define the material)*

Add material # 1

Young's Modulus 207000000000

Poisson's Ratio 0.3

Click OK.

5) Defining element group

From the "Menu Bar"

Meshing- element group *(A window will open to define the group)*

Add-Group no. 1, type 3-D solid, element sub-type –axisymmetric.

6) Defining the mesh

From the "Menu Bar"

Meshing-Mesh density-Body *(A window will open for selecting different option for meshing).*

Select Method -Use length, put element edge length 0.0045(say)

Meshing type-ruled base

Nodes per Element 8

Select brick element.

OK

7) Applying the boundary conditions

From the "Menu Bar"

Model- Boundary Conditions-Define Fixity *(A window will open to define different fixity)*

Add-Fixity name, new name e.g X-Fixed, check the x-translation box and same way define all the fixities needed.

From the "Menu Bar"

Model- Boundary Conditions-Apply Fixity *(A window will open)*

Apply to-surface

Surface #	Fixity
1	X-Fixed
4	XZ-Fixed
5	Z-Fixed
7	---
3	---

8) Applying the load

From the "Menu Bar"

Model- Loading-Apply *(A window will open to define loads)*

Load type-Pressure

Apply to-Surface

Click define (*A window will open for defining the load*)

Add- pressure # 1

Magnitude= 0.0072(say)

Add- pressure # 2

Magnitude = -0.0081(say)

Add- pressure # 3

Magnitude= 0.00519(say)

OK

From the drop down list

Select Load # 1, Site # 3, 6 7 2 etc, select time function #1

Select Load # 2 site # 4 (*Traction on nozzle end*), select time function #1

Select Load # 3 site # 10 (*Traction on vessel end*), select time function #1

9) Running the analysis

From the "Menu Bar"

Solution-Data file/run *(A window will open to create the ADINA input file)*

Give file name T-18(say) and click Save

ADINA analysis window will open and take some time for the solution. You will get a message that the solution is successfully completed. Close the entire windows.

Step-3 Post processing and results:

From the dropdown list given in the top-left corner

Select Post-processing

A new window will open for the analysis results.

Click open give the path of the file as T-18 and press open.

As the file open, the model's geometry will appear on the screen.

From the menu bar click the button for quick band plot, the whole model will show the stress contour in different colours.

The value and location of maximum and minimum stress can also be seen.

The value of maximum stress can be used to find the stress concentration factor.

Step-4 Fatigue Analysis

1) Repeat steps -1

2) *From the "Menu Bar"*

Control-Time function *(A window for defining time function will open)*

Add-Time function number 1

Function multiplier as constant

Time	Value
1	1
1.0000e20	1

Add-Time function number 2

Function multiplier as constant

Import-give the path of the note pad files to load the time step given in Table A-2

Graphical presentation of the load step can be seen by pressing "Graph" button

Applying time Step

From the "Menu Bar"

Control-Time Step *(A window will open for time steps)*

Time step name as "default"

Number of Steps	Constant Magnitude
1160	1

3) Applying seismic wave on the model

From the "Menu Bar"

Model-Load-Apply *(A window will open to apply the load)*

Load type-Displacement

Apply to-Surface

Site # *5 (should be top face of the nozzle)*, select time function # 2

Click define button (*A window will open for defining the load*)

Add- Displacement # 1

Prescribed value of translation

X-Free, Y-Free, Z= -0.001

Prescribed value of rotation

X-Free, Y-Free, Z= Free

4) Running the analysis

From the "Menu Bar"

Solution-Data file/run *(A window will open to create the ADINA input file)*

Give file name SNP-66Fatigue etc. and click OK.

ADINA Analysis window will open and take long hours (about 7-8) for the solution to be completed. You will get a message that the solution is successfully completed. Close the entire windows.

Post processing and results:

From the dropdown list given in the top-left corner

Select Post-processing

A new window will open for the analysis results.

Click open give the path of the file as T-18Fatigue and press open.

It will take about two-three hours to open the Porthole file

As the file open, the structure of the geometry will appear on the screen.

From the menu bar click the button for quick band plot, the whole model will show the stress contour in different colours.

The required graph for stress, strain and reaction can be obtained by defining the nodes and elements at which these results are needed.